

University of Southampton Research Repository

Copyright © and Moral Rights for this thesis and, where applicable, any accompanying data are retained by the author and/or other copyright owners. A copy can be downloaded for personal non-commercial research or study, without prior permission or charge. This thesis and the accompanying data cannot be reproduced or quoted extensively from without first obtaining permission in writing from the copyright holder/s. The content of the thesis and accompanying research data (where applicable) must not be changed in any way or sold commercially in any format or medium without the formal permission of the copyright holder/s.

When referring to this thesis and any accompanying data, full bibliographic details must be given, e.g.

Thesis: Zeina Nazer (2025) " CAN LOW-COST MULTI-STATIC LIDAR IMPROVE SAFETY OF CONNECTED AUTONOMOUS VEHICLES?", University of Southampton, Faculty of Engineering and Physical Sciences MPhil Thesis.

University of Southampton

Faculty of Engineering and Physical Sciences

School of Civil and Environmental Engineering

CAN LOW-COST MULTI-STATIC LIDAR IMPROVE SAFETY OF CONNECTED AUTONOMOUS VEHICLES?

by

ZEINA NAZER P.E. MSc. MBA

https://orcid.org/0000-0002-7022-9615

Thesis for the degree of Master of Philosophy in Engineering & The Environment

Under the Supervision of Prof Otto Muskens and Prof Ben Waterson

04 April 2025

University of Southampton Abstract

Faculty of Engineering and Physical Sciences

Master of Philosophy in Engineering & The Environment

CAN LOW-COST MULTI-STATIC LIDAR IMPROVE SAFETY OF CONNECTED AUTONOMOUS VEHICLES?

by

Zeina Nazer

This thesis is motivated by the following question: How can the performance of LiDAR sensors improve to reliably detect the surrounding environment at least as safely as with a competent human driver sitting in the driver's seat? This research is much needed and timely.

LiDAR (Light Detection and Ranging) sensors have several applications. In this research the focus is on LiDAR application in connected autonomous vehicles CAV in order to improve their safety. CAV depend on their perception systems to gather information about their immediate surroundings. CAV need to detect their immediate environment including nearby vehicles, pedestrians, and other obstacles. LiDAR sensors complemented with cameras and other sensors using perception algorithms can improve safety by providing more accurate estimation of the surroundings and reducing the blind spots (Li and Ibanez-Guzman 2020).

This research investigates whether a single, rotating, and expensive LiDAR can be replaced by multiple, low-cost Solid-State LiDAR and advance road safety including the safety of CAV by helping reduce blind spots. *In other terms if multi LiDAR sensors are better than one.*

This research used both Physics and Engineering laboratories to test various scenarios of LiDAR sensors in order to draw conclusions and provide recommendations.

The aim of this research is to improve LiDAR sensors on CAV to better locate objects and ultimately pedestrians. Among other requirements for vehicles to become autonomous, LiDAR sensors need to function as well as the human eye, in order to eliminate pedestrian/vehicle collisions.

LiDAR sensors fall into several ranges and types. Each type has its own advantages and disadvantages, and the cost can differ. While some have argued that LiDAR sensors are expensive, one cannot put a cost on human life. Considering this, for the CAV industry to become more sustainable, there must be a cost-effective solution for installing LiDAR sensors onto vehicles.

This research project used both laboratory and field experiments using different LiDAR techniques and scenarios in order to answer the research question "Are Multistatic or Multiple LiDAR sensors better than a single LiDAR sensor in advancing road safety of CAV by seeing more (reducing the blind spot or dead zone)?."

The conclusions drawn from this research suggest that two LiDAR sensors are better than one in reducing the blind spot, which can contribute in improving the safety of CAV. This was proven by understanding the theory of Two LiDAR setup in the Physics Lab pointing at one object using triangulation/trilateration method. The setup of two Lidar sensors combined with cameras was tested in the Engineering lab then using real life experiments pointing at a pedestrian. Using both Physics Lab and Engineering lab the two LiDAR setup proved to have fewer blind spots than one LiDAR setup.

| Tabl | e of Contents | 2 |
|------|------------------------------------------------------|----|
| Tabl | e of Tables | 6 |
| Tabl | e of Figures | 8 |
| Rese | earch Thesis: Declaration of Authorship | 11 |
| Ackr | nowledgements | 12 |
| Defi | nitions and Abbreviations | 13 |
| Cha | pter 1 Introduction | 15 |
| 1.1 | Background | 15 |
| 1.2 | Aims & Objectives | 16 |
| 1.3 | Structure of the Thesis | 16 |
| 1.4 | Methodology | 17 |
| Cha | pter 2 Literature Review | 19 |
| 2.1 | Introduction | 19 |
| 2.2 | CAV AV & Pedestrian Safety | 19 |
| | 2.2.1 Perception/Reaction Time and Stopping Distance | 20 |
| | 2.2.2 Blind Spot | 22 |
| 2.3 | CAV & ADAS | 23 |
| 2.4 | CAV & Sensors Suite | 24 |
| | 2.4.1 Cameras | 25 |
| | 2.4.2 Radar | 26 |
| | 2.4.3 Ultrasonic Sensors | 26 |
| | 2.4.4 LiDAR | 27 |
| Cha | pter 3 LiDAR Overview | 30 |
| 3.1 | Monostatic, Bistatic, Multistatic LiDAR | 30 |
| 3.2 | LiDAR Rangefinder Principles | 30 |
| | 3.2.1 Direct Time of Flight | 35 |

| | 3.2.2 | Indirect | Time of Flight | .35 |
|------|--------|-------------|--------------------------------------------|-----|
| | | 3.2.2.1 | Frequency-modulated continuous-wave (FMCW) | .35 |
| | | 3.2.2.2 | Amplitude Modulated Continuous Wave (AMCW) | .36 |
| | 3.2.3 | LiDAR Ir | naging | .36 |
| | | 3.2.3.1 | Scanning LiDAR | .36 |
| | | 3.2.3.2 | Mechanical Scanning | .36 |
| | 3.2.4 | Solid-st | ate LiDAR | .37 |
| | | 3.2.4.1 | Flash LiDAR | .38 |
| | | 3.2.4.2 | Micro-electromechanical System (MEMS) | .38 |
| | | 3.2.4.3 | Optical Phased Arrays (OPA) | .38 |
| | 3.2.5 | LiDAR R | anges | .39 |
| | 3.2.6 | LiDAR W | /avelength | .39 |
| 3.3 | LiD | AR State | -of-the-Art | .39 |
| 3.4 | No | LiDAR Op | otion | .40 |
| Cha | pter 4 | 4 LiDAF | R Theory | 42 |
| 4.1 | Intr | oduction | 1 | .42 |
| 4.2 | LiD | AR Basic | s | .42 |
| 4.3 | Tim | ne of Fligh | nt | .42 |
| 4.4 | Prir | nciples o | f Triangulation, Trilateration & Ellipse | .44 |
| Cha | nter! | 5 Jab F | xperimental Setup | 49 |
| 5.1 | | | ent | |
| J. 1 | | | ource | |
| | | | etectors/Receivers | |
| 5.2 | | | LiDAR Configuration | |
| J.2 | | | _ | |
| | | | atic LiDAR Experimental Setup | |
| F ^ | | | atic LiDAR Experimental Results | |
| 5.3 | | | LiDAR Using Diverging Lens | |
| | 5.3.1 | Monosta | atic Diverging Lens Experimental Setup | .53 |

| | 5.3.2 | Monostatic Diverging Lens Experimental Results54 |
|-----|-------------------------------------------------------------------------------------------|---------------------------------------------------|
| 5.4 | Mu | ltistatic LiDAR Configuration55 |
| | 5.4.1 | Multistatic LiDAR Experimental Setup55 |
| | 5.4.2 | Multistatic LiDAR Experimental Results56 |
| 5.5 | Mu | ltistatic LiDAR Improved Version60 |
| | 5.5.1 | Multistatic LiDAR Improved Experimental Setup61 |
| | 5.5.2 | Multistatic LiDAR Improved Experimental Results61 |
| 5.6 | Ex | perimental Results & Analysis64 |
| 5.7 | Lal | Setup Preparation for Phase II65 |
| | 5.7.1 | Leddar M16 Flash LiDAR65 |
| | 5.7.2 | M16 Leddar Physics Lab Experimental Setup68 |
| | 5.7.3 | M16 Leddar Physics Lab Data Analysis68 |
| Cha | pter | 6 Field Experimental Setup 71 |
| 6.1 | Un | derstanding Leddar M16 Sensor71 |
| | | |
| 6.2 | Le | ddar M16 Experiments on Static Single Object71 |
| 6.2 | | Two Leddar M16 and Two Cameras71 |
| 6.2 | 6.2.1 | |
| 6.2 | 6.2.1 6.2.2 | Two Leddar M16 and Two Cameras71 |
| 6.2 | 6.2.1 6.2.2 6.2.3 | Two Leddar M16 and Two Cameras |
| 6.2 | 6.2.1 6.2.2 6.2.3 6.2.4 | Two Leddar M16 and Two Cameras |
| | 6.2.1 6.2.2 6.2.3 6.2.4 Lee | Two Leddar M16 and Two Cameras |
| | 6.2.1 6.2.2 6.2.3 6.2.4 Le 6 | Two Leddar M16 and Two Cameras |
| | 6.2.1 6.2.2 6.2.3 6.2.4 Le 6.3.1 6.3.2 | Two Leddar M16 and Two Cameras |
| | 6.2.1 6.2.2 6.2.3 6.2.4 Le 6 6.3.1 6.3.2 6.3.3 | Two Leddar M16 and Two Cameras |
| 6.3 | 6.2.1 6.2.2 6.2.3 6.2.4 Le 6 6.3.1 6.3.2 6.3.3 | Two Leddar M16 and Two Cameras |
| 6.3 | 6.2.1 6.2.2 6.2.3 6.2.4 Le 6 6.3.1 6.3.2 6.3.3 pter | Two Leddar M16 and Two Cameras |
| 6.3 | 6.2.1 6.2.2 6.2.3 6.2.4 Lec 6.3.1 6.3.2 6.3.4 pter | Two Leddar M16 and Two Cameras |

| Appendix B Object Location Using Python Coding | .103 |
|------------------------------------------------|------|
| Appendix CPython Coding for Leddar M16 | .106 |
| List of References | .116 |

Table of Tables

Table of Tables

| Table 2.1 calculation of speed and stopping distance for human driver and AV | 21 |
|-----------------------------------------------------------------------------------|----|
| Table 2.2 Comparison of Radar, Camera, Sonar and LiDAR Technologies | 28 |
| Table 3.1 Summary of LiDAR Imaging Principles | 31 |
| Table 3.2 Comparison of LiDAR Experiments performed in this research work | 32 |
| Table 6.1 Position coordinates reflecting heat map for illustration for Two LiDAR | 74 |
| Table 6.2 Frequency Distribution for Two LiDAR sensors | 82 |
| Table 6.3 Frequency Distribution for One Lidar | 82 |
| Table 6.4 Paired-Samples Proportions Tests | 84 |
| Table 6.5 Paired-Samples Proportions Statistics | 85 |
| Table 6.6 Position coordinates reflecting X1 and X2 Layout 1 | 85 |
| Table 6.7 Position coordinates reflecting X1 and X2 Layout 2 | 86 |
| Table 6.8 Position coordinates reflecting X1 and X2 Layout 3 | 87 |
| Table 6.9 Position coordinates reflecting X1 and X2 Layout 4 | 88 |
| Table 6.10 Position coordinates reflecting X1 and X2 Layout 5 | 89 |
| Table 6.11 Position coordinates reflecting X1 and X2 Layout 6 | 90 |
| Table 6.12 Position coordinates reflecting X1 and X2 for X1 at P7 | 90 |
| Table 6.13 Position coordinates reflecting X1 and X2 for X1 at P5 | 91 |
| Table 6.14 Position coordinates reflecting X1 and X2 for X1 at P50 | 93 |
| Table 6.15 Position coordinates reflecting X1 and X2 for X2 at P48 | 94 |
| Table 6.16 Position coordinates reflecting X1 and X2 for X1 at P48 | 95 |
| Table 6.17 Frequency Distribution for Two Lidars | 96 |
| Table 6.18 Frequency Distribution for One Lidar. | 96 |
| Table 6.19 Paired-Samples Proportions Tests | 98 |

Table of Tables

| Table 6.20 Paired-Samples Proportions Statistics | 98 |
|--------------------------------------------------|----|
| | |

Table of Figures

Table of Figures

| Figure 2.1 Presenting stopping distance and vehicle speed for human driver vs CAV22 |
|----------------------------------------------------------------------------------------------------|
| Figure 2.2 Blind Spot of Pedestrian seen by one LiDAR and two LiDARs at 5m distance 23 |
| Figure 2.3 Blind Spot of Pedestrian seen by one LiDAR and two LiDARs at 50m distance 23 |
| Figure 2.4 CAV & Sensors (Yeong. D.J. 2021)25 |
| Figure 4.1 Describing the concept of ToF measurement43 |
| Figure 4.2 3D-Multistatic LiDAR principle using multiple sensors and Trilateration45 |
| Figure 4.3 2D- Ellipse using two detectors to determine object position using Mathematica 46 |
| Figure 4.4 Object detection using ellipse with two detectors using Python48 |
| Figure 4.5 Object detection using Trilateration of three detectors using Python48 |
| Figure 4.6 Object detection using Trilateration of four detectors using Python |
| Figure 5.1 Monostatic LiDAR Experimental Setup Looking at one object |
| Figure 5.2 Monostatic LiDAR: Time Traces measured by the Linear LiDAR setup53 |
| Figure 5.3 Time trace vs object distance for the single beam setup (cm vs ns)53 |
| Figure 5.4 Single Beam LiDAR Experiment with one detector using a diverging lens54 |
| Figure 5.5 Diverging LiDAR: Time Traces measuring object at various distances54 |
| Figure 5.6 Time trace vs object distance for the diverging beam setup |
| Figure 5.7 Multistatic LiDAR: Single Beam LiDAR Experiment with Two Detectors Using Triangulation |
| Figure 5.8 Measure of Power Meter Using Heat Map57 |
| Figure 5.9 Detected light intensity of detectors 1 and 2 |
| Figure 5.10 Aperture angles of receivers 1 and 2 |
| Figure 5.11 Useable overlap area |
| Figure 5.12 Time delay for two detectors |
| Figure 5.13 Peak reflected light intensity for each detector |

Table of Figures

| Figure 5.14 Improved version of Multistatic LiDAR: Two Detectors Using Triangulation61 |
|---------------------------------------------------------------------------------------------|
| Figure 5.15 Intensity of Det2 (new detector) vs Det162 |
| Figure 5.16 Peak reflected light intensity for each detector Improved Version62 |
| Figure 5.17 Useable overlap area Improved Version measured in cm |
| Figure 5.18 Time delay for two detectors Improved Version |
| Figure 5.19 Illustration of Leddar M16 illumination Area and Detection Zone |
| Figure 5.20 LeddarM16 mounted with a Logitech camera67 |
| Figure 5.21 LabVIEW of LeddarM16 Experiment |
| Figure 5.22 Flash LiDAR operating principal Source: (Lemmetti et al. 2021)67 |
| Figure 5.23 object measurement at 20cm distance actual vs measured |
| Figure 5.24 object measurement at 120cm distance actual vs measured |
| Figure 5.25 Lab setup of Two Leddar M16 each combined with a camera pointing at one object. |
| 69 |
| Figure 5.26 Initial Results viewing one object using Triangulation in Physics Lab70 |
| Figure 6.1 Two Leddar M16 – Two cameras showing the side view of the Engineering |
| experimental setup72 |
| Figure 6.2 Two Leddar M16 – Two cameras showing the front view of the Engineering |
| experimental setup73 |
| Figure 6.3 Full dataset object position using two Leddar M16 sensors |
| Figure 6.4 Heat Map for two Leddar M16 sensors |
| Figure 6.5 One Leddar M16, one camera setup |
| Figure 6.6 One Leddar M16 sensor looking at position X79 |
| Figure 6.7 One camera looking at position X |
| Figure 6.8 Heat map for one Leddar M16 sensor |
| Figure 6.9 Full Dataset of X1 at P7 using two Leddar M16 sensors |
| Figure 6.10 Full Dataset of X1 at P5 using two Leddar M16 sensors |

Table of Figures

| Figure 6.11 Full Dataset of X1 at P50 using two Leddar M16 sensors |
|--------------------------------------------------------------------------------------------|
| Figure 6.12 Full Dataset of X1 at P3 using two Leddar M16 sensors |
| Figure 6.13 Full Dataset of X1 at P48 using two Leddar M16 sensors90 |
| Figure 6.14 Full Dataset of X1 at P7 using one Leddar M16 sensor |
| Figure 6.15 Full Dataset of X1 at P5 using one Leddar M16 sensor |
| Figure 6.16 Single camera images for X1 at P5 using one Leddar M16 sensor |
| Figure 6.17 Overlay for Single camera and Leddar M16 sensor for X1 at P5 and X2 at P2393 |
| Figure 6.18 Full Dataset of X1 at P50 using one Leddar M16 sensor93 |
| Figure 6.19 Overlay for Single camera and Leddar M16 sensor for X1 at P50 and X2 at P23 94 |
| Figure 6.20 Full Dataset of X1 at P3 using one Leddar M16 sensor94 |
| Figure 6.21 Full Dataset of X1 at P48 using one Leddar M16 sensor95 |
| Figure 6.22 Full Dataset of X1 at P48 using one Leddar M16 sensor95 |

Research Thesis: Declaration of Authorship

Research Thesis: Declaration of Authorship

Print name: ZEINA NAZER

Title of thesis: "CAN LOW-COST MULTI-STATIC LIDAR IMPROVE SAFETY OF CONNECTED AUTONOMOUS VEHICLES?"

I declare that this thesis and the work presented in it are my own and has been generated by me as the result of my own original research.

I confirm that:

- This work was done wholly or mainly while in candidature for a research degree at this University;
- 2. Where any part of this thesis has previously been submitted for a degree or any other qualification at this University or any other institution, this has been clearly stated;
- 3. Where I have consulted the published work of others, this is always clearly attributed;
- 4. Where I have quoted from the work of others, the source is always given. With the exception of such quotations, this thesis is entirely my own work;
- 5. I have acknowledged all main sources of help;
- 6. Where the thesis is based on work done by myself jointly with others, I have made clear exactly what was done by others and what I have contributed myself;
- 7. None of this work has been published before submission.

| Się | gnature: 2 | Z.N | NDate:04/04/2025 |
|-----|------------|-----|------------------|
|-----|------------|-----|------------------|

Acknowledgements

Acknowledgements

I would like to thank Prof Otto Muskens and Prof Ben Waterson for their continuous support and encouragement. Special thanks go to The Engineering and Physical Sciences Research Council (EPSRC) and The Defence Science and Technology Laboratory (DSTL) for their funding.

I would also like also to thank my mom and sisters Zahira & Rima for their emotional support.

I would like to thank Lina, Mona, Mirna, Maya, Nada, Noura & Khadijah for being there for me.

I would like to thank Dr Peter Wiecha for his contribution in the Deep Learning part. I also would like to thank Integrated Nanophotonics, Transport Research Groups, Student Advice and the Enabling Services.

Special thanks go to my mentor and role model Dr Wassim Habbal for showing me the way.

This thesis is dedicated to my mother Wafa my ultimate role model.

Definitions and Abbreviations

AD Autonomous Driving

ADAS Advanced Driver Assistance Systems

AI...... Artificial Intelligence

AMCW Amplitude Modulated Continuous Wave

APD Avalanche Photodiode

AV..... Autonomous Vehicles

BSI..... British Standards Institute

CAV Connected Autonomous Vehicles

CMOS...... Complementary Metal-Oxide-Semiconductor

DARPA Defence Advanced Research Projects Agency in US

DSTL Defence Science and Technology Laboratory

EM Electromagnetic

EOM Electro-Optic Modulator

EPSRC Engineering & Physical Sciences Research Council

FMCW.....Frequency Modulated Continuous Wave

FoV Field of View

GPS Global Positioning System

IMU...... Inertial navigation measurement unit

IR.....Infrared

ITS Intelligent Transport Systems

LiDAR..... Light Detection and Ranging

MEMS Micro-Electromechanical Systems

ML Machine Learning

MLS Mobile LiDAR System

NHTSA...... National Highway Traffic Safety Administration in USA

NIRA...... Near Infrared Reflectance Accessory

Definitions and Abbreviations

WHO......World Health Organization

Chapter 1 Introduction

1.1 Background

Improvements to road safety in the United Kingdom (UK) and elsewhere are minimal since road traffic accidents are commonplace. The CAV claim to reduce traffic accidents by reducing human errors, the principal cause of collision, the traffic accidents will be reduced (Bucsuházy et al. 2020). Their work conducted qualitative and quantitative analyses to determine the factors causing traffic accidents, the research found that inattention of drivers regardless of their gender or age played a key role in the occurrence of traffic accidents. Inattention included distraction and inexperience of drivers.

CAV claim to reduce traffic accidents by reducing human errors if they can detect objects without making mistakes like humans do. If all CAV were to be equipped with the appropriate hardware and software, then human errors could be eliminated. LiDAR have several applications and use of the technology has been increasing rapidly. Nevertheless, LiDAR use for CAV remains debatable. Major companies including Waymo, Cruise and Uber that are testing for autonomous vehicles use LiDAR along other sensors while Tesla autonomous cars operate without LiDAR (William Poor 2023). Notably, this thesis does not promote CAV or LiDAR sensors, but explores solutions for improving safety of CAV if they were to use LiDAR sensors.

There is a limited amount of literature on Multistatic LiDAR sensors for automotive applications to optimize object location and reduce blind spots (Kim and Park 2020) (Jim Hyen Park 2008) For example, research on the placement of Multiple LiDAR sensors on Autonomous vehicles was performed and concluded with identifying an optimal position that reduced blind spots. To achieve this, a LiDAR occupancy grid was used to formulate the work mathematically, and experiments were performed on solid-state LiDAR sensors mounted on a vehicle (Kim and Park 2020)

Other previous work concluded that Multistatic radar can improve image resolution (Doughty, Woodbridge, and Baker 2007) ("Multistatic Radars" 2004) as can the combination of Multistatic radar with deep learning by reducing blind spots (Angelov et al. 2018) as it is possible to combine deep learning with lasers to access the hidden environment (Caramazza et al. 2018).

A LiDAR sensor combined with a deep learning camera enabled significantly better image reconstruction from fewer measurements (Johnson et al. 2021). The application and flexibility of deep learning techniques and how it can be combined with LiDAR sensors for traffic signals suggests that it can give better results (Gouda et al. 2022)

Recent work was conducted on the use of Multistatic Radar for automotive applications at Politecnico university in Milan(Vince 2022)

Their work concluded there is a gap in Multistatic LiDAR in the application of CAV. The combination with neural network could provide advanced results. (Caramazza et al. 2018) (Johnson et al. 2021)(Gouda et al. 2022) (Kim and Park 2020) (Jim Hyen Park 2008).

Some of the previous work concluded that Multistatic radar can improve resolution (Doughty, Woodbridge, and Baker 2007b) ("Multistatic Radars" 2004) in combination with deep learning.(Angelov et al. 2018) Deep Learning has become indispensable in the design and implementation of autonomous vehicles.

The work of this thesis takes the previous work a step further and includes cameras and a triangulation method to locate an object, while reducing the blind spots. The key areas in this research are LiDAR theory and practice, triangulation, pedestrian safety, autonomous vehicles, Advanced Driver Assistance Systems (ADAS), physics laboratory and engineering laboratory experiments. This study will consider all these areas in order to improve pedestrian safety.

1.2 Aims & Objectives

The ultimate aim of this work is to explore if Multiple/ Multistatic LiDAR sensors are better than Monostatic LiDAR in finding blind spots and providing better image resolution and reducing blind spots. These in application could lead to improving road safety. In order to set the scene, this thesis will begin by understanding how a single LiDAR sensor works in a laboratory environment and then investigate Multiple LiDAR systems by looking at a single object using triangulation method focusing on optimal LiDAR sensors placement to reduce blind spots.

A Fianium laser will be used in the laboratory using triangulation under different scenarios, starting with conventional LiDAR and looking into different scenarios of LiDAR combined with other sensors. The emphasis in this work started with optics improvements through experiments combined with data analysis and laboratory measurements. After the optimal lab setup was reached, the second part of the experiment was performed in a real-life environment using solid-state LiDAR sensors combined with cameras pointing at single and multiple objects.

The project compares the results of theoretical LiDAR sensors versus field experiment solid-state M16 Leddartech sensors combined with cameras for testing and validation in a real-life controlled environment.

1.3 Structure of the Thesis

The key areas in this research are LiDAR theory and types, pedestrian safety, connected autonomous vehicles, ADAS, triangulation, physics and engineering lab experiments. This study will interconnect all these areas in order to improve pedestrian safety.

This research will investigate LiDAR systems in different scenarios, addressing the overall research question of this thesis. First, the aims & objectives of this thesis are set in order to identify research gaps and challenges that need overcoming. The methodology used throughout the studies is described (Chapter 1).

(Chapter 2) will cover the Literature review including pedestrian safety, blind spot, CAV and sensors used in CAV including LiDAR, Radar, and Cameras.

(Chapter 3) covers LiDAR overview including several types and the state-of-the-art.

(Chapter 4) reviews LiDAR theory and the principles of Time of Flight, Triangulation, Trilateration and Ellipse.

Different experimentations of LiDAR scenarios will take place in the physics lab with complexity added in order to identify an improved setup will be covered in (Chapter 5).

The results will be then analysed and discussed. Following this, field experiments will be performed using two solid-state LiDAR sensors combined with cameras using triangulation to detect objects in (Chapter 6).

The results will be analysed and discussed in detail. The project will include testing and validation of data collected from lab experiments and field experiments. From the results of the

previous chapters, conclusions will be drawn, and recommendations will be made for future work (Chapter 7) of Multistatic compared to single LiDAR systems for reducing blind spots.

1.4 Methodology

This section presents an overview of the methodology to be followed in this project. This will cover the plan and experiments showing what Multistatic LiDAR is capable of.

This work starts by an overview of LiDAR sensor types, ranges and state-of-the-art design. Then it looks into the theory of LiDAR and triangulation method and defines the concept of Multistatic LiDAR sensors. Phase I in the University of Southampton, UK, Physics Laboratory will utilise a Fianium laser used with triangulation under different scenarios. This will commence with conventional LiDAR and investigating different scenarios of LiDAR combined with other sensors. The emphasis of this work was to investigate optics improvements through experiments combined with data analysis and lab measurements.

Once optimal lab setup was reached, a Phase II experiment was performed in a real-life environment using solid-state LiDAR (SSL) sensors combined with cameras pointing at single and multiple objects, static and moving. The use of triangulation method helps focus on optimal LiDAR sensors placement to reduce blind spots.

The project then compares the results of theoretical LiDAR sensors and the field experiment using solid-state Leddar M16 sensors combined with cameras.

The aim of this research is to explore whether Multistatic LiDAR system combined with cameras can enhance the safety of pedestrians. By improving the performance LiDAR sensors, fully autonomous vehicles will improve and become more reliable. This can be achieved by investigating Multistatic LiDAR systems, both in theory and in practice. The theory Multistatic LiDAR investigation was performed in the laboratory environment on an optics bench with a laser and two detectors pointing at one object using triangulation. The real-world experiment will include two SSL sensors, Leddar M16 sensors combined with cameras mounted on the front of a medium size vehicle on both sides pointing at one object using triangulation in an indoor environment with minimum objects in the room to avoid background noise. This stage will also include static object representing a pedestrian. Following the real-world experiment, the project will include testing and validation of data collected from lab experiments and practical experiments representing the real world in order to draw conclusion about Multistatic LiDAR systems.

A proposed future study, adding complexity to the work achieved here, may have multiple static objects as well as moving single objects and moving multiple objects using triangulation 2 LiDAR sensors with possible additional LiDAR sensor (a total of 3 LiDAR sensors) mounted in the middle in front of the car and on both sides in the front of the vehicle.

The project also considered off-the-shelf SSL combined with a camera to test for one static object. Results were analysed, and recommendations were drawn on how to improve the performance and other requirements of the different LiDAR experiments in the lab environment. The project investigates the state-of-the-art of automotive LiDAR sensors. The project will also explore the several types of LiDAR sensors from a literature review of both academia and industry. The theoretical experiments include:

- 1) Laboratory experiments for conventional LiDAR using a diverging lens.
- 2) Introduction of Multistatic LiDAR and laboratory experiments and introducing triangulation

3) Improving the lab setup using triangulation pointing at a static single object.

Experimental setup Phase II includes running experiments of Solid State LiDAR sensors in a real-world environment. The experiment was run in Bolderwood Innovation Centre B176 at the University of Southampton, UK.

The tasks performed in the real-life experiments consist of mounting 2 Lidar sensors and cameras on both sides of the front of a medium size vehicle pointing at a pedestrian using triangulation in order to explore the potential performance improvement of Multistatic LiDAR combined solutions. The idea is to investigate ways to improve the performance of Multistatic compact SSL systems to potentially form the basis of a pedestrian warning system for the autonomous vehicles.

The experiment took place in a closed environment with minimum objects in the room. The tasks include:

- Testing Leddar M16 combined with a camera on optic bench in a laboratory to understand how it works and programming Leddar M16 sensors using a Python programme.
- 2) Mounting 2 Leddar M16 sensors combined with cameras mounted on a tripod in a larger room representing real world situation looking at a static person representing a pedestrian. Collected data using this setup at 63 positions of the pedestrian at a distance difference of 50 cm. The room size is 4 m × 5.5 m.
- 3) Mounting 2 Leddar M16 sensors combined with cameras mounted on a tripod in a larger room representing real world situation looking at multiple objects.
- 4) Analysing results of Phase II and comparing results with Phase I experiment and drawing conclusions and recommendations for future work.

Chapter 2 Literature Review

2.1 Introduction

The world has become increasingly urbanised, with over 55% of the population living in cities and urban areas. This shift is set to increase to increase to more than double by 2050, at which point around 7 in 10 people will live in cities or urban areas equating to 70% of the world's population (The World Bank Group 2024).

This rapid pace and scale of urbanization brings significant challenges, including the increased usage of motor vehicles and thus an increase in congestion and traffic accidents. Despite the advancement and maturity of technologies, the number of fatalities caused by car accidents remains remarkably high.

According to the World Health Organisation (WHO), approximately 1.19 million people die each year as a result of road traffic crashes and more than 50% of traffic deaths including non-motorised road users: pedestrians, cyclists, and motorcyclists (WHO site 2023).

A fully autonomous car allows passengers to travel without a steering wheel, pedals, or the need to monitor the vehicle. Its key societal benefits stem from eliminating human error in driving, with an expected 90% reduction in fatalities. Additional advantages include fewer traffic jams, lower fuel emissions, and improved mobility for aging and disabled populations.

This shift will also drive new ownership and business models, reshaping transportation. While autonomous cars will lead due to market demand, other unmanned vehicles—on land, in the air, and at sea—will progressively follow, from trains to vessels.

However, achieving full autonomy requires highly reliable sensor suites capable of continuously monitoring the vehicle's environment. These systems must integrate diverse technologies with different working principles and failure modes to handle all possible scenarios. A combination of radar, video cameras, and LiDAR—enhanced by deep learning—will likely serve most use cases, with LiDAR at the core.

The push for autonomous vehicles has significantly altered LiDAR requirements compared to traditional remote sensing. Automotive LiDAR systems must deliver long-range detection, high spatial resolution, real-time processing, and resistance to solar interference—pushing the technology to its limits.

Various LiDAR configurations have emerged to meet these demands, including short- and long-range systems with narrow or wide fields of view. Early solutions used high-speed rotating wheels and stacked detectors to achieve necessary performance levels. However, large-scale automotive adoption requires additional refinements: sensors must be industrialized for mass production, designed for reliability, and compact enough to fit seamlessly into vehicles—all while maintaining affordability.

2.2 CAV AV & Pedestrian Safety

Transport and mobility play a critical role in our daily life. The choice of mode of transport makes a significant difference when it comes to pedestrian safety, as different modes of transport have different safety implications. Even when people are driving to work or taking the bus, they are

pedestrians at some point during the day. Pedestrians are people travelling by foot rather than using vehicles. Pedestrians become vulnerable road users, meaning that they are more at risk of injuries than drivers and passengers in vehicles.

In this research Connected Autonomous Vehicles (CAV) and Autonomous Vehicles (AV) mean the same thing as this work does not cover the connected side of vehicles, i.e. vehicle to vehicle, vehicle to infrastructure, etc. and only discusses the autonomous side. While connected vehicles are already in place, autonomous vehicles are still in development (Cprime, n.d.).

Government legislation should therefore focus on how connectivity can help avoid accidents in the development of CAV. VANET system (Vehicular Ad-Hoc Network) is a group of AV connected by a wireless network. The main purpose is to provide safety and comfort to drivers.

Although governments are working on reducing accidents with infrastructure improvements, they are not able to eliminate accidents caused by human factors.

The purpose of the safety system in an automotive is to protect other road users as well as the vehicle occupants. This can be achieved with the vehicle sensors such as radar, LiDAR and cameras collecting data from the surrounding environment of the vehicle.

As CAV eliminate the impact of human errors on the cause of traffic accidents, they are expected to dramatically reduce traffic accidents (Petrović, Mijailović, and Pešić 2020).

The paper concluded that not enough data was proven to make this assumption due to the fact that CAV are still in the testing phase, so the sample of traffic accidents is limited, and the technology is not mature yet. The human errors referred to in this paper include vehicle speed, driver's inattention, perceptual errors, wrong driving decisions and late detection are the main causes of traffic accidents (Rumar 1990).

2.2.1 Perception/Reaction Time and Stopping Distance

Understanding the stopping distance is important to design safer roads for pedestrians. Further, perception reaction time differs between different drivers depending on their age and their state of mind. This information is important in determining the LiDAR frame rate when designing for ADAS and autonomous vehicles to take into consideration the stopping distance and the average perception reaction times for drivers and the CAV. The frame rate is limited by the distance the LiDAR design will allow the car to move forward during the frame period (Paul F. McManamon 2019b).

Previous research proposed a Hybrid VANET based driver alert system integrating a pedestrian body unit in a VANET by sending signals giving an alert system to driver to give more reaction time (Dahlia Sam E. Evangelin Cyril RAJ Velanganny 2015)

The policy on Geometric Design of Highways and Streets at the American Association of State Highway & Transportation Officials (AASHTO) defines the formula of the stopping distance (AASHTO 2018). The perception reaction for an alert driver is 1 second, 1.5 seconds for an average driver and between 2 to 2.5 seconds for an elderly or tired driver. The reaction of Autonomous Vehicle is 0.1 second. While CAV are still in the testing phase, they are expected to eliminate human errors which are the main cause of traffic accidents using sensors to reduce P/R to 0.1 second vs 2-2.5 seconds P/R for an average driver.

The Stopping distance is measured as follow (Paul F. McManamon 2019)

$$Ds = (0.278 tv + v^2/(254 (f + G)))$$
(AASHTO)

Where:

Ds = stopping distance, measured in metres; t = perception-reaction time in seconds

v = speed of the car in km/h; G = grade or slope of the road, uphill or downhill.

f = friction coefficient between tyres and road, f ranges between 0.3 on wet road and 0.7 on dry road.

To better explain the stopping distance equation, let us make some assumptions:

G=0 for a flat road,

f= 0.7 for dry road

t= 2.5 seconds for human and t= 0.1 for CAV.

Therefore, for the speed of 20mph which is the average speed in urban areas, the human needs 28.2 m as a safe stopping distance when seeing an object or a pedestrian, while the CAV needs for the same speed 6.7m in order to safely stop.

As for the motorway speed of 70mph, the human driver requires a safe stopping distance of 150m while the CAV needs a safe stopping distance of 74.5m.

Those numbers are presented in table 2.1 below and in Figure 2.1. We also conclude that reliable sensors for CAV should be designed to see at a distance of 150m. While many state-of-the-art LiDAR sensors are designed to see beyond 150m for the sake of road safety 150m is enough to be designed for.

To put in context, the real-life experiment will be undertaken for CAV in an urban area (speed 20mph) where stopping distance is 6.7m. as the space available is 5m, we assume a speed of 17mph as highlighted in table 2.1 below. For that same distance of 5m space available, the human driver should be driving as a speed of 4.2mph.

The real-life experiment will be discussed in chapter 6. Section 2.2.1 presents a justification of the experiment and puts everything in context.

Table 2.1 calculation of speed and stopping distance for human driver and AV

| ٧ | | Human | |
|-----------|----------|-------------------|-------------------|
| (mph) | v (km/h) | (m) | AV (m) |
| 4.2 | 6.818043 | <mark>5.00</mark> | 0.450991 |
| 5 | 8.0467 | 5.956626 | 0.587868 |
| 10 | 16.0934 | 12.64159 | 1.904076 |
| 15 | 24.1401 | 20.0549 | 3.948622 |
| 17 | 27.44693 | 23.31259 | <mark>5.00</mark> |
| 20 | 32.1868 | 28.19654 | 6.721509 |
| 25 | 40.2335 | 37.06653 | 10.22273 |
| 30 | 48.2802 | 46.66485 | 14.4523 |
| 35 | 56.3269 | 56.99151 | 19.41021 |
| 40 | 64.3736 | 68.04652 | 25.09645 |
| 45 | 72.4203 | 79.82986 | 31.51103 |
| 50 | 80.467 | 92.34154 | 38.65396 |
| 55 | 88.5137 | 105.5816 | 46.52522 |
| 60 | 96.5604 | 119.5499 | 55.12482 |
| 65 | 104.6071 | 134.2466 | 64.45276 |
| 70 | 112.6538 | 149.6717 | 74.50905 |

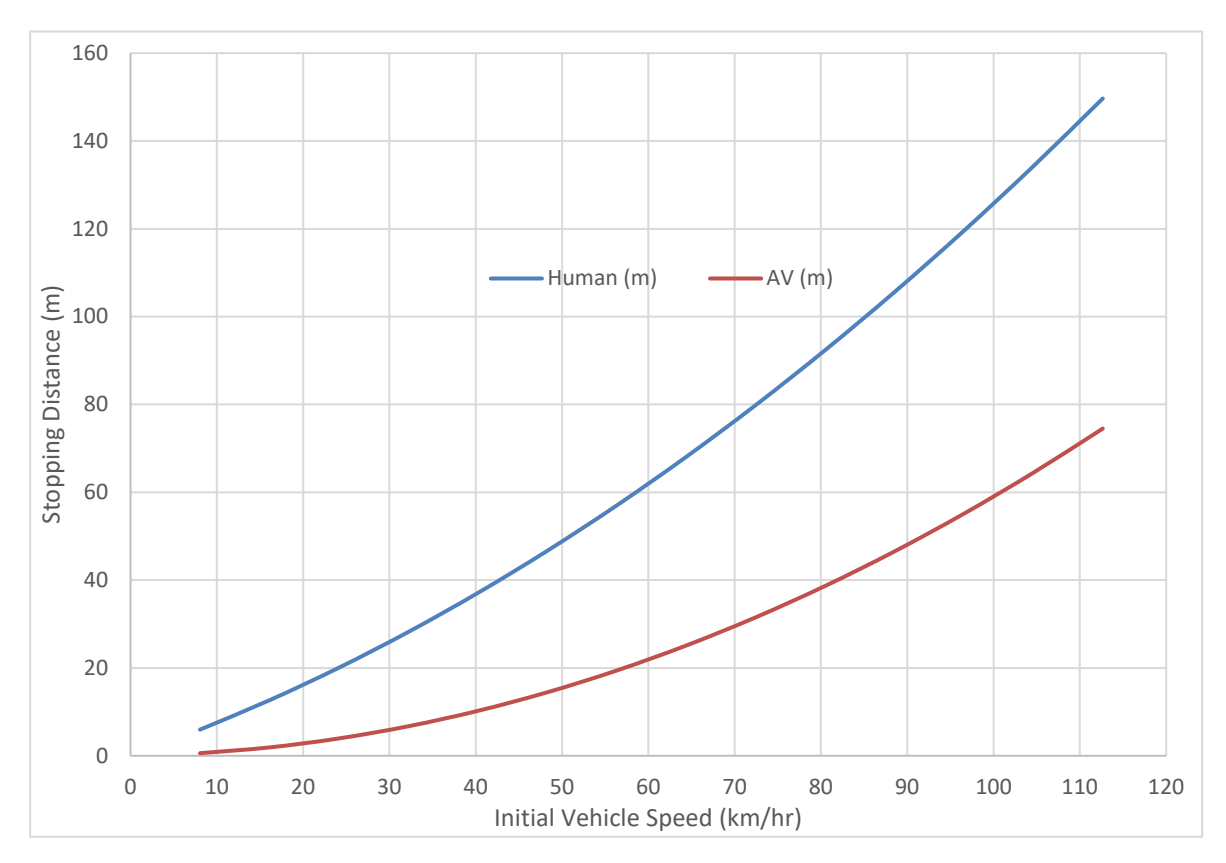


Figure 2.1 Presenting stopping distance and vehicle speed for human driver vs CAV.

2.2.2 Blind Spot

The main challenge faced in pedestrian safety is the potential conflict between the vehicles and the pedestrian and the blind spots. Blind spot is defined at the area not seen due to obstruction. Missing these obstructed areas can lead to traffic accidents. A safe system should be designed by reducing blind spots. As of today, CAV did not achieve the safety promised.

When a LiDAR is pointed at an object or pedestrian, the area hidden behind the pedestrian is the blind spot. Blind spots are better presented graphically. Based on Figures 2.2 and 2.3 we can see graphically that blind spots (black area seen) are larger for one LiDAR than for two LiDARS pointing at an object or a pedestrian. This will be proven experimentally in later chapters.

Figures 2.2 and 2.3 show 50cm width object at a 5m distance and 50m distance seen by one LiDAR and two LiDAR sensors.

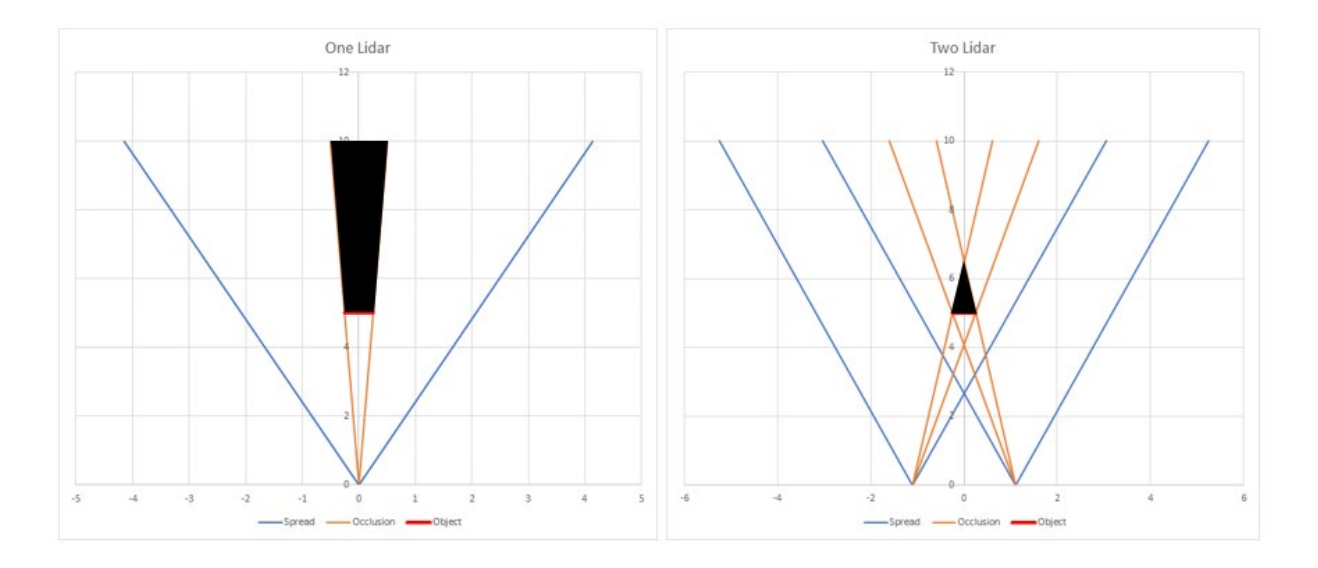


Figure 2.2 Blind Spot of Pedestrian seen by one LiDAR and two LiDARs at 5m distance.

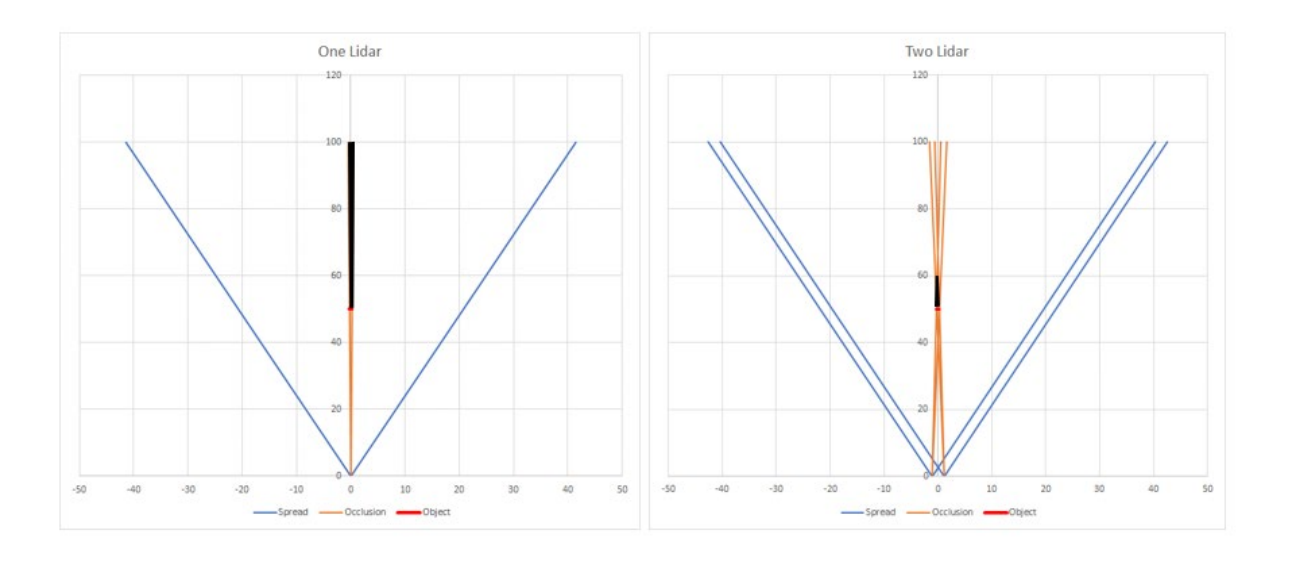


Figure 2.3 Blind Spot of Pedestrian seen by one LiDAR and two LiDARs at 50m distance.

2.3 CAV & ADAS

The lifetime of a typical car ranges between 10-12 years (Hearst Autos Research 2020)

ADAS should aim for a long-term solution rather than retrofitting for the short term. (Sensor fusion) consisting of merging different data flows and (sensor suite) consisting of sensors and transmitter connected to the sensors are important factors in ADAS in order to ensure fast response times for vehicles.

This furthers advancement in sensor technology – including sensor imaging, radar, LiDAR sensors, and artificial intelligence to enabled ADAS and autonomous vehicles. Sensor fusion enables obstacle detection, collision avoidance systems, blind spot monitoring and low visibility conditions among other safety features. In order to enable autonomous navigation, ADAS need reliable sensing of the environment surrounding the vehicle using image sensors (cameras), Radar and LiDAR. Other sensors include ultrasonic sensors. The combination of

those sensors can form sensor suite. They are installed inside and outside the vehicles to enable the autonomous perception algorithms in order to make decisions.

The global CAV industry is growing at a fast pace. Fully synchronizing the operation of sensors through fusion allows CAV to monitor their surroundings and warn drivers of potential road hazards and take independent actions of the driver to prevent collisions. In order to achieve full autonomy, artificial intelligence is required to process and integrate the data from the sensor suite of LiDAR sensors, cameras, radars and ultrasonic sensors.

CAV is being tested on streets, mapping surrounding areas in great detail, to allow the vehicle's computer control systems to draw on an extensive dataset based on the fixed environment. This supplement real-time observations of other vehicles, pedestrians, trees, traffic lights, and other moving features by its suite of onboard sensors. To ensure the successful adoption of CAV, safety is key. Millions of miles have been driven around the world with CAV to ensure they are safer than human drivers; some driven in dedicated roads, others by using simulations and high-fidelity virtual environments in labs.

2.4 CAV & Sensors Suite

Previous research investigated optimizing the LiDAR sensor's position to reduce black spots using a LiDAR occupancy grid system formulating the issue into an optimization problem. They used a genetic algorithm with commercial LiDAR sensors without adding more sensors which was proposed for future work (Kim and Park 2020)

Other previous work on multiple LiDAR testing using infrastructure-based LiDAR to detect and track pedestrians and vehicles at intersections (Zhao et al. 2023)

The LiDAR sensors used are Velodyne's Puck LiDAR sensor (previously VLP-16) ranging to 100 m compared to the Leddar M16 LiDAR sensor used in this project ranging to 165 m. Based on their work, they concluded that sixteen channel sensors were not enough and that 64 or 128 channels might give better results. This could improve the tracking accuracy and detection range. Their work could also be improved by adding cameras to LiDAR sensors as is the case in this thesis.

Other work on optimizing the roadside LiDAR configuration include (Ge et al. 2023)included an analytical simulation model to analyse and quantify the detection of blind spots and the impact on vehicle detection and tracking capabilities in CAV applications (Ge et al. 2023)

The size of blind spot is determined by the height and titled angles of the LiDAR sensors as proven by experimentation.

While this research focuses on LiDAR, it is important to understand that other sensors are also essential for the car to become autonomous. When a vehicle is in Autonomous Driving (AD) mode, it must be able to reliably identify objects. This can be done by combining a variety of sensors, while verifying that what the vehicle is detecting is accurate. The three sensors are the camera, radar and LiDAR. When working together, these sensors provide the vehicle information of its surroundings. This aids detection of the speed and distance of nearby objects, as well as their three-dimensional shape, while tracking the acceleration and location of the vehicle in relation to the objects (Burke 2019).

In addition to different technologies used in autonomous vehicles, sufficient overlap between technologies is important in order to improve safety. Such a technology is sensor fusion, which is the concept of using multiple sensor technologies to generate an accurate and reliable map of the environment around the vehicle (Motaz Khader 2020)

To detect objects over a short range using radar, ultrasound is typically used. Ultrasonic waves have limitations from strong attenuation in air at a distance. Alternatively, for LiDAR, cameras use colour and are easily available at a low cost; however, cameras require significant processing to extract useful information and depend strongly on ambient light conditions. Both LiDAR and radar have common and complementary features that can map surroundings and measure object velocity. Advanced sensor technologies can detect objects in their field of view (FoV). For example, ranging sensors provide higher accuracy and positioning of other road users such as pedestrians, cyclists, and other vehicles. Hence, advanced technology is essential for the development of CAV.

Figure 2.4 below presents the combined sensors used in CAV. This figure presents LiDAR sensors complemented with cameras, radar, and ultrasounds. Using perception algorithms can improve safety by providing more accurate estimation of the surroundings of CAV. LiDAR adds "eyes" to CAV by sending laser pulses outward, they map out their environments. CAV need to quickly develop an image of the world around them to avoid hitting any surrounding. Ultrasound sensors are used to detect objects over a short-range using radar. Cameras use colour, and are low-cost; however, cameras require significant processing to extract useful information and depend strongly on ambient light conditions. Ranging sensors provide higher accuracy and positioning of other road users. Both LiDAR and radar have common and complementary features that can map surroundings and measure object velocity.

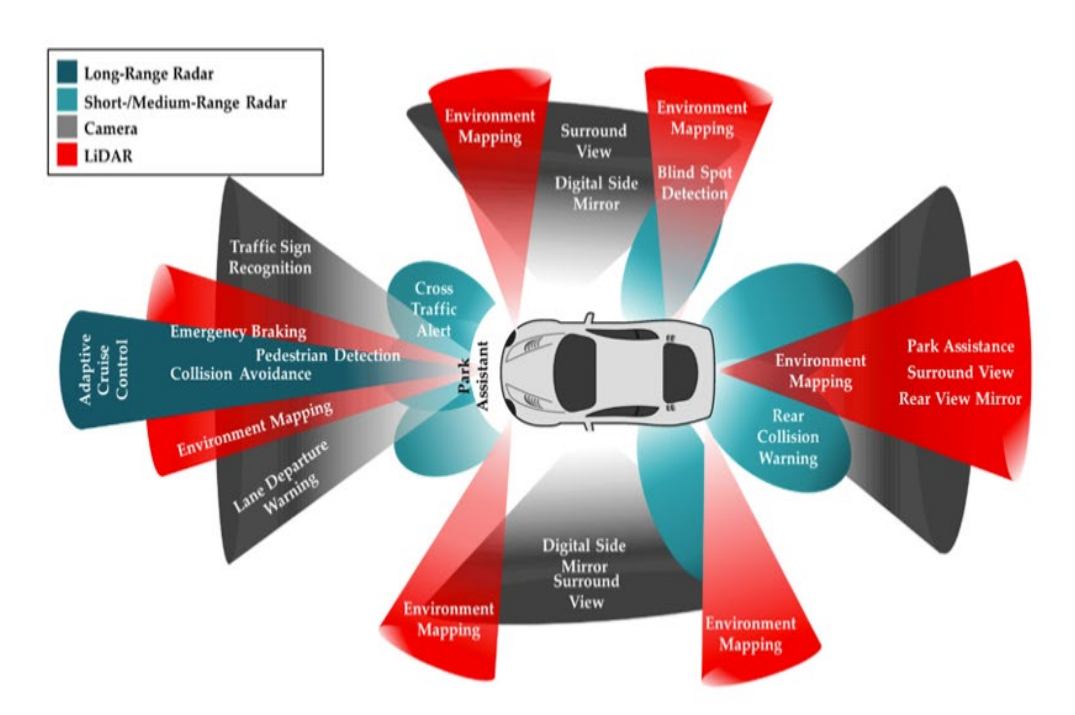


Figure 2.4 CAV & Sensors (Yeong. D.J. 2021)

Source: Yeong, D.J.; Velasco-Hernandez, G.; Barry, J.; Walsh, J. 2021. https://doi.org/10.3390/s21062140

2.4.1 Cameras

Cameras produce photos and videos; they are the most accurate way to create a visual representation of the environment surrounding autonomous vehicles. However, camera systems rely on devices placed on all sides of the car, providing a 360° view. While some cameras have a wide field of view of 120° with a shorter range, others focus on a narrower view to provide long-range images. Additionally, there are fish-eye cameras with super-wide lenses that provide a panoramic view, including the rear of the vehicle for autonomous parking.

Cameras can distinguish details of the surrounding environment, but the distances of those objects need to be exactly identified for CAV. Additionally, cameras are not able to detect objects in low-visibility conditions, like fog, rain, or night (Burke 2019)

2.4.2 Radar

Radar (Radio Detection and Ranging), a cheaper and older alternative to LiDAR, is traditionally used to detect ships, aircraft, and weather and it works by transmitting radio waves in pulses (Zhang et al. 2023).

Once waves reach an object, some of the incident rays are reflected and return to the sensor, providing information on the speed and location of the object by using the time taken for the signal to return (Gottinger et al., n.d.)

To achieve this, radar uses a transmitter and an antenna that emits radio waves. When this radiation is reflected and/or scattering by the object, the antenna receives it.

Radar transmitter works in conjunction with waveguides and amplifiers in order to produce strong radio wave signals. The waves are then transmitted by the antenna and receiver, thus converting the identification of an object into a video that is viewed by the operator (Bole, Wall, and Norris 2014)

Nevertheless, Radar can operate in a wider range of environments than LiDAR. LiDAR is limited in night-time, rain, and fog (Zhang et al. 2023)

Radar is not sensitive to environmental changes as it uses radio waves which are not affected by external debris. Radar also has a longer operating distance than LiDAR (Bole, Wall, and Norris 2014).

Like the vehicle's cameras, Radar sensors surround the car to detect objects at every angle. They are able to determine speed and distance. However, they cannot distinguish between several types of vehicles.

2.4.3 Ultrasonic Sensors

Ultrasonic sensors measure the distance and the presence of a target object by sending a sound pulse, above the range of human hearing (ultrasonic), toward the target and then measuring the time it takes the sound echo to return. (Ignatious, El-Sayed, and Khan 2023)

It is important to note that the attenuation of high-frequency ultrasound in air significantly limits its effective range. Attenuation is influenced by both frequency—where higher frequencies result in greater attenuation—and humidity levels in the air. Due to these factors, ultrasound ranging sensors typically have a measurement range limited to just a few meters. (Sonbul 2014)

Another key limitation of ultrasound is the propagation speed of sound waves in air, which is approximately 340 meters per second. Over a 10-meter distance, this results in a response latency of around 60 milliseconds—a substantial delay relative to the response time required for Connected and Autonomous Vehicles (CAVs). Consequently, ultrasound is unlikely to be effective for applications requiring measurements beyond a few meters in driver assistance systems.

The ultrasound sensors are beneficial for use in CAV. Ultrasound is used to sense nearby objects for parking but does not possess the required capabilities for driving. They measure the distance between to objects by sending and receiving ultrasonic pulses. Hence, ultrasound

relays information regarding an objects proximity. Ultrasonic sensors are not affected by colours unless object material absorbs sound, readings will be unreliable (Arrow.com 2018)

2.4.4 **LiDAR**

LiDAR was developed in the 1960s for military purposes and weather applications. However, during the 2000s LiDAR emerged an innovative technology for CAV applications, traffic management and urban environments, focusing on safety. LiDAR is similar to microwave radar, except that it uses a shorter wavelength. Instead of using sound or radio waves, LiDAR utilizes laser light pulses, hence mapping surroundings at the speed of light. LiDAR can map positions and distances more accurately than Radar. LiDAR uses a large amount of short laser pulses forming point clouds that can then be implemented into machine learning to provide more accurate results useful for autonomous vehicles. Due to LiDAR short light pulses, it can detect smaller objects than Radar can detect (Critchley 2019).

As LiDAR brings its own flashlight, it can see at night using Near-Infrared ((P.F. McManamon 2015)NIR) wavelengths. This means that LiDAR can have increased angular resolution associated with the shorter wavelengths operating day and night (Novitsky and Philbrick 2005). LiDAR is categorised as laser class 1, thus does not cause damaging radiation during operation for the eyes.

LiDAR utilizes laser light pulses, mapping their surroundings at the speed of light. LiDAR, compared with microwave Radar, uses shorter wavelength, higher resolution, near-infrared light (Bo Liu Yu Yang Jiang Shuo 2019).

To avoid eye damage, LiDAR systems are designed in such a way that their light source is classified as class 1. The laser works using high-voltage electricity that causes emission of an intense light beam exciting some of the atoms in a cylindrical ruby crystal to higher energy levels. At a certain energy level, some atoms emit photons. LiDAR, compared with microwave Radar, uses shorter wavelength, higher resolution, near-infrared light (Bo Liu Yu Yang Jiang Shuo 2019).

LiDAR can map positions and distances more accurately than Radar since it uses a large amount of short laser pulses forming point clouds that can then be implemented into machine learning to provide more accurate results useful for autonomous vehicles. "LiDAR can also detect smaller objects than Radar can because of the short light pulses (Critchley 2019).

Notably, LiDAR has increased angular resolution associated with the shorter wavelengths meaning it can operate in both the day and night (P.F. McManamon 2015).

LiDAR is a remote sensing mechanism used for CAV to detect their surroundings. Table 2.2 below compares the different sensors systems used in ADAS and autonomous vehicles. For LiDAR to become an integral part of CAV and ADAS, the main requirements for LiDAR sensors are to be low-cost and highly reliable, whilst meeting the performance specifications of ranging and detection of low-reflectivity objects (Dai et al. 2022).

Long range LiDAR are placed on top or at the front of the vehicles and refers to forward-facing devices. Short range applies to side-looking and rear-view installations and are placed on the sides of the vehicle. It is not possible to get a 360° field of view (FOV) from one single system and it is required to install several LiDAR sensors on the vehicle in order to have a full view, including blind spots (Thakur 2016).

Table 2.2 Comparison of Radar, Camera, Sonar and LiDAR Technologies

| Sensor | Advantages | Disadvantages | Applications |
|------------------------------------------------------------------|----------------------------------------------------------------------------------------------------------------------------------------------------------------------------------------------------------------------------------------------------------------------------|--------------------------------------------------------------------------------------------------------------------------------------------------------------------------------------------------------------------------------------------------------------------------------------------------------------------------------------------------------------------------------------------------------------------------------------------------------------|-----------------------------------------------------------------------------------------------------------------|
| Camera (Imaging sensors) | High angular resolution High Colour recognition Easily available Low cost Reliable in traffic signs Reliable in object edge precision High lane detection | Limited depth resolution/perception Limited in measuring object velocity Limited depth range Limited dynamic ranges with shadows Works poorly at night. Affected by rain/fog. Significant processing needed to extract useful information. | Lane departure warning Forward collision warning Traffic signs recognition |
| Radar short/ medium Range (24GHz) (1-60m typical range) | High depth resolution High horizonal FoV Low cost and compact size due to increased integration (in this context of CAV) High depth range High immunity to weather conditions: rain, fog, snow Measure object velocity | limited to resolve small features, as distances increase. Low vertical field of view Complex processing Difficult to filter clutter at low speed. Limited in object edge precision Limited in lane detection Limited in colour recognition | Blind spot detection Forward collision warning |
| LiDAR Flash (typical range 50m) | High angular resolution High horizonal FoV for solid-state LiDAR and widest FoV of 360 degrees rotation for mechanical LiDAR High depth resolution High depth range High object edge precision High low-light performance, Improve perception. Improve navigation systems. | Low immunity to weather conditions, with low performance due to scattering. Performing better using IR 1,550nm wavelength. Limited in measuring object velocity Limited in detecting objects at close distances. Limited in lane detection Limited in colour recognition Excessive cost compared to other sensors. Bulky size of mechanical scanning LiDAR, however size shrinking especially with industry shift to solid-state LiDAR More energy efficient | Blind spot detection Forward collision warning |
| LiDAR Scanning (range 200m) | More traditional Covers more areas as it turns 360 degrees. Improve perception. Improve navigation systems. | Takes more time due to rotation. Collects lots of unnecessary data that could confuse the data processing. More expensive High energy consumption | Mapping environment |
| SONAR/ ultrasonic sensors | -Sound Navigation and RangingHigh performance for nearby objectsUltrasonic sensors work by emitting high-frequency sound waves and analysing the reflections. | Poor performance in regard to far away objects because of low velocity of sound, long delay of signal to come back and attenuation of sound in the air. | -Ultrasound sensors are used to detect objects over a short-range using SonarPark assists -collision avoidance. |

Chapter 3 LiDAR Overview

3.1 Monostatic, Bistatic, Multistatic LiDAR

LiDAR is a technique useful for CAV since it can map positions and distances more accurately than Radar. LiDAR brings its own flash and can see at night. LiDAR can also detect smaller objects than Radar can be due to its short light pulses. An introduction to LiDAR and its features was given in Section 2.4.4. The following chapter will discuss those features in more detail. There will be a review of three types of LiDAR: Monostatic, Bistatic and Multistatic. Additionally, this chapter will review numerous measurement principles and their relevance to CAV.

A monostatic LiDAR system (or conventional LiDAR) comprises of a transmitter and receiver that are in same location. Alternatively, a bistatic LiDAR system comprises of a transmitter and receiver that are separated by a distance. The term "Multistatic LiDAR system" refers to a combination of the conventional monostatic LiDAR with additional receivers whose outward optical axes point in different directions and are not co-aligned with the direction of the transmitted laser beam (Mishchenko et al. 2016)

Multistatic LiDAR systems (Jin Hyen Park 2008) contain a combination of spatially diverse monostatic or Bistatic LiDAR components with a shared area of coverage. Limited research was conducted on Multistatic Radar and Multistatic LiDAR in the application of CAV. Some work included (Fölster, Rohling, and Member 2005) and (Doughty, Woodbridge, and Baker 2007) and (Emery and Camps 2017).

Previous research on Multistatic Radar concluded it can improve image resolution compared to Monostatic Radar; this can be applicable to Multistatic LiDAR.

Radar and LiDAR are similar in technique (see Section 2.4.4). Radar emits radio waves while LiDAR uses lasers with lower wavelength and higher accuracy, allowing detection of smaller objects. Deep Learning combined with Multistatic Radar showed satisfactory results in improving image resolution (Caramazza et al. 2018).

Deep learning has become an indispensable technique in the design and implementation of CAV (see Section 2.3). Further, an experiment combining a Multistatic LiDAR with a diffuser will have divided the energy along multiple scattering directions. In such a situation, there is limited influence of background illumination due to using high energy laser pulses. Therefore, by using a diverging source instead of a single beam, the object can be seen at any point in space, rather than directly in front of the beam. According to (O'Hagan, Doughty, and Inggs 2017), the project uses an adapted time of flight LiDAR system which is analogous to Multistatic Radar.

There are several advantages offered from the spatial diversity of Multistatic over conventional monostatic and bistatic radar due to the use of a diverging beam. This beam enables observation of objects by using multiple transmitter-receiver pairs. This allows an observer to view multiple aspects of the object, thereby increasing the image resolution and allowing more potentially useful information.

3.2 LiDAR Rangefinder Principles

There are two principles used to operate based on the type of signal modulation of the laser beam. direct pulsed Time of Flight (ToF) and indirect. The indirect ToF falls into

two types: continuous wave frequency modulated approach (FMCW), and continuous wave amplitude modulated approach (AMCW)

ToF LiDAR (incoherent) transmitter emits a pulse, hits an object and returns, the receiver receives the return wave and calculates the difference in reception t between the two and multiplies it by the speed of light to achieve distance measurement between objects. Direct ToF LiDAR has two types of beam steering, **Mechanical LiDAR** and **solid-state LiDAR**, which is spinning scanning and solid-state scanning as well as **Flash LiDAR**. LiDAR imaging principles, Mechanical and Solid State are summarised in Table 3.1 below.

Table 3.1 Summary of LiDAR Imaging Principles

| | Mechanical | MEM | ОРА | Flash LiDAR | AMCW | FMCW |
|------------|------------|-------------|------------|---------------|----------------|-----------------|
| | Scanners | Scanners | | (Solid State) | (indirect ToF) | (indirect ToF) |
| | | | | (Direct ToF) | (incoherent) | (coherent) |
| | | | | (incoherent) | | |
| Principle | Galvos, | MEMs | Phased | -Pulsed flood | Pixelated | |
| | rotating | micromirror | arrays of | illumination. | Phase meters | |
| | mirrors | | antennas | -short in | | |
| | | | | duration | | |
| Advantages | 360 degree | Low-cost, | Full solid | Fast frame | Commercial | -enables |
| | FOV in | compact, | state | rate | | improvements in |
| | horizontal | lightweight | | | | resolution of |
| | | | | | | range |
| | | | | | | measurements. |
| | | | | | | -operates with |
| | | | | | | minimal optical |
| | | | | | | power |
| | | | | | | -high dynamic |

range allows

FMCW to perform

more reliably in

the rain.

| | management, linearity | for ling range | Blind spots | only | |
|-------------|--------------------------|----------------|----------------|------|--|
| elements, l | linearity | range | | | |
| | | Tarigo | unless several | | |
| Bulky, | | | are used | | |
| redundant | | | | | |
| data | | | | | |
| collected | | | | | |

FMCW LiDAR transmitting a continuous beam with a frequency that varies steadily over time. Since the frequency of the source beam is constantly changing, differences in beam transmission distance result in differences in frequency.

AMCW LiDAR is like ToF system, it emits a signal that measures the time of the laser reflection back. However, ToF emit only one pulse, and AMCW LiDAR modulates by varying the polar current in the laser diode to adjust the intensity of the emitted light.

FLASH LiDAR does not scan but directly emits a large area of laser light to cover the detection area for a short time, an array of laser beams that are emitted simultaneously over a wide area to provide a 3D view of the surrounding environment, it can capture an entire scene in a single flash.

LiDAR rangefinder is the measure of the distance to the target or object using a laser beam. There are two principles used to operate based on the type of signal modulation of the laser beam. These principles fall into two types: direct pulsed ToF and indirect ToF. The indirect ToF falls into two types: continuous wave frequency modulated approach (FMCW), and continuous wave amplitude modulated approach (AMCW) (Royo and Ballesta-Garcia 2019). Table 3.2 below illustrates the difference between the different LiDAR experiments conducted in this research work including their advantages and disadvantages and difference in the cost.

Table 3.2 Comparison of LiDAR Experiments performed in this research work.

| | Fianium Laser | Multiple Solid State LeddarTech | Mechanical Scanning LiDAR |
|-----------|-----------------------------------------------------------|---------------------------------------------------------------------------------------------------------------------|---------------------------------------------------------------------------------------------------------------------------------|
| Principle | Direct ToF Lab based. Flash, 2 detectors, pointing at | Direct ToF 16 channel detectors Only looks at common coverage area if 2 Leddar are used. With different time base | Direct ToF provides a high SNR over a wide FoV, they have long range and good reliability, however, are more expensive than SSL |

| | common with | and can provide 360° maps, if | with increased |
|------------|--------------------|--------------------------------|---------------------------|
| | same time base. | properly combined with other | maintenance costs and |
| | | sensors. | the reduction of the |
| | | Solid State LiDARs have | overall lifespan of the |
| | | multiple implementation | system. MSL have |
| | | methods including MEMS, | limited speed of rotation |
| | | OPA and Flash LiDAR. | < 100 Hz, affecting the |
| | | Flash SSL uses a beam that is | accuracy of detecting |
| | | diffused through emission | nearby vehicles and |
| | | options to diverge the beam | differentiating vehicle |
| | | over the entire FoV and | types at high speeds. |
| | | doesn't have the physical | They also have |
| | | limitation of MSL, they can | limitations in detecting |
| | | achieve higher measurement | dark and non-reflective |
| | | rates for better profiling and | objects and are prone to |
| | | high-speed vehicle detection. | performance |
| | | The LeddarM16 used in this | deterioration in bad |
| | | project is SSL with high- | weather conditions due |
| | | precision detection | to their dependency on |
| | | capabilities. It can locate | highly collimated lasers. |
| | | obstacles such as fixed | |
| | | structures, vehicles, | |
| | | pedestrians, and cyclists | |
| | | uses laser flash illumination | |
| | | with various FoV options and | |
| | | measurement rates of up to | |
| | | 100Hz. | |
| | | | |
| Advantages | 168ps with 5cm | Resolution of 50cm looking | |
| | resolution | at up to 500cm. larger shared | |
| | experiment | coverage area. | |
| | looking at up to | | |
| | 120cm. more | | |
| | difficult to align | | |
| | <u> </u> | | |

| | for longer | | |
|---------------|-------------------|------------------------------|----------------------|
| | distance. | | |
| Disadvantages | Costly, difficult | Limited range, Blind spots | |
| | to align for | unless several are used. | |
| | longer distance. | | |
| | Shared coverage | | |
| | area was small | | |
| | | | |
| | | | |
| Cost | £20,000 data | £1,000 per unit with 2 units | £20,000 for rotating |
| | collected by the | used commercial off-the- | |
| | computer, | shelve application | |
| | 2 detectors at | | |
| | £4,000 each | | |
| | £60,000 for | | |
| | Fianium laser. | | |
| | This is a | | |
| | Research setup | | |
| | not matched for | | |
| | integration | | |

The first principle is the direct-detection laser rangefinder type also known as pulsed lasers using their time of flight (ToF), this is incoherent-detection laser rangefinders. The second principle is the indirectly measured distance and velocity of the object from the Doppler effect, this is known as the frequently modulated continuous wave (FMCW). These are coherent-detection laser rangefinders (Li and Ibanez-Guzman 2020).

In the first principle, LiDAR imaging uses Time of Flight (ToF) where the optical signal is projected to the target and the reflected (detected) signal is processed to determine the distance between the transmitter and the object using the speed of light (Royo and Ballesta-Garcia 2019)

This distance is measured based on the round-trip delay of light waves that travel to the target object, and the intensity may be modulated or phased. To measure the intensity, certain measurement principles must be adhered to.

The direct ToF imaging system is incoherent LiDAR, meaning the photons are not in phase with one another and have different frequency and wavelengths. Hence, both pulsed and AMCW LiDAR are incoherent. Alternatively, coherent light will have photons sharing the same frequency and wavelengths that are in phase with one another, meaning coherent LiDAR utilises an indirect ToF that is FMCW. In addition to coherence, the direct ToF LiDAR has two types of beam steering that describes as a technique for changing the relative phases of radio

frequencies signals in the case of Radars. In the case of LiDAR, beam steering is described as mechanical LiDAR and solid-state LiDAR, which is spinning scanning and solid-state scanning as well as Flash LiDAR (Royo and Ballesta-Garcia 2019). Each of those approaches have different capabilities and applications that will be discussed in this chapter.

3.2.1 Direct Time of Flight

The pulsed direct ToF approach directly measures the round-trip time between the light pulse emitted by the laser to the target and the return. It is incoherent, short in duration and is measured in nanoseconds (ns). The pulsed direct TOF adopts the indirect detection of intensity, which is stable, robust and produces resolution in centimetres (cm). The measurements have minimal influence of ambient light due to the high energy laser pulses. Nevertheless, at long ranges, the Signal-to-Noise Ratio (SNR) is low and the ToF approach surpasses the emission limit fixed by eye-safety levels. Hence, the pulsed direct ToF is unsuitable over longer ranges (Lopac et al. 2022).

The detectors used for the direct ToF approach are sensitive to light and need to be enclosed in dark cases to avoid nuisances which leads to an increase in the cost of the system (Zhang et al. 2023).

Nevertheless, the pulsed ToF LiDAR is the most commonly used for autonomous vehicles due to its simple operation and its ability to perform well both indoors and outdoors (Royo and Ballesta-Garcia 2019).

The pulsed direct ToF LiDAR can detect movement by comparing successive scans. The ToF LiDAR uses a wavelength in (NIR) of 805 nm, 905 nm and 940 nm and they are all safe for the human eyes with typical depth resolution of 1 cm (Armenta 2021).

3.2.2 Indirect Time of Flight

Indirect ToF include both AMCW and FMCW measurement principles as discussed below.

3.2.2.1 Frequency-modulated continuous-wave (FMCW)

The FMCW is an indirect and coherent ToF LiDAR. The FMCW approach presents many advantages in the use of autonomous vehicles, as its coherent detection scheme enables improvements in resolution of range measurements between one and two orders of magnitude when compared to the other methods (Royo and Ballesta-Garcia 2019).

FMCW techniques operate with minimal optical power and the high dynamic range allows FMCW to perform more reliably in the rain compared to other LiDAR types (Crouch 2019).

The coherent LiDAR is used to develop solid-state LiDAR systems. It can measure velocity directly and at high precision for moving objects and it is unaffected by ambient light (Piggott 2022)

Coherent LiDAR is a 3D imaging technology proving more advantages than traditional LiDAR systems. The coherent LiDAR operates by sensing Doppler shift of light and can achieve high depth accuracies. Many coherent LiDAR are monostatic and thus sharing the transition and receiving paths.

The FMCW LiDAR used for autonomous vehicles has a single continuous wave beam that is split into two parts and modulated. One part of the beam is focused onto a target whilst the other serves as a reference signal. Compared to direct ToF, the FMCW approach relatively new

the use of autonomous vehicles. As it is possible to integrate FMCW on a single chip in the use of autonomous vehicles, this makes this approach attractive eventually. FMCW is used both indoors and outdoors with typical depth of resolution of 0.1cm.

3.2.2.2 Amplitude Modulated Continuous Wave (AMCW)

The AMCW is a compromise between FMCW and dToF. AMCW operates as a ToF system, emitting a signal and measuring the time it takes for that signal to return. However, this method sends more complex pattern making AMCW more resistant to interference than a dToF system which only emits a single pulse. Additionally, AMCW methods are well-developed and efficient for indoor environments with stable electronics architectures working in parallel in every pixel and are established commercially.

3.2.3 LiDAR Imaging

LiDAR imaging principles are based on a 3D imaging with a 360° view to achieve its full capacity. This can be achieved via two different methods: scanning or Flash LiDAR.

Scanning LiDAR uses collimated narrow laser beam to scan a point or line of light pulses across the field of view. The angular resolution of the system is determined through the angular width and the scan rate. The return light is collected by an imaging optic that has a single point detector for a 2D scan and a linear array of detectors for a line scan. The scanning techniques include mechanical varieties and solid-state scanning which includes optical phased arrays.

The second imaging principle is flash LiDAR, where the laser illuminates the full field of view using diverging beam and does not need narrow beam, where the detector is able to determine the angular resolution of the system. Flash LiDAR is both simple, cheap and still meets the eye safety requirements. The eye is much more resistant to radiation at wavelengths longer than 1400 nm. Many scanning systems are being designed at 1550 nm wavelength. Flash systems have different eye safety strategies since the laser is not a narrow beam (Warren 2019)

3.2.3.1 Scanning LiDAR

Scanning systems use a beam steering component to cover all the angular positions of the field of view by modifying the angular direction of the incident beam (Thakur 2016).

Many commercial systems for autonomous vehicles rely on scanning LiDAR. The limitations of this technology include the precision, field of view covered, the speed and the spatial resolution of the images. Laser scanning system performance requires an understanding of the interaction of the work and the wavelength, radiation duration, and power of the laser, as well as damage to the optical elements of the scanning system. For the use of autonomous vehicles, scanning is divided into mechanical scanning, MEMS and OPA, each method will be described below. Alternative working principles such as liquid crystals waveguides are possible however they are beyond this study and will not be covered.

3.2.3.2 Mechanical Scanning

Mechanical scanning LiDAR is a rotating system including rotating mirrors and galvanometric positioning of mirrors to achieve scanning by creating a full 360° horizontal field of view (FoV), however the vertical range is limited. The mechanical aspect provides a high SNR over a wide FoV resulting in a large implementation (Motaz Khader 2020).

Currently, a mechanical spinning scanner on top of the vehicle is the most common LiDAR being evaluated for autonomous vehicles. Mechanical LiDAR is expensive with its own limitations including blind spots around the vehicle (see section 2.4.4). The blind spot limitations are resolved by using additional LiDARs mounted on the vehicle sides and corners, increasing the cost of the system.

Mechanical scanning collects data over a wide area of up to a 360° FOV by using a rotating mirror to steer a light beam or rotating laser and receiver. Mechanical scanning LiDAR uses high-power, collimated laser beams that focus the reflected signal on the receiver through the use of highly focused optics (Paschotta 2020). A collimated beam is a light with rays that are parallel such that there is negligible spreading as it propagates. A perfectly collimated beam, with no divergence, will not disperse over distance.

Simple mechanical scanning LiDAR uses a single laser source that rotates to capture a single horizontal line of data points following each cycle. A complex mechanical LiDAR uses multiple emitter/receiver combinations (up to 128) that rotate mechanically to capture multiple horizontal lines of data points over 360° to provide a detailed map of the surroundings (see section 2.4.4). They provide a high SNR over a wide FOV, they have long range and good reliability, however, are more expensive than solid state LiDAR due to the increased maintenance costs and the reduction of the overall lifespan of the system. Other limitations of mechanical scanning LiDAR are the limited speed of rotation to 100 Hz or less, which affects the accuracy of detecting nearby vehicles and differentiating vehicle types at high speeds. They also have limitations in detecting dark and non-reflective objects and are prone to performance deterioration in adverse weather conditions due to their dependency on highly collimated lasers (John Dinan 2021).

3.2.4 Solid-state LiDAR

Solid-state LiDAR (SSL) sensors are increasingly being used in automotive LiDAR.

Solid-state LiDAR marks a major leap forward in LiDAR technology. Unlike traditional systems that depend on mechanical components like spinning mirrors or rotating assemblies, solid-state LiDAR uses only electronic or optical mechanisms to direct laser beams. Just as solid-state drives (SSDs) transformed data storage, solid-state LiDAR delivers faster performance, greater reliability, enhanced durability, and lower power consumption than traditional mechanical lidar systems.

The development of solid-state LiDAR has been largely propelled by advancements in the autonomous vehicle industry, which has invested heavily in this cutting-edge technology.

The SSL technology was developed to deliver greater reliability, more compact designs, lower manufacturing and maintenance costs, reduced power consumption, and enhanced durability in harsh conditions such as shock, vibration, and extreme weather, higher performance, and greater reliability than the rotating LiDAR units (Adam Frost 2018).

While most autonomous vehicles require 3D LiDAR systems, solid-state 2D LiDAR systems are capable of object identification and distance measurement (Adam Frost 2018).

A combination of SSL sensors grouped on a vehicle would still be less costly compared to a single rotating LiDAR and can provide 360° maps, if located such that all angles are covered such like a single rotating 360° LiDAR sensor. SSL is applicable to electronic tolling and traffic management, and is thus relevant to CAV. Also, SSL is being increasingly available. SSLs have multiple implementation methods including microelectromechanical systems (MEMS) systems integrating mechanical and electrical components on a silicon chip, optical phased array (OPA) LiDAR, leveraging arrays of integrated optical emitters and detectors on silicon chips and Flash LiDAR, which illuminates entire scene in one burst, and will be discussed in the subsequent sections.

3.2.4.1 Flash LiDAR

Flash LiDAR illuminates the entire field of view with a diverging laser beam with a single pulse (Teschler 2021).

Compared to the scanning LiDAR, a collimated laser beam is used to illuminate one point at a time. "LiDARs can use two different types of light emission: collimated beams and diffused beams." (John Dinan 2021).

Flash SSL uses a beam that is diffused through emitting laser pulses to diverge the beam over the entire FOV, whereas the mechanical scanning LiDAR uses collimated beams.

In flash LiDAR, the emitted light pulse is dispersed in all directions, significantly reducing the SNR, while in ToF cameras limits the measured ranges to a few meters (Royo and Ballesta-Garcia 2019).

Flash SSL solutions do not have the physical limitation of mechanical LiDAR, they are able to achieve higher measurement rates for better profiling and high-speed vehicle detection. In addition, flash SSL systems achieve better temperature range compared to mechanical LiDAR (John Dinan 2021).

The LeddarM16 used in this project is a solid-state flash LiDAR with high-precision detection capabilities. The LeddarM16 can locate obstacles such as fixed structures, vehicles, pedestrians, and cyclists uses laser flash illumination with various FOV options and measurement rates of up to 100Hz.

3.2.4.2 Micro-electromechanical System (MEMS)

Micro-electromechanical system (MEMS) scanning uses actuated micromirrors with electromagnetic actuators for scanning the field of view that are supported by expanding optics ("MEMS Sensors," n.d.).

The range of MEMS is medium to long, with good reliability at a low cost and compact size. The MEMS uses electromechanical scanning hardware as a substitute to the mechanical equivalent, described in section 3.3.3.2. The receiver light collection aperture that determines the SNR is in millimetres (mm). Multiple mirrors are needed in order to move the laser beam in multiple dimensions with the alignment process susceptible to shocks and vibrations encountered in moving vehicles (Motaz Khader 2020).

MEMS have many advantages including their compact size, light weight and low power consumption. This makes MEMS one of the preferred LiDAR solutions for autonomous vehicles and has a growing demand in the automotive sector as well as in robotics (S Holmström et al. 2014).

3.2.4.3 Optical Phased Arrays (OPA)

Optical phased arrays (OPA) operate by directing a beam from an array of optical antennas towards an object. The optical antenna purpose is to convert the energy of free propagating radiation to local energy. They operate similar to radiowave and microwave antennas (Hecht 2013).

It is an emerging type of solid-state technologies that operates in a similar fashion to microwave phased arrays, described later in section 3.3.4.2. The emitted fields from each antenna interfere

to steer far-field patterns. The OPA component can achieve a high turning speed with a stable phase with a wide field of view detecting targets at a long distance (Wu et al. 2022).

Optical beam steering by phase modulation was developed in 1990 with the phased arrays in radio explored over the past one hundred years.

In an OPA system, an optical phase modulator controls the velocity of light as it passes through the lens. This helps to eliminate the mechanical moving parts. OPA has recently gained interest as an alternative to traditional mechanical beam steering since it has a large steering range at high speed. While OPA is still under testing for long-range LiDAR, it has grown in interest in academia and the industry as a developing technology. However, OPA is operating commercially in short and mid-range purposes. OPA combined with FMCW could be useful in LiDAR systems since they could contribute to increasing reliability and reducing costs (Piatek 2017).

3.2.5 LiDAR Ranges

The types of LiDAR with the measurement process are TOF, direct ToF and indirect ToF (FMCW and RMCW or AMCW). The beam steering includes mechanical and solid state (scanned and solid beam). Photodetector receivers have several types.

3.2.6 LiDAR Wavelength

In recent years, LiDAR manufacturers have ranged from known automotive Tier-1s to start-ups across the globe. The majority of these companies operate their LiDAR at NIR wavelengths. SWIR wavelengths are mostly used in FMCW. For NIR wavelengths, the photons fired by the laser in a LiDAR system, intended to be reflected off objects and received by the detector, have to compete with ambient photons coming from the sun (Hadji 2021b). At 905 nm, the solar irradiance is around 3 times higher than at 1550 nm.

A pedestrian eye standing in the path of a LiDAR's emission path should not be damaged by a laser being fired in their direction (Li and Ibanez-Guzman 2020).

The International Standards on Safety for Laser product (IEC-60825) is a specification that dictates how much the maximum permissible exposure is across the different wavelengths of light (Hadji 2021) and (Yole Developpement 2018).

3.3 LiDAR State-of-the-Art

CAV is predicted to be worth £63 billion by 2035 according to the UK Department for Transport. Are we there yet? The rooftop versions sold by industry leader can cost as much as £60,000, while thanks to state-of-the-art Solid-State LiDAR cost per unit aims to be reduced to £600.

In this research study, the cost of Fianium is £40,000 while 1 unit of Solid state LiDAR is £1000, 2 are used, therefore the cost in this experiment for both units of Solid State LiDAR is £2,000.

As the technologies advance, the relationship between supply and demand applies and consumer costs are important in determining the balance between them. Many emerging technologies and technologies enabled business models could be promising solutions to existing transport systems aiming to reduce cost and make travel more user-friendly.

As LiDAR sensors become more affordable and the demand in cities is increasing, there are large investments in LiDAR and automotive sensors. These investments have resulted in a boom of the LiDAR technology platform. LiDAR technology has been commercialised for massmarket use with growth for the LiDAR market projected to £3Billion in 2025 with the automotive

segment expected to be the main driver for LiDAR technologies according to (Yole Developpement 2018).

SSL sensors are replacing the mechanical rotating expensive LiDAR sensor mounted on top of the vehicle. They are compact, powerful, and remarkably less costly. They are part of the sensor suite interfacing with the computerized navigation and control system of CAV along with other sensors. However, artificial intelligence software is needed to gather data from all sensors, process it and create a single robotic sensory system.

SSL is expected to work in short and long range, with narrow and wide FoV. It has to have high spatial resolution, high tolerance to the sunlight and are expected to work well in adverse weather. (Adam Frost 2018) They also are expected to have real-time performance. The prototypes also need to scale-up for mass production at a worthwhile cost and with compact sizes in order to fit on the vehicles as fixed or rotating. The Emerging Technology of LiDAR was described in a conference proceeding (Lemmetti et al. 2021). LiDAR sensors are still not offered as mass-production and the small SSL sensors are still not widely spread. Additionally, the available sensors in the market are designed for short and medium range (50-100m) applications. The long range scanning LiDAR sensors designed with optimal solutions (i.e. maximum efficiency with less power consumption and maximum eye safety are still not developed. Flash LiDAR sensors, if designed for long distance can provide less power density and fast data collection while maintaining eye safety.

3.4 No LiDAR Option

Currently all major AV manufactures including General Motors, Google Waymo, Amazon Zoox, Apple cars, Audi, BMW, Volvo and many others use LiDAR sensors in their AV operation. Tesla AV do not use LiDAR sensors and depend on cameras and computer software to detect their surrounding environment. Arguably, some of the fatal accidents of the Tesla auto-pilot car could have been avoided if Tesla cars were equipped with LiDAR sensors. Tesla's forward-looking camera and radar could not identify vehicles at 200 m away, while LiDAR would have located incoming vehicles in time for a suitably programmed car to apply the brakes (German Sharabock 2020).

While there is no available data on the number of AV on US roads, as of 2021, there have been over 80 companies testing approximately 1,400 AV and trucks and other vehicles in over 36 states.

A recent report by US-NHTSA on autonomous vehicles car crashes reported that 70% of car crashes linked with autonomous vehicles in the US were with Tesla (US-NHTSA 2022). Based on the data, 400 crashes were reported with 273 of these accidents involved in Tesla cars with 5 of these accidents being fatal. The 5 fatal accidents reported with Tesla vehicles involved form a small number compared to the reported yearly fatal accidents caused by human drivers (43,000 according to the US Insurance Institute for Highway Safety). However, all these fatal accidents were caused with Tesla AV involved, in addition to the 273 car accidents out of 400 in total.

In addition to Tesla, a recent research work by the US Southwest Research Institute (SwRI) developed Autonomous Driving based on cameras without using LiDAR and Radar sensors. The research work developed in March 2024 claims to potentially deliver accurate mapping capabilities for cameras. This work is applicable in military solutions and off-roads and not in urban areas and on-roads. The work is based on software solution identifying nearby objects using cameras as the only sensors (Crowe 2024) and (Paleja 2024).

While this research work may be successful in off-roads and in military applications, it is still at early stages, and it is too soon to conclude its success in replacing LIDAR sensors with

cameras. Additionally, this research work was not tested in urban areas so it is too early to conclude if it will be applicable and successful in urban areas and on motorways.

There have been other startups and research centres trying to design AD without including LiDAR sensors in their AD solutions based on the claim that LiDAR sensors are too expensive. However, no major work has been proven able to replace LiDAR sensors to date. Thus, LiDAR sensors remain essential in the design of AV complemented with other sensors.

Chapter 4 LiDAR Theory

4.1 Introduction

The type of LiDAR sensors deployed on CAV play an important role in the cost and safety of the CAV. Therefore, it is important to understand how to measure the key parameters of LiDAR sensors including the specifications, the range, resolution, frame rate and FoV and what is the relationship between those parameters in order for LiDAR sensors to perform well. This chapter sets the scene by understanding the principles and basics of LiDAR sensors. The equations in this chapter take mathematical approach in order to determine how LiDAR is measured and improved.

4.2 LiDAR Basics

Basic metrics of LiDAR include the wavelength, detection range, transmitted power, the FoV precision accuracy (in percentage), resolution (pixels per in ppi), pulse rate (Hz), scan rate (Hz) and Signal too Noise Ratio (dB). The pulsed light of LiDAR emitted and reaches an object with unknown distance. The incident light beam is then reflected by the object and measured by the detector. In this case, the LiDAR used a factor of two, as light is traveling to and from the object. The intensity of the reflected light may be plotted against time.

4.3 Time of Flight

The range of target object is measured by calculating the round-trip delay of light signals emitted by the laser to the object. The round-trip delay is known as Time of Flight (ToF). ToF can be obtained by modulating the frequency, phase, intensity (amongst others) of the transmitted light The time of the modulation pattern detected at the receiver is measured with using different metrics and imaging techniques to determine the ToF.

Equation 1 describes the principle of ToF how the distance of the object is measured. As the speed of light is constant, with the time of flight traveling twice from laser to object back to detector. Assuming the distance from laser to object and distance from object to detector are similar, then using equation 1, the distance of the object can be measured.

 $R = c \times \Delta t/2$ Equation 1

R = variable object distance (m)

c = speed of light (m/s) $\approx 3 \times 10^8$ m/s

 $\Delta t = time of flight (s)$

Figure 4.1 below demonstrates the concept of ToF measurement.

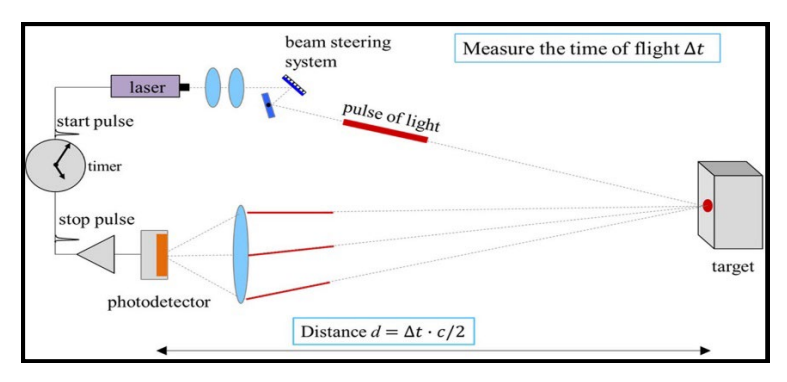


Figure 4.1 Describing the concept of ToF measurement.

(Warren 2019)

The LiDAR FoV is the angle in which the signals are emitted, both vertically and horizontally. For a full FoV, a 360 rotating can be used, alternatively combining the output of several sensors with a smaller FoV covering 360 can be used.

Equation 2 is also a basic one in showing the relationship between the frequency and wavelength.

 $f \times \lambda = c$ Equation 2

f = frequency (Hz or 1/s)

 λ = wavelength (m)

The energy, power and irradiance are calculated in Equations 3,4 and 5 below. These equations show how the wavelength affects the range and safety. The equations show the maximum permissible exposure (MPE) of Light to human eyes without causing damage. It is limited by eye safety regulations ("IEC60825-1 Safety of Laser Products," n.d.).

In practical applications, 905 nm and 1550 nm are the most common wavelength used for LiDAR in autonomous vehicles applications.

 $E = h \times f$ Equation 3

E = energy of photons (J)

h = Plank's constant

P = E/t Equation 4

P = power (W or J/s)

 $E_2 = P/A$ Equation 5

 E_2 = Irradiance (W/m²)

$$A = area (m^2)$$

The LiDAR range presents the maximum possible distance at which an object can be detected. The signal-to-noise ration SNR is a key parameter used to differ between the background noise and the object reflected signal, which helps determine the maximum LiDAR range. Therefore, the signal-to noise ratio is the measure of the strength of a signal versus the background noise. In the case of AV, the background noise sources in LiDAR detect any source of light such as the sunlight, car headlights, road lighting, etc. forming in some cases missed or false object detections (Leddartech 2022).

Equations 6 calculates the Signal to Noise Ratio. The SNR is directly proportional to receiver power, the detector's intrinsic gain and the detector's sensitivity. This is why the measurements are made in dark room since the room light can be detected by the LiDAR detectors. This is why the detectors in the Physics experiments presented in chapter 5 are enclosed in dark boxes to reduce the noise effect of the room light. In order to achieve higher range, higher power must be received, or waveform processing systems must be optimised, and front end signal acquisition must be achieved. (Piatek 2017).

$$SNR(R) = \frac{P(R)S_{\lambda}M}{\sqrt{2eB[(P(R)+P_B)S_{\lambda}+I_D]FM^2 + \frac{4kTB}{R_0}}}$$
(Piatek 2017) Equation 6

 S_{λ} = Detector's sensitivity B = Detection bandwidth

PB= Background light optical power M = Detector's intrinsic gain

T = temperature in degrees Celsius ID = Detector's dark current

e = elementary charge k = Boltzmann constant F = Detector's excess noise factor

Equation 7 presents the basic LiDAR equation. The equation shows that power received is directly proportional to power transmitted and aperture area of the receiver and is inversely proportional to the distance of the object. The power received plans an important role in calculating the LiDAR range as it plays an important role in determining the SNR. The LiDAR range is determined by the background noise and the signals of photons detected by the photodetector.

$$P(R) = P_0 \rho \frac{A_0}{\pi R^2} \eta_0 \exp(-2\gamma R)$$
 (Piatek 2017) **Equation 7**

P(R) = power received P_0 = Peak power transmitted

 ρ = target reflectivity A₀ = aperture area of the receiver

ηο = receiving optics transmission γ= atmospheric extinction coefficient

4.4 Principles of Triangulation, Trilateration & Ellipse

The working principle of "**Triangulation**" LiDAR ToF works on the basis of triangulation sensors measure the location of the object within the field of view (FoV) of the detecting object within

few inches with high accuracy requirements. ToF sensors derive range from the time it takes for the light to travel from the sensor to the object and return. The laser emits an infrared laser signal that will be reflected by the target object. The beam passes through the lens. By construction, triangles are built. The distance to the object is nonlinearly proportional to the angle of the reflected light. Using the triangles similarities concepts, the actual distance to the target object is measured.

The working principle of "**Trilateration/Multilateration**" LiDAR ToF works on the basis of using multiple sensors to locate one object or multiple objects. It is measuring the distance from three or multiple reference positions by using ToF technique and using three distances to compute the object position. The node will be found at the intersection of three circles centred at each reference point. This works in Multistatic LiDAR setup and is illustrated in Figure 4.2 below (Gentile 2019).

Therefore, triangulation works with triangles similarities concepts and angles and trilateration works with distance in order to position the object (GIS 2023).

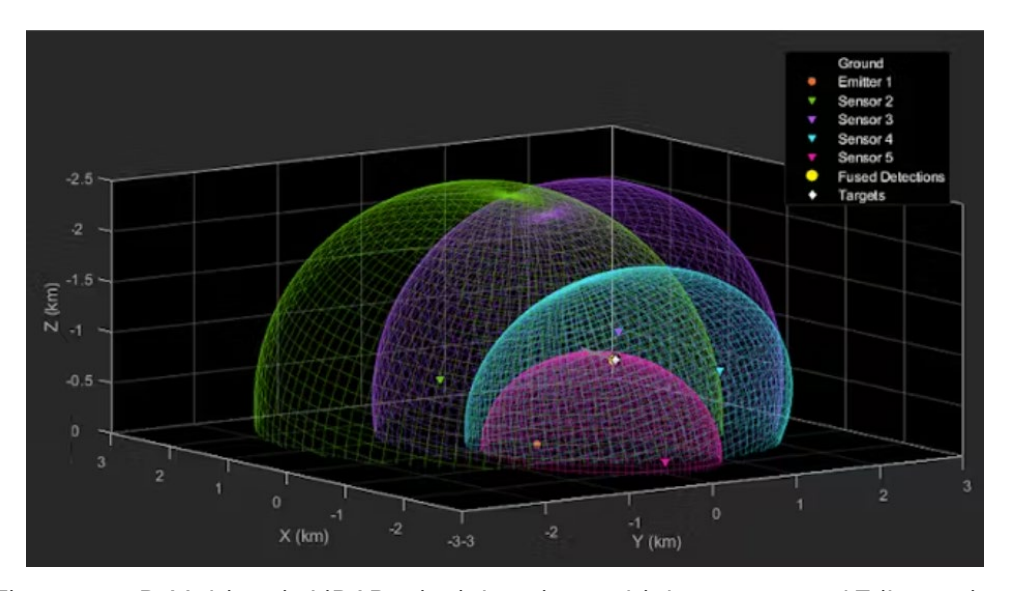


Figure 4.2 3D-Multistatic LiDAR principle using multiple sensors and Trilateration.

(Gentile 2019)

The definitions of triangulation and trilateration change based on different sources. While (Gentile 2019)considers Figure 4.2 trilateration, it is considered triangulation based on (Bosch 2001) With three ellipses, whereby three detectors point at one object, only one position of the object is possible where all three ellipses meet. This phenomenon is called triangulation and is described in detail in a laser ranging paper (Bosch 2001).

The working principle of "**Ellipse**" is using bistatic measurement, which is two detectors. It is described by using a single source, single detector and a single object. The object position will be located on an ellipse, with all points on the ellipse having a constant path to the light, as in Equation 9. With two detectors pointing at one object, the object can only be seen in 2D at two positions where the two ellipses (plan view) intersect.

In a monostatic LiDAR setup, the detector and light source are in the same location. Assuming a constant light intensity, if the detector and light source are not in same location, the total distance travelled by the light is equivalent to the distance between the source and the object and the distance from the object to the detector with total distance D.

$$R(in\ meters) = D = d_1 + d_2 = constant = 2a$$

Equation 8

$$a = (d_1 + d_2)/2$$
;

$$b = \sqrt{(a^2 - (\frac{x_1}{2})^2)}$$

$$d_1 = \sqrt{(x^2 + y^2)}$$

$$d_2 = \sqrt{((x^1 - x^2)^2 + y^2)}$$

$$\frac{x^2}{a^2} + \frac{y^2}{b^2} = 1$$

Equation 9

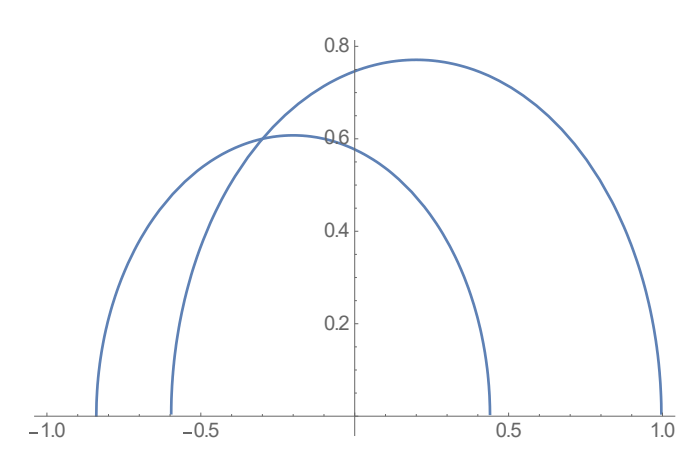


Figure 4.3 2D- Ellipse using two detectors to determine object position using Mathematica.

When three or more detectors are used it is possible to locate a single object as only one point can be seen at the intersection of the ellipses. This is the concept of triangulation/trilateration and reconstruction using the intersection of multiple ellipses. Alternatively, the concept of triangulation is possible if one object is found identifying its peak or maximum time signal. In the case of multiple objects being detected, the peaks will not be identified to each corresponding object; they will only inform of the presence of those objects in the space.

The principle of triangulation/trilateration works using multiple detectors or a single detector using multiple positions to calculate the location of one object. Using two detectors, the position of the object can be on one of the two points of intersections between two ellipses with D being constant at all points on the ellipse. With a third detector, the position of the object can be as one point only of intersections between three ellipses.

The position of the object can be determined through the calculation of all three ellipses. The ellipse equation can be solved analytically using Mathematica (version 12) or using a Python code provided by Dr Peter Wiecha. The Mathematica script determined the object position is shown in Figure 4.4 with the generated code included in Appendix A. The set of coordinates satisfying all three ellipses is the only location that the object can be in 2D. The triangulation method allows the object to be seen by the detectors at any position.

This means the analytical triangulation method and ellipse equation rely on the distance being known for a single object from three detectors will need to be coupled with other methods. Figure 4.5 and 4.6 below is generated by the Python code developed by Dr Peter Wiecha. The setup is using one source and two detectors. The position of the object can only be on an ellipse with constant path length between the source and the detector at all points. Using two or three detectors seeing one object, this can also be calculated using the ellipse concept generated in Mathematica or using Python code attached in Appendix B.

This project assumes a constant light intensity in all directions with a diverging source of light. When measuring the ToF to a single object by a detector at multiple points, the object position can be located at the intersection of two or three ellipses. To do this, a set up with a diverging source must be devised, applied by a diffuser, and the distance measurement from time of flight confirmed. By using a diverging source, instead of a single beam, the object can be seen at any point in space, rather than directly in front of the beam.

As previously described with conventional LiDAR the light is emitted as a straight line. When adding a diffuser, the ToF measurement with one detector and one diffuser, it will converge or diverge where the object is known to be traveling along an ellipse. By repeating the ToF measurement with two detectors, the object's position can be found intersecting between two ellipses drawn from the FoV of the detectors.

Using the ellipse concept, an object location can be determined as a point along an ellipse, one object can be found on one side of the table (see Equations 8 and 9). If more than one object is detected, the time trace will produce multiple peaks, each corresponding to a different object.

When using two or more detectors the position of the object is located more accurately. The analytical method of triangulation works well when locating a single object, however if more than one object is detected, it becomes more cumbersome and more complex computing methods will be needed.

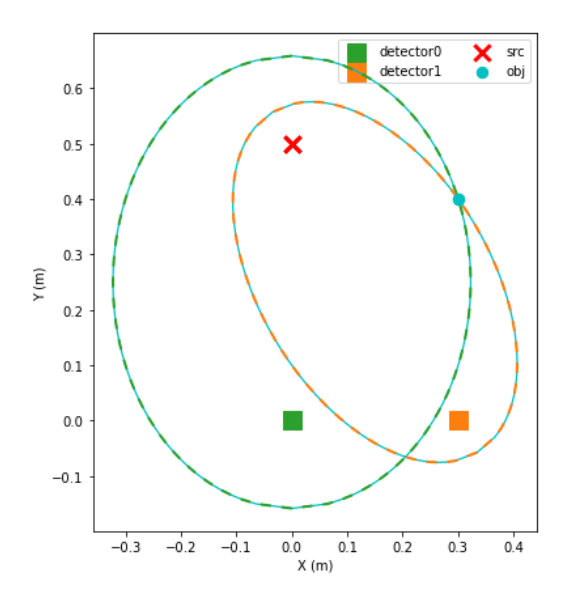


Figure 4.4 Object detection using ellipse with two detectors using Python.

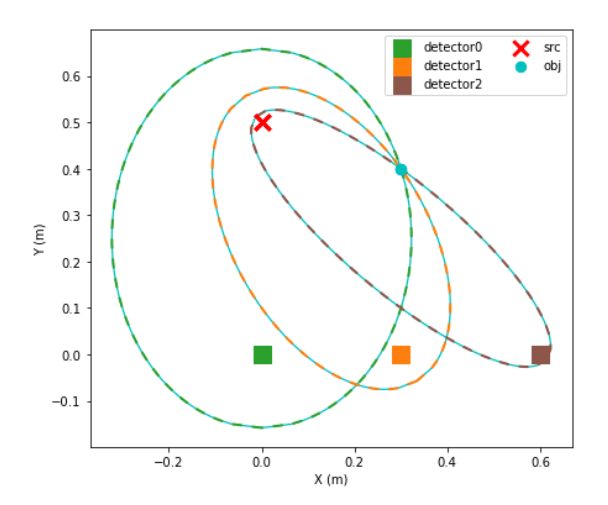


Figure 4.5 Object detection using Trilateration of three detectors using Python.

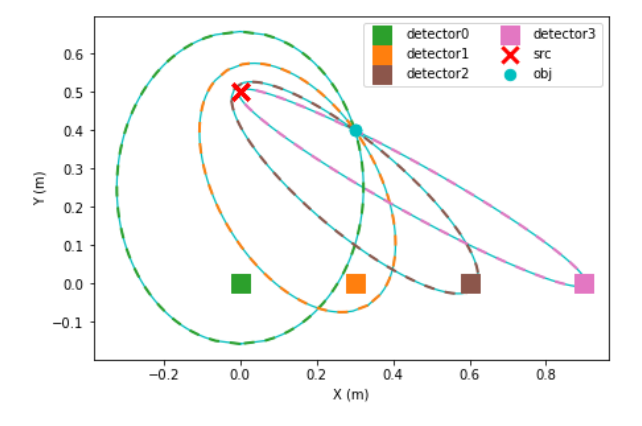


Figure 4.6 Object detection using Trilateration of four detectors using Python.

Chapter 5 Lab Experimental Setup

This chapter covers the LiDAR experimental setup in the Physics Laboratory, starting from a conventional Monostatic LiDAR simple experiment to the triangulation of a Multistatic LiDAR system.

At the start of the project, there was an existing optical setup that consisted of a dual beam LiDAR utilised by another research group, where participating in collecting data helped in gaining great insights. This project was useful to the present research to learn how LiDAR works, as it includes ToF ranging, imaging, scattering and accuracy under highly scattering environment for object detection and distance measurement.

5.1 Lab Equipment

The three main components to the LiDAR sensor in this experiment are: the laser source, the optical systems for pointing the LiDAR, and photodetectors/receivers to detect photons of light (Paul F. McManamon 2019)

Depending on the application, lasers with wavelengths between 600-1000 nm or 1550 nm can be used for long-range imaging, because the wavelengths do not affect the human eye ("IEC60825-1 Safety of Laser Products," n.d.).

5.1.1 Laser Source

LiDAR systems utilise a diode laser or a diode-pumped solid-state laser, which can be divided into bulk solid-state lasers and fibre lasers. Diode lasers can be very efficient and can be inexpensive. They have broad laser line width and broad beam. Diode lasers are useful to pump a solid-state medium that can be Q-switched to obtain higher peak power.

The solid-state laser may also have narrower linewidth and beam divergence closer to the diffraction limit. Alternatively, Fiber lasers tend to be limited in peak power because of limited gain area in the fibre.

In the experiments described here, the Supercontinuum Fianium laser is used with wavelength range 400 nm to 1500 nm. This is essential for the ToF measurements as one pulse can be distinguished from another, at 10 picoseconds. The laser beam is modulated, sent to the object and returned scattering to a detector as a functioning ToF LiDAR.

A higher laser wavelength of a 1550nm-based system, such as that of the Supercontinuum Fianium laser, has an advantage from a performance perspective, as it allows for more photons to be emitted and returned to the detector, eye shade is needed in this case. A sufficient eye-safe design has to be employed regardless of the laser wavelength by considering the energy per pulse and the size of the laser aperture. The one used here is suitable because of eye safety.

With a 905 nm wavelength LiDAR, the peak power can be increased by either of these factors given different optics and laser parameters (Hadji 2021b).

5.1.2 Photodetectors/Receivers

As mentioned in (section 4.1), LiDAR receivers may consist of a single detector or an array of detectors. Recently, high-bandwidth arrays have become available so that can measure the range of each pixel based on the time of return of a reflected laser pulse. To increase the SNR in the receiver, two main approaches have been used. For direct detection LiDAR, it is possible to make use of the gain on the receiver to increase the receiver SNR. With gain coming prior to detection, it is usually achieved via a detector or an array after detection by generating multiple electrons per received photon.

Avalanche Photodiodes (APDs) are the most prominent type of sensor used in coherent LiDAR and provide a moderate amount of gain. However, APDs also need to operate in a linear mode to integrate the signal from the received photons. It also requires high-bias voltages with poor uniformity (Hadji 2021)

The linear APD in receivers can help overcome the limited brightness of diode-laser beams. One example of an APD is the Geiger-mode which always generates the maximum number of electrons with photon is received. The Geiger mode is when the diode is operating slightly above breakdown threshold voltage.

"APD operations can be divided into several regimes depending on the magnitude of the reverse bias voltage. At low applied voltages, a small photoresponse will be detected. As the reverse bias voltage is increased, an output current is detected that is proportional to the incident optical power with a gain of unity" (Nikzad 2020).

Single Photon Avalanche Diode (SPAD) is another type of sensor that is becoming increasingly used in LiDAR that are built on single photon in direct ToF. SPAD has a large gain and is able to produce a measurable current output from every photon detected. SPAD has a low voltage, excellent uniformity and works in Geiger mode.

The SPAD is able to detect single photons, providing short duration trigger pulses that can be counted. ("Single-photon avalanche diode) The detection is executed in a dark room to prevent ambient light affecting the results; light is taken via an optical fibre with detectors kept in a dark black box to reduce noise.

When the reflected light reaches the photon receiver, the light is coupled to an optical fibre and sent to the photon counter where the intensity of light is measured following each pulse. While Leddar M16 sensors use APD, the other sensors such as CMOS used in digital cameras use SPAD. CMOS stands for Complementary metal-oxide Semiconductor used in microchips.

Optical systems and computing apertures are needed to point both the transmitter and the receiver. A single aperture can be used for both the transmitter and the receiver, or these apertures can be separate. When an optical system is pointed for transmission or for receiving, it uses either mechanical or non-mechanical pointing approaches. A simple pointing scheme can be a mirror that is tilted. There are many mechanical approaches to pointing an optical system. The effect of these mechanical pointing systems is to change the tilt of the optical wavefront.

For the Fianium laser, a trigger diode is used, which is fed by a glass slide in the line of fire of the laser that reflects 4% of the laser output towards the trigger diode. When light hits the glass, some light reflects off the glass while the rest keeps going through the glass and the light is refracted.

This gives the detector a time to begin the measurements, i.e., t₀. Before the light is emitted, a small portion of each pulse is directed into the trigger diode to begin the ToF measurement. Interlock is used to shut off the laser beam for eye safety reasons. Hence, this project evaluated on a scattering object to reduce light reflection on the object surface.

A magnetic mount is used for the detector to allow for a change of position, in case of multiple detector locations. In this project, the magnetic mounts were used with three bases that correspond to the horizontal movement of the detector in three distinct positions. The DPC-230 computer programme is used, which is a photon correlator module that records absolute photon times in up to 16 parallel detection channels ("DPC-230 TCSPC Module - Becker & Hickl GmbH") SPCM64 used with LabVIEW.

5.2 Monostatic LiDAR Configuration

The purpose of this experiment is to explore the ToF LiDAR using a conventional pulsed laser. The setup used a pulsed Fianium laser with a 1050 nm wavelength and data was collected and analysed using Origin (version 2019). Then the Python code was developed to output the positions of reflecting objects from the raw LiDAR data using two detectors. Python was used in those experiments to analyse the data collected to view a single object; in further steps the project will use deep learning to view multiple objects.

5.2.1 Monostatic LiDAR Experimental Setup

This experiment included a conventional simple single beam LiDAR experiment using a Fianium Supercontinuum laser system to view one object and to investigate the concept of triangulation, discussed in section 4.3, while moving the detector to three different positions.

The object is located on an optical bench with the FoV mounted with black walls to reduce the surrounding noise, setup is illustrated in Figure 5.1 where the black box represents the lens. The light is coupled to an optical fibre and sent to the photon counter where the intensity of light is measured following each pulse.

A laser beam originating from high-power fibre broadband pulsed laser-producing photons at a wavelength of 400 nm to 1500 nm. While a conventional, single detector LiDAR has limited FoV, Multidetector LiDAR might have increased FoV, while compromising on the accuracy level (see section 4.1), this will be determined in the following experiments.

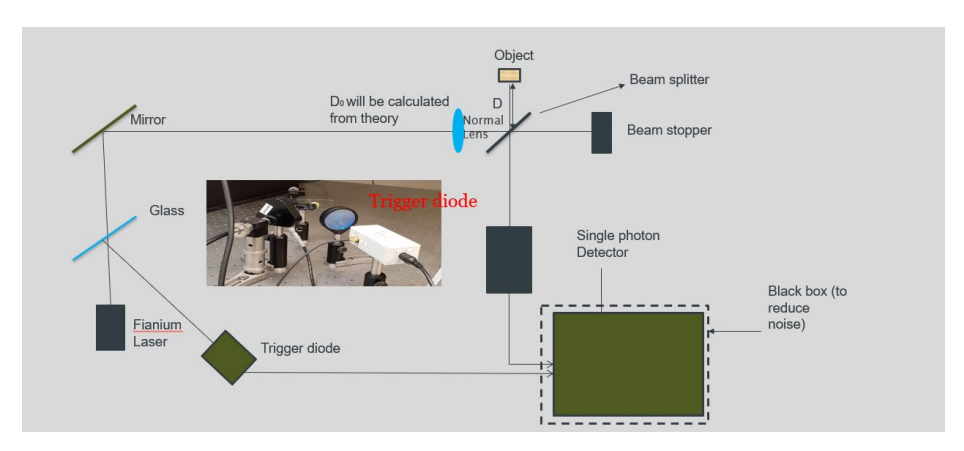


Figure 5.1 Monostatic LiDAR Experimental Setup Looking at one object.

5.2.2 Monostatic LiDAR Experimental Results

In this setup, the project measures the time trace at various locations between the object and the detector with an increment of a distance of 5 cm. A linear relationship is expected, as given in Equation $c=\frac{2D+d}{\Delta t}$, here D is the fixed distance of the light traveling within the setup; it is the distance between the source and the detector. Here, it is possible to calculate the theoretical gradient using Equation y=a+bx, where the intercept will give the value of D.

In the experimental results, the highest peak points correspond to the object's position at each location. Other subsequent peaks are produced by reflections from other objects surrounding the setup, such as the walls in the lab and the shadow of the object. The peaks are caused by the emitted light reflecting from the surface of the objects. The time between the light emitted and the peak detected corresponds to the x-axis position of the peak, giving precise information of the distance that the light has travelled. There is the reflected object, the reflectivity of the object to help identify the object targeted. Also, the back wall enclosing the laser setup gave background peaks, although much smaller than the project under study. This can be eliminated by taking measurements of peaks without the object, then taking measurement with the object and subtracting to eliminate the back wall effect.

Figure 5.2 (credit Ana Hammer) shows the photon counts over time when the room light is switched off. Measurements are taken in a dark room to reduce any noise that would affect the results. This could also be done by using a filter to allow in only laser light. In this experiment, the object was moved parallel to the movement of the detector for 5 to 60 cm. The detector software used was (SPCM).

The data were analysed with Ana Hammer using Origin. The files were converted to .asc from .sdt so that they can be used in Python coding or imported into Origin. The shifting time traces produced are shown by the same object at various distances away from the light source. The first strongest peak is produced by the object and subsequent smaller peaks are produced by other reflections from within the lab, such as the wall or the object's shadow.

The width of the peaks can be attributed to the resolution in the time domain with the shortest channel of the detector being 164 ps. This experiment was then repeated using a diverging laser source to confirm that this would still give a reliable distance measurement, with the only difference (as expected) being a lower number of photons counts due to the beam intensity being spread rather than being confined to the spot of the single beam laser. Figure 5.3 (credit Ana Hammer) shows the distance calculated in cm between the source and the object. Error bars are given by the standard deviation of three experimental runs of the experiment. The slope (measured gradient) of 0.066 \pm 0.00043 ns/cm agrees with the value predicted from theory, with an intercept of 118.066 \pm 0.015 ns. The predicted gradient was 0.066 ns/cm where $c=3\times10^8$ m/s.

$$y = a + bx$$
 and $c = \frac{2D + d}{\Delta t}$

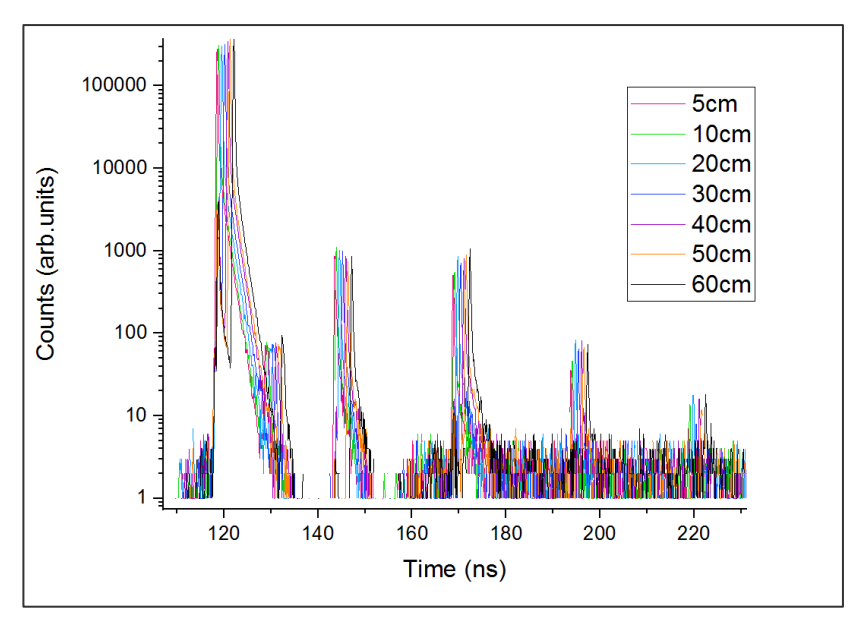


Figure 5.2 Monostatic LiDAR: Time Traces measured by the Linear LiDAR setup.

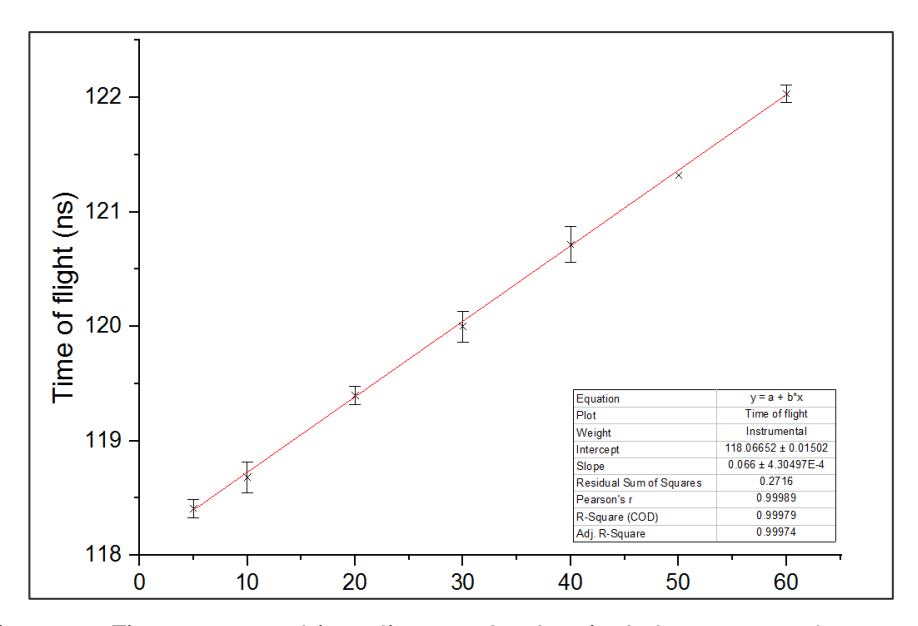


Figure 5.3 Time trace vs object distance for the single beam setup (cm vs ns)

5.3 Monostatic LiDAR Using Diverging Lens

5.3.1 Monostatic Diverging Lens Experimental Setup

This setup repeats the initial experiment, while adding a diverging lens and collimation (as described in section 5.2 above). The process of collimation is used to collimate the beam into the vertical direction, so the beam diverges horizontally. The divergence creates a cone of light or FoV that can see the object by spreading the laser pulse over the entire effective area of detection, which is the optical bench measuring 1 $\rm m^2$, illuminating the object at any position within the study area. The collimation here is used to maximise the intensity of the beam for the object to reflect to the detector. The expected result seen here is that the count number of photons decreases due to the divergence, as the beam is spreading the photons onto

a larger area. Thus, a larger area is covered with the intensity of the beam decreasing. The experimental setup is shown in Figure 5.4 where the black box unlabelled represents the lens.

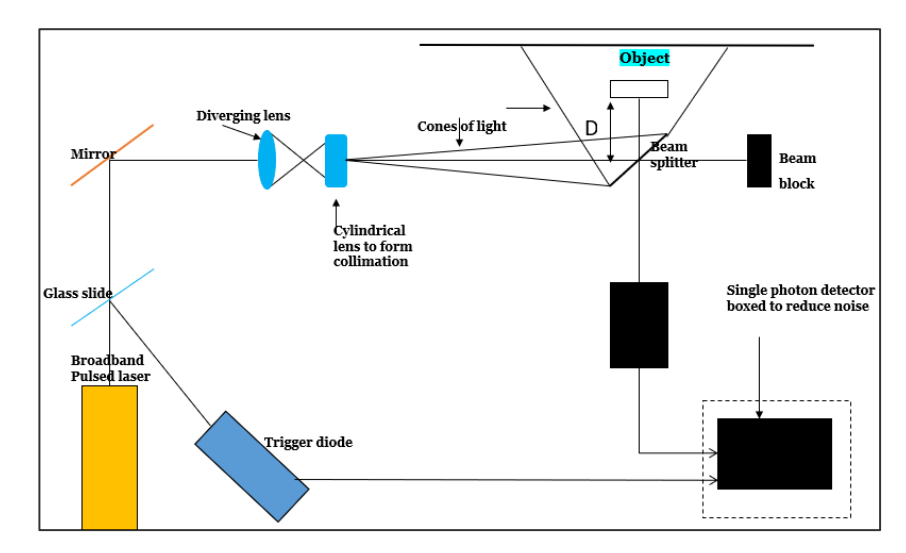


Figure 5.4 Single Beam LiDAR Experiment with one detector using a diverging lens.

5.3.2 Monostatic Diverging Lens Experimental Results

The data were analysed with Ana Hammer using Origin. The files were converted to .asc from .sdt so that they can be used in coding or imported into Origin. Figure 5.5 below shows the shifting time traces produced by the same object at various distances away from the light source. The first strongest peak is produced by the object and subsequent smaller peaks are produced by other reflections from within the lab. The peaks are of less magnitude than the previous experiment due to the diverging lens. In Figure 5.5 (credit Ana Hammer), the Y axis is the log count, while X axis in nanoseconds (ns).

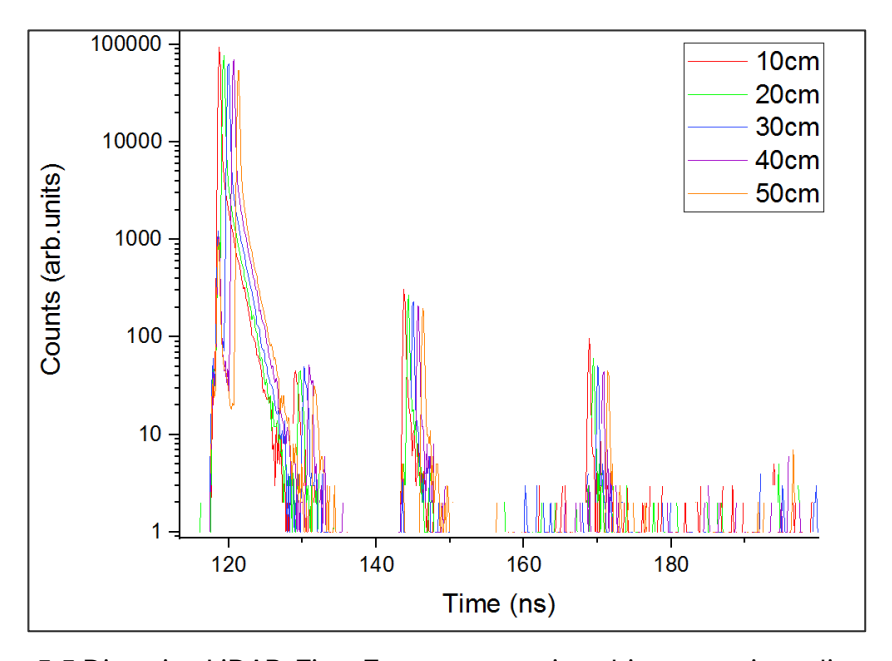


Figure 5.5 Diverging LiDAR: Time Traces measuring object at various distances.

Figure 5.6 (credit Ana Hammer) shows the relationship between the distance of light source to the object versus the time of flight. The intensity of the peaks is lower than the initial

experiment. This is expected due to the application of the diverging lens. Y in ns while X is in cm.

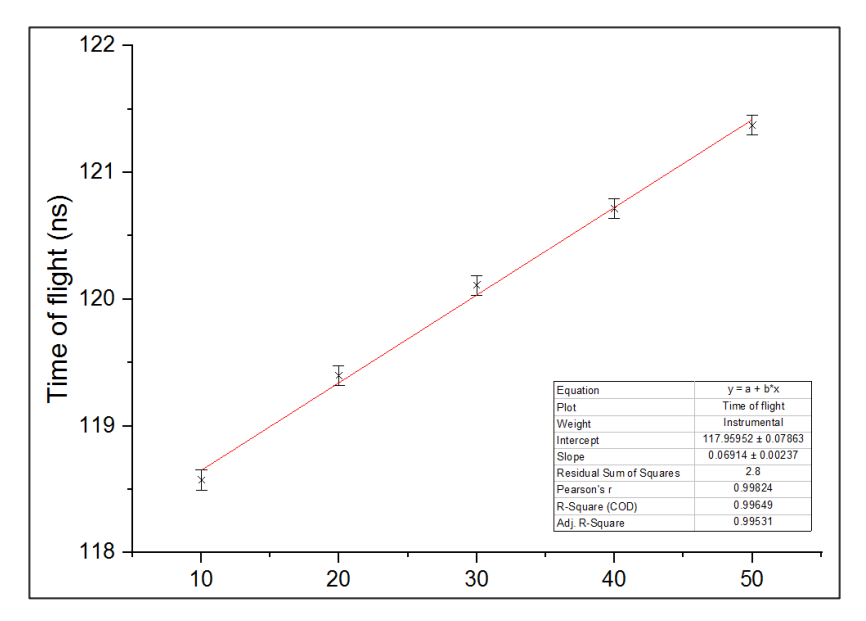


Figure 5.6 Time trace vs object distance for the diverging beam setup.

5.4 Multistatic LiDAR Configuration

The Multistatic sensor setup is achieved by modifying the design of the source-detector arrangement, described in section 4.6, and separating them (Jim Hyen Park 2008).

The set up here works by triangulating the position of an object, described in detail in section 4.2. The setup includes a diffuser and two detectors (Detector 1 and Detector 2) with Detector 1 at angle 64° and Detector 2 at angle 92°. The diffusers increase the FoV for the entire area without the need to move components in the setup. The same Fianium laser is used as for the previous experiments.

The setup will scan the entire FoV instead of building a point cloud of measured objects. The scan is conducted using the diverging lens to create a flash that illuminates the surroundings. This facilitates measurement of the returning photons by the detectors. Having two detectors will create an overlapping FoV; this will help to calculate the position of the reflected objects. This is best illustrated using Figure 5.7 below. In this figure, it is clear how the intersection of the down-range profiles within an area illuminated by multiple beam widths permits to distinguish the two objects as seen in Figure 5.7.

5.4.1 Multistatic LiDAR Experimental Setup

This data was analysed with Daniel Smyth, an MPhil student. The experimental setup includes a the Fianium supercontinuum laser, as used in the previous experiment. This setup uses two detectors instead of one detector to utilise triangulation concept described in section 4.2. Here, collimation is used as previously described, also slits and irises optics are added to the setup to define the beam. There are four steps followed in this experiment which include measuring the source power distribution, characterizing the aperture angle of the receivers, determining the overlap area, and finding the time delay for each object position.

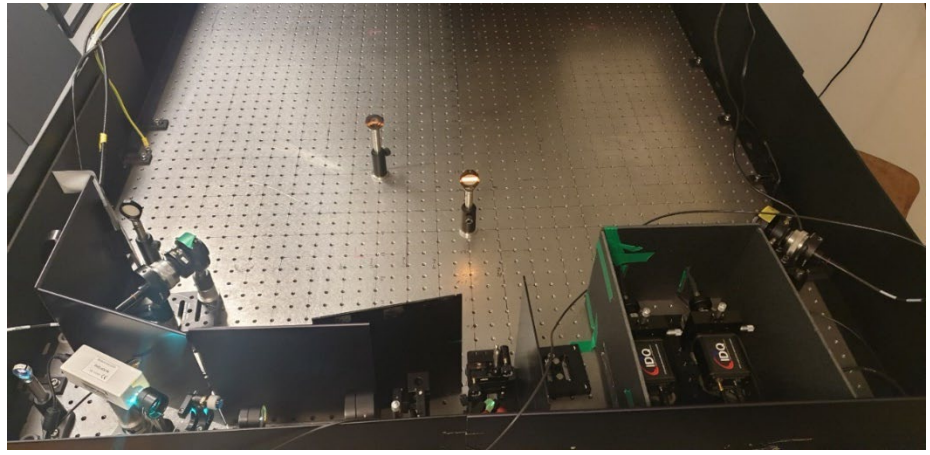


Figure 5.7 Multistatic LiDAR: Single Beam LiDAR Experiment with Two Detectors Using

Triangulation

5.4.2 Multistatic LiDAR Experimental Results

Four steps were followed in the laboratory, they were repeated until higher image resolution was reached (fewer dark zones).

- Step 1: measure the source power distribution.
- Step 2: characterise the aperture angle of the receivers.
- Step 3: determine the overlap area.
- Step 4: find time delay for each object position.

Step 1: Measure the source power distribution.

The power distribution was measured via two different methods and then results were compared to ensure validity. The first method was using (Newport optical power meter) to measure the peak for the object at various locations on the optic bench. The second method was to measure the peak of the object using both detectors for object various positions on the optic bench. All Python scripts were provided by Dr Peter Wiecha and are included in Appendix B. In this setup the first step was to measure the source power distribution using a power meter.

Point cloud data was obtained by positioning the object along the test area and moved from -50 cm to 55 cm on the x-axis and from 15 cm to 105 cm on the y-axis, using increments of 5 cm. The aim is to measure the beam using power meter directly from the light source and to compare that with measurements taken using the detectors. Figure 5.8 below represents the heat map, where the highest intensity of viewed object is viewed in the yellow area. The FoV calculated in this experiment shows the high intensity area to be $50 \times 80 \text{ cm}^2$.

Y (cm)

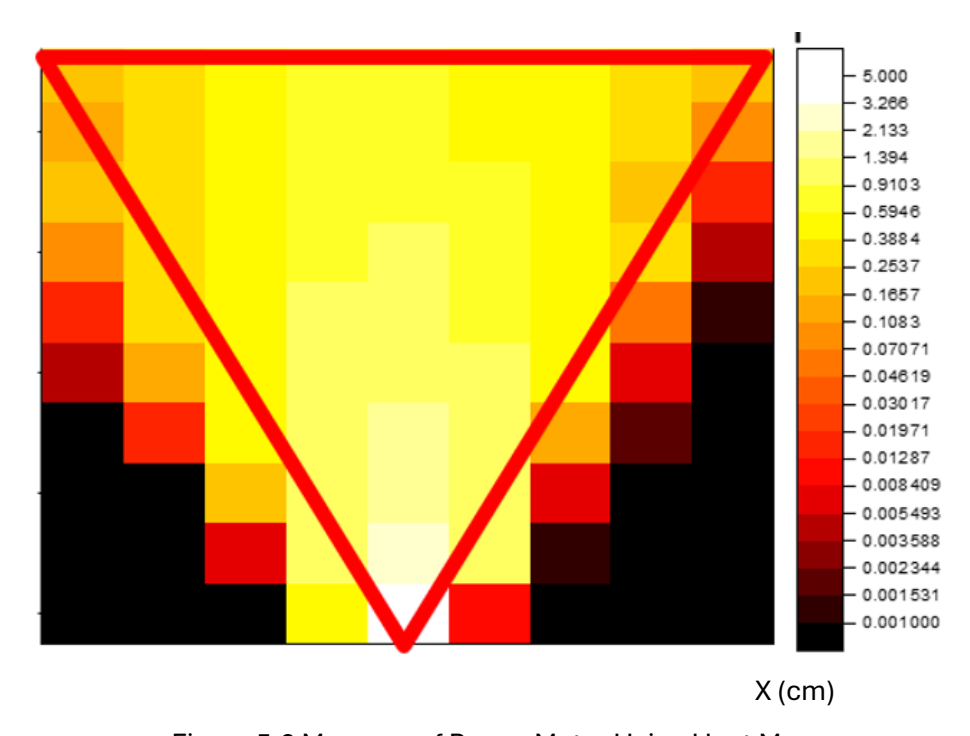


Figure 5.8 Measure of Power Meter Using Heat Map

(Python script credit of Dr Peter Wiecha provided in Appendix)

Figure 5.9 below shows the peak of the object from both Detector 1 and 2, which is the main point of interest. This will allow to find the distance the light has travelled from the source to the object then to detector. This will allow application of the ellipse concept discussed in Chapter 3 to be able to determine the location of the object using the ellipse equation (Equation 8) to find the position of the object using both detectors. Since there are two intersecting points on both ellipses, there are two object positions.

Those points increase in the case of multiple objects, as described in section 5.4.1.

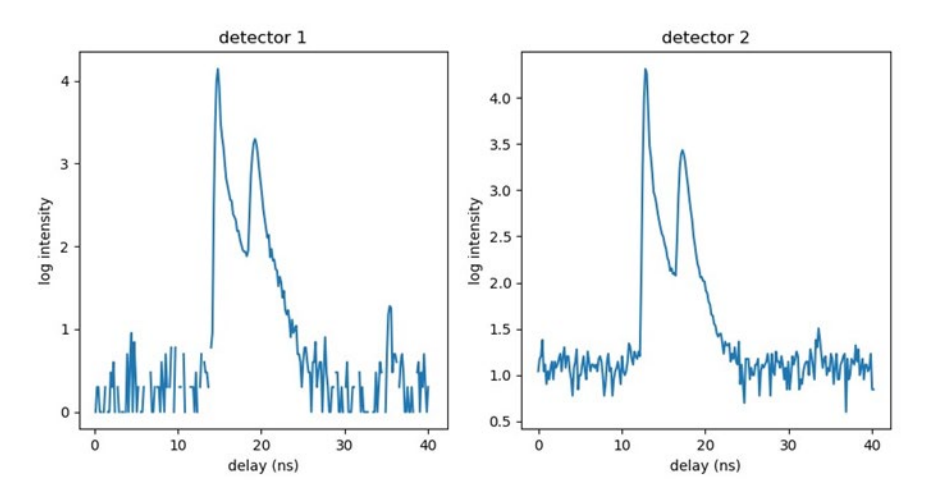


Figure 5.9 Detected light intensity of detectors 1 and 2.

Step 2: Characterise the aperture angle of the receivers.

In this step, the aperture angle of the two receivers was determined. Figure 5.10 below shows the aperture angles of receivers 1 and 2 with the increased FoV using the diffusers described in section 5.4. The main purpose of adding the diffusers was because LiDAR photon detector FoV is narrow. In this setup, there was a high degree of random light scattering, therefore, it is expected that some light will be lost. Hence, the sensitivity of is reduced. However, the aperture angle of the detectors is maximized (in this particular setup).

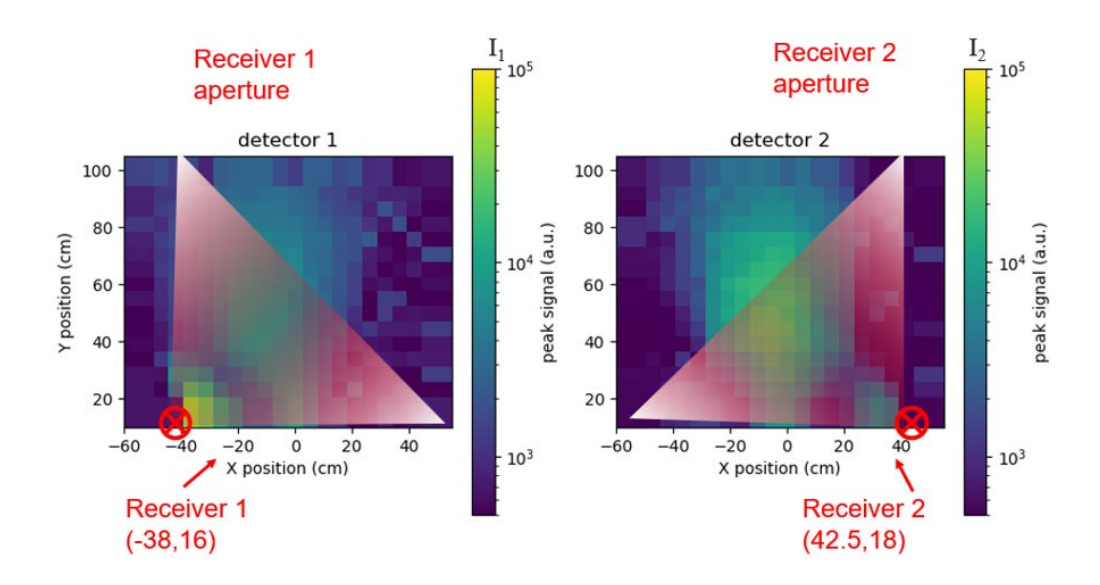


Figure 5.10 Aperture angles of receivers 1 and 2.

Step 3: Determine the overlap area.

In this step, the useable overlap area needs to be determined. This can be done by using Python script for detector overlap. The result is the diagram shown in Figure 5.11, where the peak position of the object is at x = -10cm and y = +60cm. This result is consistent with the power meter measurements taken in previous steps in section 5.4.1.

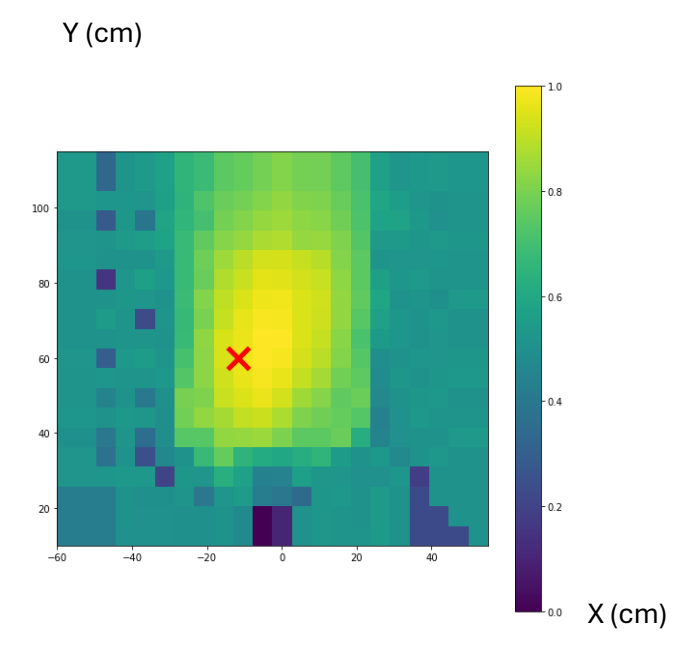


Figure 5.11 Useable overlap area.

Step 4: Find time delay for each object position.

In Figure 5.12, the x-axis position of the peak corresponds to the time taken between the light emitted and the peak detected. This is extremely helpful, as it gives precise position of the light travelled. The useable area shows the time delay for both detectors.

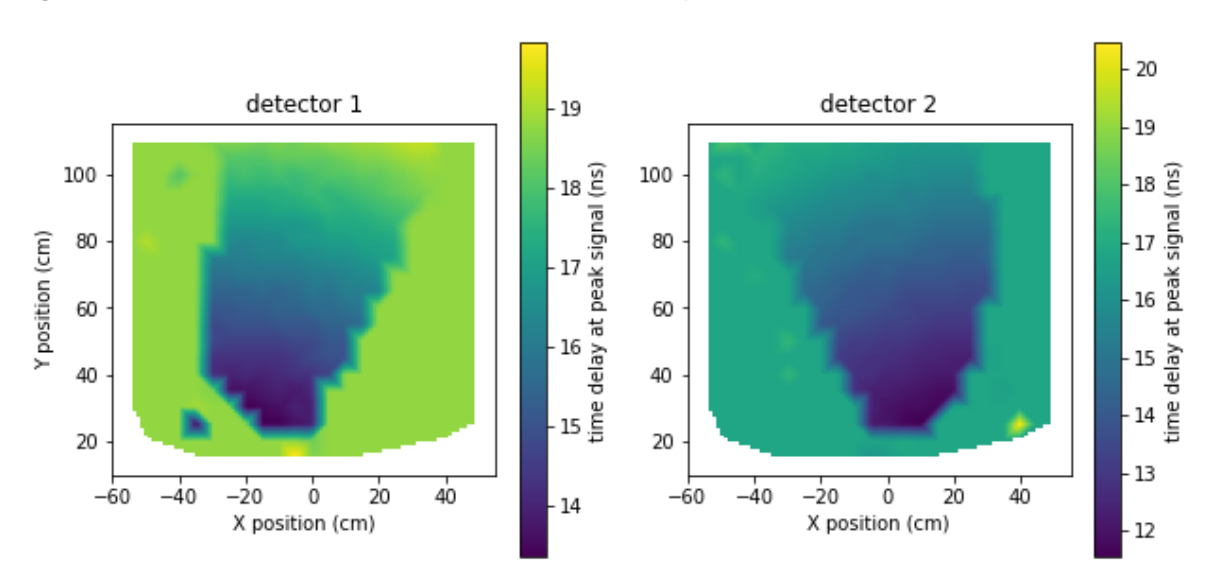


Figure 5.12 Time delay for two detectors.

Figure 5.13 shows the peak light intensity received by each detector corresponding to each object position. Here, the overlap area of both detectors helps determine the position of the object by using triangulation.

(i1 * i2)/ max is the calculation of overlapped area.

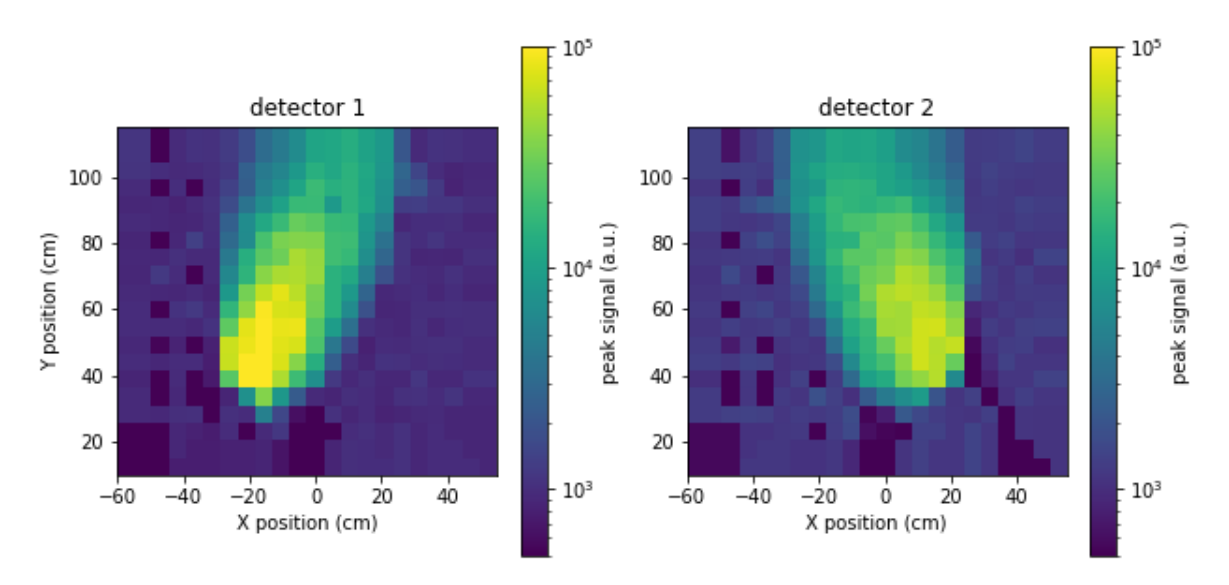


Figure 5.13 Peak reflected light intensity for each detector.

The approach used in this study provides a wider FoV using the divergence lens and the diffuser. In the case of point cloud LiDAR, the FoV is wider, however, compromising on the intensity.

In this original setup of Multistatic LiDAR using diffusers, we achieved simultaneous data acquisition with two detectors; we defined a shared coverage area of 50 × 80 cm². The source angle is limited the available area and there were dark corners (blind spots), which we will try to resolve in the improved version (section 5.4). Also, the aperture of the receivers could be improved further.

In this experiment, we used Multistatic LiDAR with Fianium LiDAR, using a diverging lens and diffuser with two detectors with diffusers applied close to the receivers to extend the angle of view. We looked at a scattering object. Data was collected and analysed using Python to analyse 424 positions of the object. The peak point was at (-5, 65).

5.5 Multistatic LiDAR Improved Version

This is a Multistatic LiDAR with Fianium laser, using diffuser and removing the lens with two detectors with diffusers identifying for a circular beam object. Data was collected and analysed using Python to analyse 395 positions of the object. Due to the improvement of the experimental setup, some area was lost from the optical bench. Therefore, fewer locations were tested for the object compared to the previous experiment. In this new set up, as we

replaced the diverging lens with the diffuser, we moved 10 cm upwards, losing 29 positions of the object.

5.5.1 Multistatic LiDAR Improved Experimental Setup

Here the setup replaces Detector 2 with a new Detector that has a 2.5 times stronger intensity with setup shown in Figure 5.14 below. Both the receivers remain in the same position. The setup replaces the object with a homogenous brass cylinder to avoid reflection from the object surface that adds more noise.

In a Monostatic LiDAR system, the light is reflected to the detector from the object in a straight line and is focused down onto an optical fibre bundle. When working with the diverging source and placing the object at some position within the cone of projected light, the light is scattering towards the detector at many different angles. This means that the incident light on the detector will not be focused onto the same point every time; it will be focused anywhere within a horizontal range. If the light is not received by the detector, then there will be no signal generated. With no adaptations to the setup to resolve this issue, a signal can only be seen a few millimetres either side of the direct beam centre. As soon as the object moves outside the range of the direct beam centre, its peak can no longer be observed and whatever is in the path of the direct beam dominates, even if it is an absorbing material. Here the aim is to compare returning photon counts using the new detector.

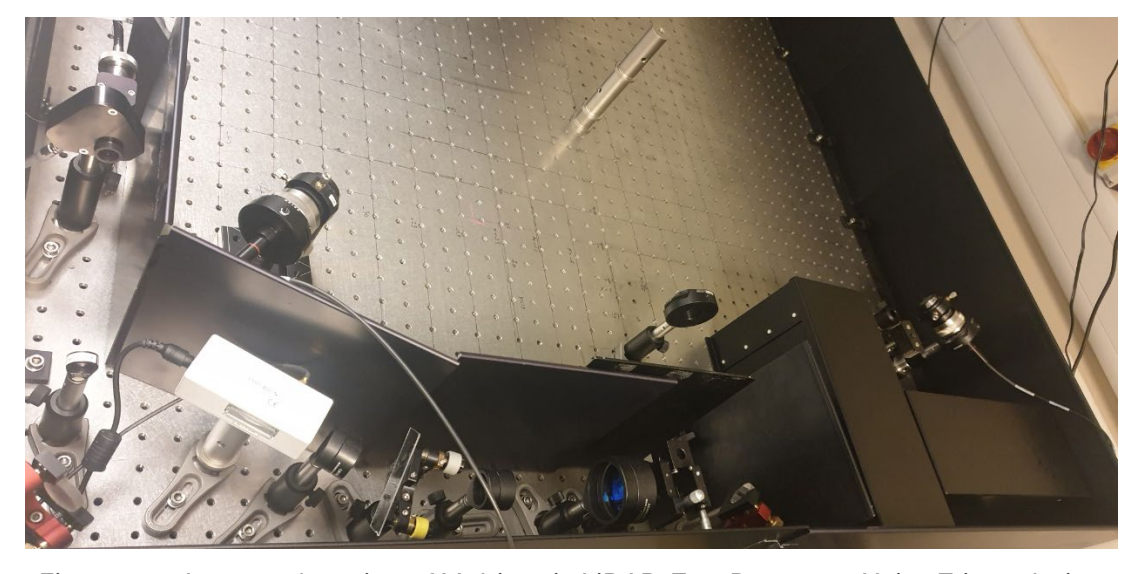


Figure 5.14 Improved version of Multistatic LiDAR: Two Detectors Using Triangulation

5.5.2 Multistatic LiDAR Improved Experimental Results

Step 1: Measure the source power distribution.

The same steps are followed in this improved setup as described in section 5.2; however, we expect an improvement given the new detector replacing the old one is more powerful, as shown in Figure 5.13. The new detector called det2 has more than twice the intensity of det1 (Detector 1). The diverging lens is removed and is replaced by a diffusor, which is expected to cover a wider FoV.

The power distribution was measured via two different methods and then results were compared. The first method was using the power meter to measure the peak of object on different locations through the optic bench. The second method was by measuring the peak of object using both detectors for object different positions on the optic bench. In this step, the beam intensity is measured with the room lights off to avoid unnecessary noise. To obtain a point cloud, the object is positioned along the test area for the x-axis, moving from -50 cm to 55 cm and for the y-axis at 15 cm to 105 cm, changing position at 5 cm intervals. The goal is to measure the beam using power meter directly from the light source compared to measurement using the detectors. In this setup the FoV is doubled as shown in Figure 5.15 below.

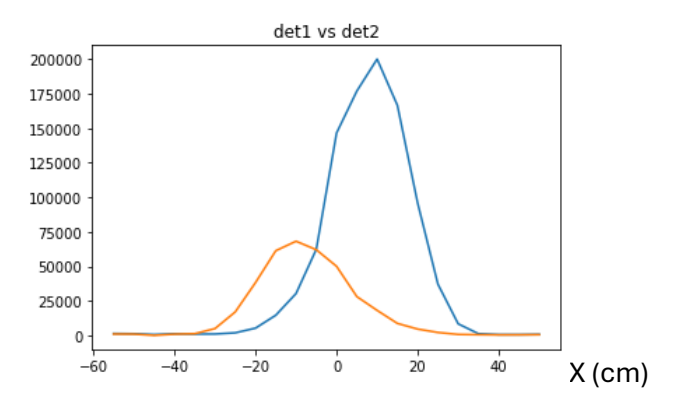


Figure 5.15 Intensity of Det2 (new detector) vs Det1.

Step 2: Characterise the aperture angle of the receivers.

In this step, the aperture angle of the two receivers was determined. Figure 5.16 below shows the increased FoV using diffusers. This was an improvement, as the LiDAR photon detector FoV is narrow. There was scattering of light throughout the testing area, which meant some light was expected to be lost to the surrounding area. Hence, the sensitivity in this case in reduced, however, the angle with which the detectors are spotting the object is maximized (in this particular setup).

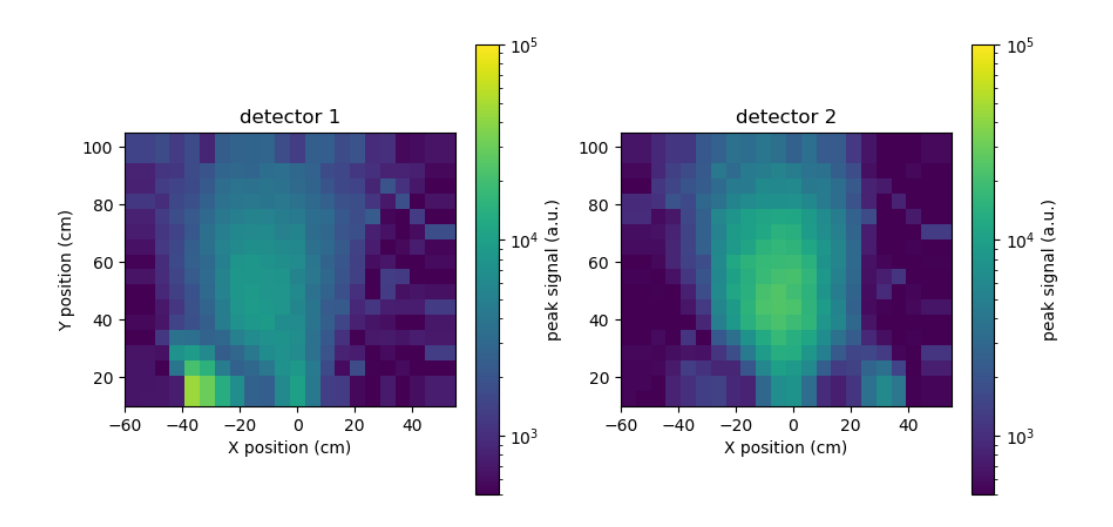


Figure 5.16 Peak reflected light intensity for each detector Improved Version

Step 3: Determine the overlap area.

In this step, the useable overlap area was determined. This can be done by using Python script for detectors overlap (see Appendix A). The result is the diagram shown in Figure 5.17 below where the peak position of the object is at position x = -5 and y = +45. This result is consistent with the power meter measurements taken in previous steps.

Y(cm)

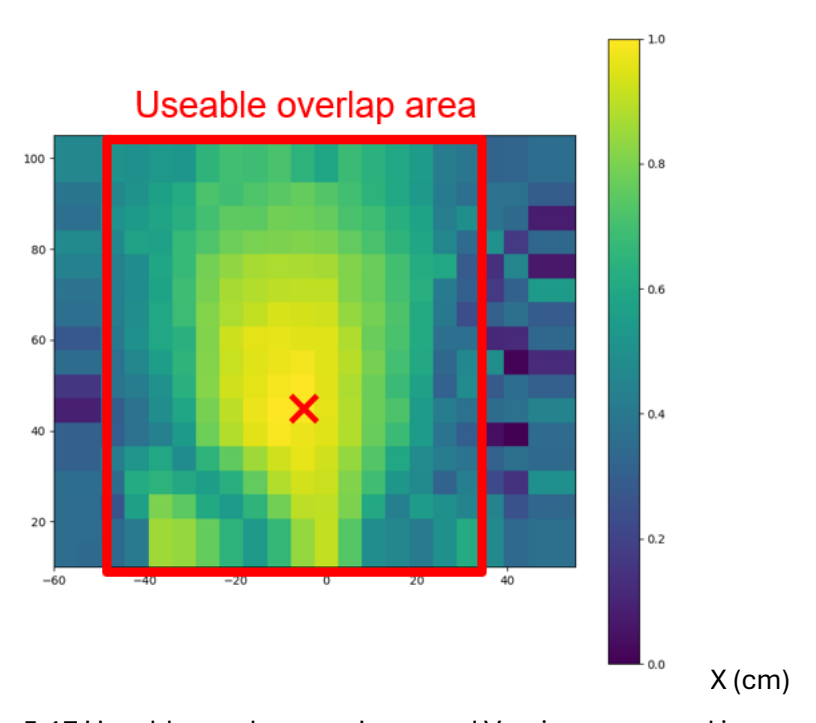


Figure 5.17 Useable overlap area Improved Version measured in cm.

Step 4: Find time delay for each object position.

Here, the x-axis position of the peak corresponds to the time taken between the light emitted and the peak detected. This gives the precise position of the object. Here the useable area shows the time delay for both detectors. Figure 5.18 shows the peak light intensity received by each detector corresponding to each object position. The overlap area of both detectors helps determine the position of the object.

This approach, using a diffuser, provides a wider FoV but compromises on the sensitivity. In the case of point cloud LiDAR, the view is single point at a time.

With this improved setup, simultaneous data acquisition was achieved using two detectors, one detector being double the power of the other detector. The defined shared coverage area was $100 \times 80 \text{ cm}^2$ – double the coverage area from the previous setup. The source angle is no longer limiting the available area, so there are no dark areas, and the aperture of the receivers has improved.

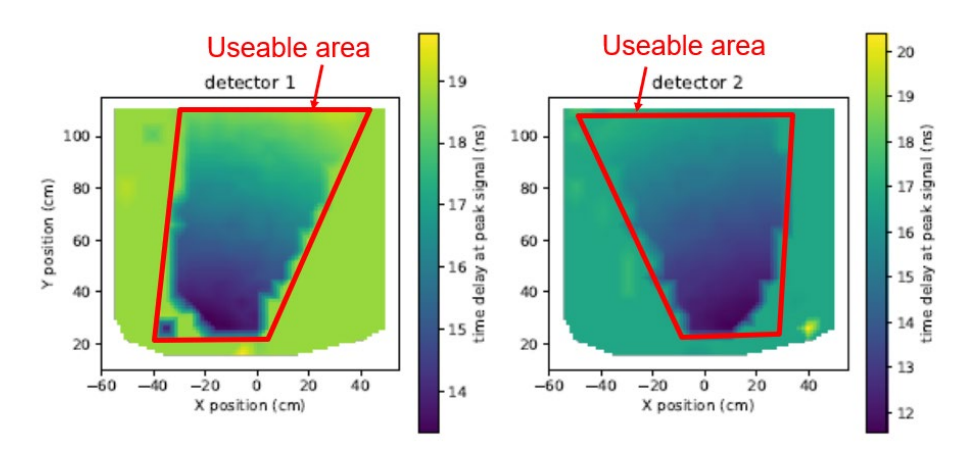


Figure 5.18 Time delay for two detectors Improved Version

5.6 Experimental Results & Analysis

This research is aiming to explore whether multi-static LiDAR systems could provide improved safety measures that could benefit in the application of autonomous vehicles. This chapter investigated the ToF LiDAR's capabilities in three different experiments while detecting one object. The project used the conventional Monostatic single detector LiDAR; then Multistatic LiDAR using triangulation with two detectors and a diverging lens to identify one object. The third experiment was an improved version of Multistatic LiDAR, using a diffuser and one of the two detectors was replaced with a new detector with double the intensity. The Multistatic LiDAR setup was used with a diverging lens to spread a laser pulse over the entire effective area of detection. This allowed the object positioned anywhere in the study area to be illuminated without the need to adjust the laser. The data was analysed using LabVIEW, Origin and Python. The purpose was to understand the behaviour of laboratory Multistatic LiDAR when detecting one static object. The lab results shown in this chapter demonstrate the impact of triangulation on increasing the field of view especially with the addition of diverging lens.

When using triangulation/trilateration of the single beam LiDAR with two detectors, we achieved simultaneous data acquisition. We were able to define a shared coverage area of 50 × 80 cm². We noticed the source angle is limiting the available area (dark areas in Figures 5.9 and 5.15). Additionally, the aperture of receivers could be further improved since it was limited in this setup. This was achieved in the improved version of the Multistatic detection where the coverage field of view was doubled to 100 × 80 cm² with no dark areas around the source angle. This could be explained with the use of the diverging lens and the increase in the new detector intensity being double. Additionally, the setup was improved by adding absorbing walls around the study area to reduce the noise, taking the data with the room light off and changing the detector angles to increase the FoV. This implicates that by using the right optics and using 2 LiDAR sensors we get better view of the object than using a single LiDAR sensor.

In previous chapters, we investigated the state-of-the-art Automotive LiDAR sensors and explored the different types of LiDAR sensors by conducting a literature review of academic and industrial studies. This chapter completed the first phase of laboratory experiments, starting with conventional LiDAR using diverging lens and examined Multistatic LiDAR and completed lab experiments for improved setup using triangulation pointing at a static single object.

We conclude here that the principle of detection works but it is limited with the technology used. This can be useful in different applications where the area of study is limited to (1x1)m2. This is a good start to understand the concept of triangulation/ trilateration/ ToF/Multistatic LiDAR. Phase II of this research works applies those principles in real life looking at longer distances and detecting a pedestrian which is the focus of this research.

The ToF Lidar concept emits light and returns with information about the object. The Flash LiDAR used in field experiments in Phase II operates using 16 channels and detect the objects. The similarity of both LiDAR types occurs when adding diverging lens to ToF LiDAR. Flash LiDAR eliminates an area using a number of channels differing based on the model. When using triangulation of multiple LiDAR sensors both TOF and Flash LiDARS become similar in that they both have a FoV with varied sizes and different information of detected objects returned.

5.7 Lab Setup Preparation for Phase II

5.7.1 Leddar M16 Flash LiDAR

Leddar M16 (Light-emitting diode detection and ranging) is a sensing technology based on laser illumination and the ToF principle. Leddar M16 is a Flash SSL created by the company LeddarTech. The product Leddar M16 Laser M16R-75J008 was chosen to be performed in the experiments of this project for many reasons. The main one being the state-of-the-art SSL provided at low cost and made available for research purposes. Other similar LiDAR sensors were more expensive and were not available to purchase as single unit and were only provided with their expensive software (LeddarTech 2019).

Leddar M16 is a unique sensing technology based on laser illumination using infrared spectrum and ToF principle. The Leddar M16R-75J0008, M16LSR sensor is an advanced state-of-the-art SSL solution and flash illumination multi-element sensing module laser - 48° × 3°. It is designed without a motorized mechanism, with wide operating temperature ranges, and an all-weather performance. Hence, it is suited for outdoor operation, without sensitivity to ambient light variations. The Leddar M16 has high precision detection capabilities; it is claimed by Leddartech, the manufacturer, to be able to locate obstacles such as fixed structures, vehicles, pedestrians, and cyclists. This is beneficial in order to better locate the surroundings of the CAV in order to improve safety.

Leddar M16 uses 16-segment photodetector array and provides multiple detection and ranging segments. Leddar M16 laser emitters illuminate the target area, and the multichannel sensor receiver collects the backscatter of the emitted light and measures the time it takes for the emitted light to return back to the sensor. The full-waveform analysis enables the measurement of distance and the detection of multiple objects in each of the 16 segments. detection and distance. However, it does not detect hidden objects if fully covered by the front objects.

Figure 5.19 below describes the illumination area and the 16 detection segments which provide the profile of the targeted object. Figures 5.20, 5.21, and 5.22 illustrates the operational setup of Leddar M16 with camera and with Labview.

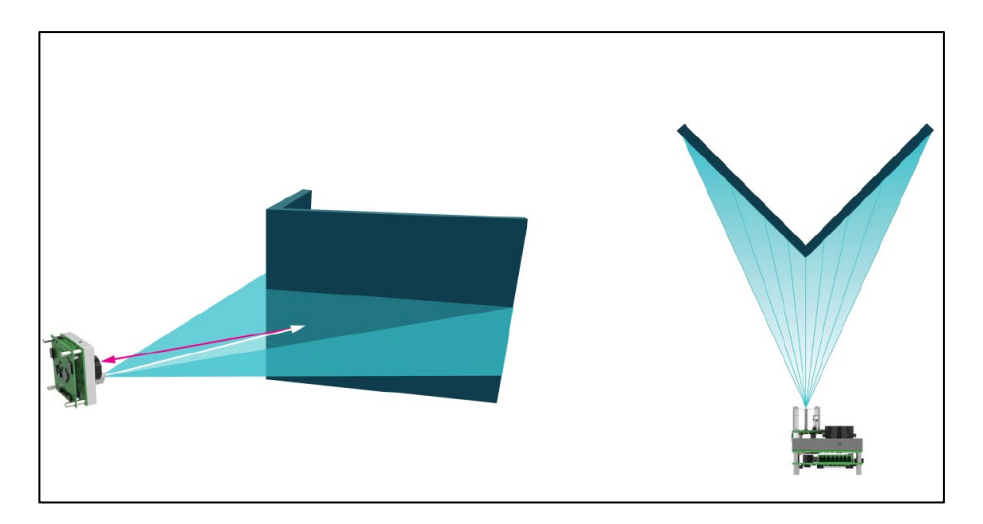


Figure 5.19 Illustration of Leddar M16 illumination Area and Detection Zone

(LeddarTech 2019)

Leddar M16 flashes 16 independent detection segments to detect simultaneously and continuously multiple objects with lateral discrimination. The sensor also performs precise multitarget detection and measurement in applications such as electronic tolling, vehicle counting and profiling, speed measurement, and traffic light automation. This makes it an ideal choice for experimenting in this project (Leddartech 2022).

Leddar M16 sensor acquires an input waveform for each segment. Multiple acquisitions are used to perform accumulations and oversampling and generate a final waveform that is then processed using LabVIEW to detect the presence of objects and measure their position.

Leddar M16 uses laser sources to achieve longer ranges, providing a narrower vertical FoV with a detection range of up to 165 m. Leddar M16 is setup in this experiment is mounted with a camera and data-acquisition using the LabVIEW (version 2021) programming environment to detect the presence of objects and measure their position.

The novelty of this experiment is correlating the camera with segmented LiDAR. In this setup the distance will be taken of a screen where only central elements registered the correct distance. In chapter 6, the project will include real-time analysis using deep learning using Python (version 3.8), which will consist of collision avoidance analysis applied in a field experiment.

Leddar M16 sensor acquires an input waveform for each segment. Multiple acquisitions are used to perform accumulations and oversampling and generate a final waveform that is then processed using LabVIEW to detect the presence of objects and measure their position.

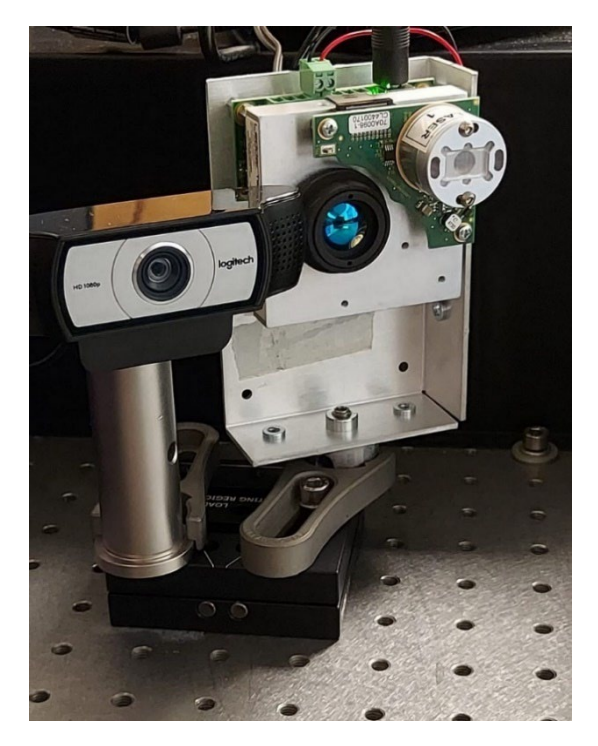


Figure 5.20 LeddarM16 mounted with a Logitech camera.

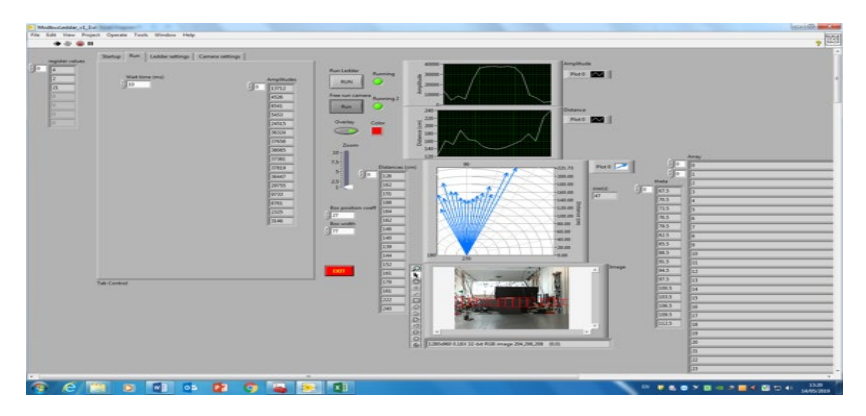


Figure 5.21 LabVIEW of LeddarM16 Experiment.

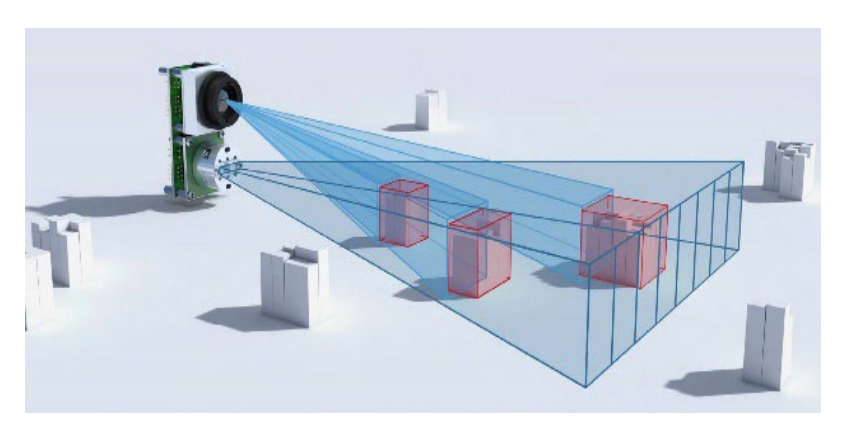


Figure 5.22 Flash LiDAR operating principal Source: (Lemmetti et al. 2021)

5.7.2 M16 Leddar Physics Lab Experimental Setup

M16 sensor was tested in the lab and data was collected for object distance ranging from 20cm to 150cm. Figure 5.23 shows the measured distances of the object versus the actual distance at a distance of 20cm. Channels numbered 2 to 13 show almost exact distances of object for the measured distances versus the actual distances. The discrepancy is only shown at channels 15 and 16. Which proves this sensor to be accurate at shorter distances.

5.7.3 M16 Leddar Physics Lab Data Analysis

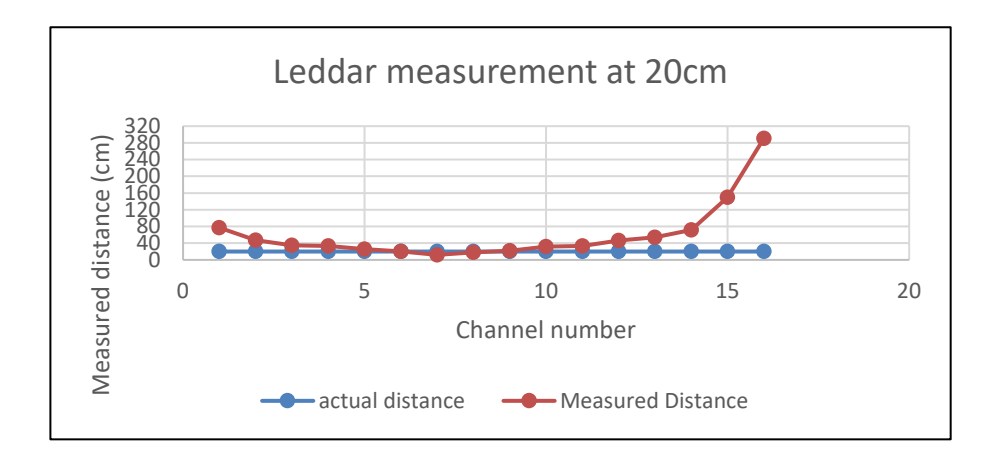


Figure 5.23 object measurement at 20cm distance actual vs measured.

Figure 5.24 shows the measured distances of the object versus the actual distance at a distance of 120cm. Here the discrepancy is higher as the object moves farther. This shows that the accuracy of the distance measured reduces at longer distances. Here channels 1,7,8,9,10,11 show approximately same measurements of actual versus measured distance of the object, with high discrepancy for channels 15 and 16.

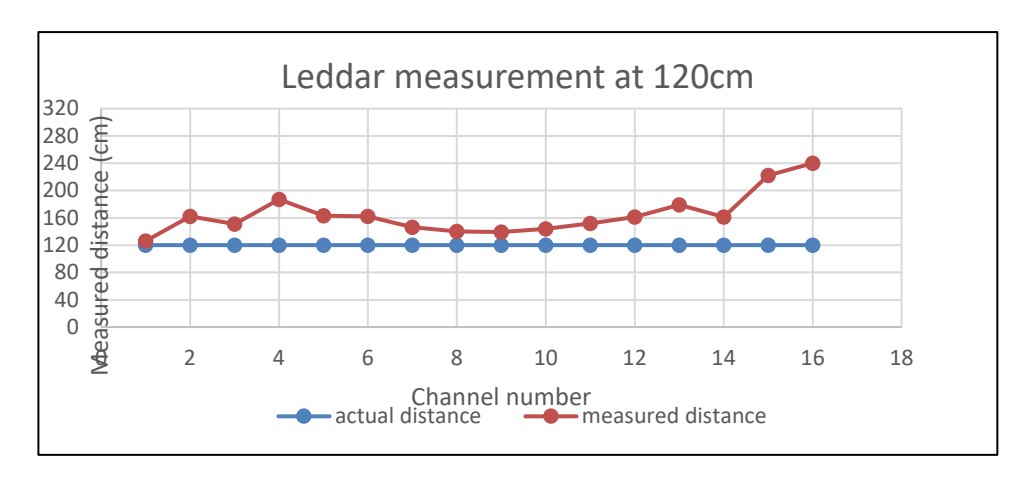


Figure 5.24 object measurement at 120cm distance actual vs measured.

Part B of the Flash LiDAR experimental setup will use triangulation of 2 Leddar M16 combined with cameras pointing at one object. We started this process in this Physics Lab for demonstration purposes and we will continue this part of the experiment in the Engineering building where a larger room is available to run this experiment on a human being. Figure 5.25 is a demonstration of 2 Leddar M16 each combined with a camera pointing at one object. Figure 5.26 shows Labview combined with Python viewing the object using triangulation.



Figure 5.25 Lab setup of Two Leddar M16 each combined with a camera pointing at one object.

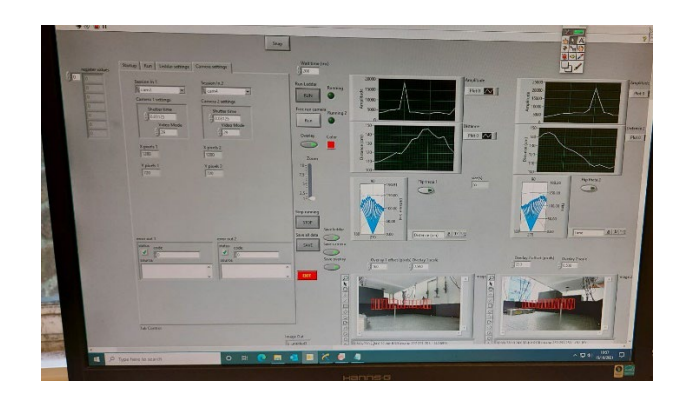


Figure 5.26 Initial Results viewing one object using Triangulation in Physics Lab

Chapter 6 Field Experimental Setup

The previous lab experimental setup of Multistatic LiDAR systems used triangulation in the laboratory including the expensive Fianium Laser, photodetectors, receivers, optical systems and computing systems. The experiment was performed on an optic bench with dimensions 1.5mx1.5m looking at an object. This chapter covers the field experimental setup which will include two low cost Solid-State Flash LiDAR sensors combined with cameras using triangulation following similar procedure to that described in Chapter 5. However, the current experiment will be conducted over a much larger area looking at humans (considered pedestrians), as opposed to the optical bench used in chapter 5. The purpose is to compare theoretical Multistatic LiDAR and practical Multistatic LiDAR using triangulation.

6.1 Understanding Leddar M16 Sensor

The experimental setup starts by understanding the solid-state Leddar M16 combined with a camera, originally tested in the on the optical bench for the Leddar M16 sensor. The experimental setup will then use triangulation with two Leddar M16 combined with two cameras pointing at one static object and later on multiple objects.

As described in section 5.7, the M16 sensor was tested in the Physics laboratory, and data was collected for the object's distance from the Leddars, and cameras setup was 20 cm to 120 cm as these were the limits of the optical bench. The results showed that this sensor is accurate at shorter distance (20 cm) and less accurate in longer distances (120 cm). Section 6.2 tests the Leddar M16 sensor at longer distance up to 500 cm.

6.2 Leddar M16 Experiments on Static Single Object

6.2.1 Two Leddar M16 and Two Cameras

In this experiment, the original proposal was to conduct it in a controlled setting using a Land Rover Discovery Sport HSE laboratory vehicle. The intention was to attach the equipment onto the front windows of the vehicle. However, due to various constraints (e.g., no dedicated room was available, no space was there to test on the Land Rover Discovery, change of setup for each experiment conducted) this plan could not be carried out. As a result, an alternate arrangement was followed.

In this modified setup, the vehicle was substituted with two tripods. The equipment was affixed to these tripods, ensuring they were at a similar height as the vehicle. The objectives of the experiment remained unchanged – to study the interaction between the Leddar M16 setup and the studied object or pedestrian. In this case, the researcher acted as the pedestrian, standing at 63 different spots inside the room. The experiment was conducted within a room measuring $5 \times 5 \, \text{m}^2$, located in Bolderwood campus, University of Southampton. This controlled environment ensured consistent conditions for the experiment's execution.

The equipment configuration consisted of two Leddar M16 sensors and two cameras. These were positioned at a distance of 220 cm from each other, and their heights were set to 122 cm on the tripods. To facilitate data analysis and control, a computer running Python and LabVIEW were employed. These measurements are taken to correspond to the position of the

side mirrors of Landrover as measured using from the vehicle used as the driving simulator at the University of Southampton. Rather than deploying the LiDAR sensors on the vehicle, the experiment was performed in an equivalent setup in a dedicated room in order to keep the experiment setup. Figures 6.1 and 6.2 below show the side view and front view of Two Leddar M16-Two Cameras setup in the Engineering lab.

Specific measurements were critical to the experiment's accuracy:

- 1. The distance between Leddar M16 Sensor 1 and Camera 1 was 15 cm.
- 2. The separation between Camera 1 and Camera 2 was 205cm.
- 3. Leddar M16 sensors were angled at 60° towards Point P5 (coordinates: 0, 250 cm).
- 4. The pedestrian or object being observed was designated as "X."

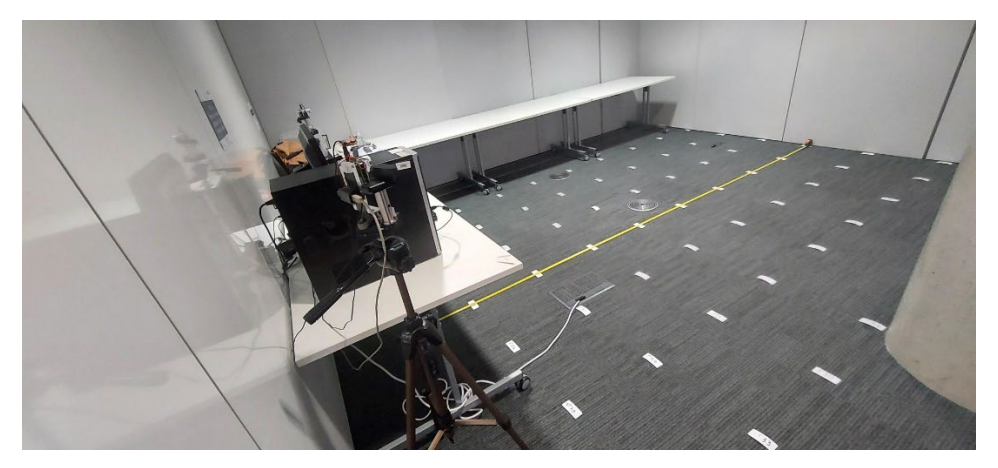


Figure 6.1 Two Leddar M16 – Two cameras showing the side view of the Engineering experimental setup.

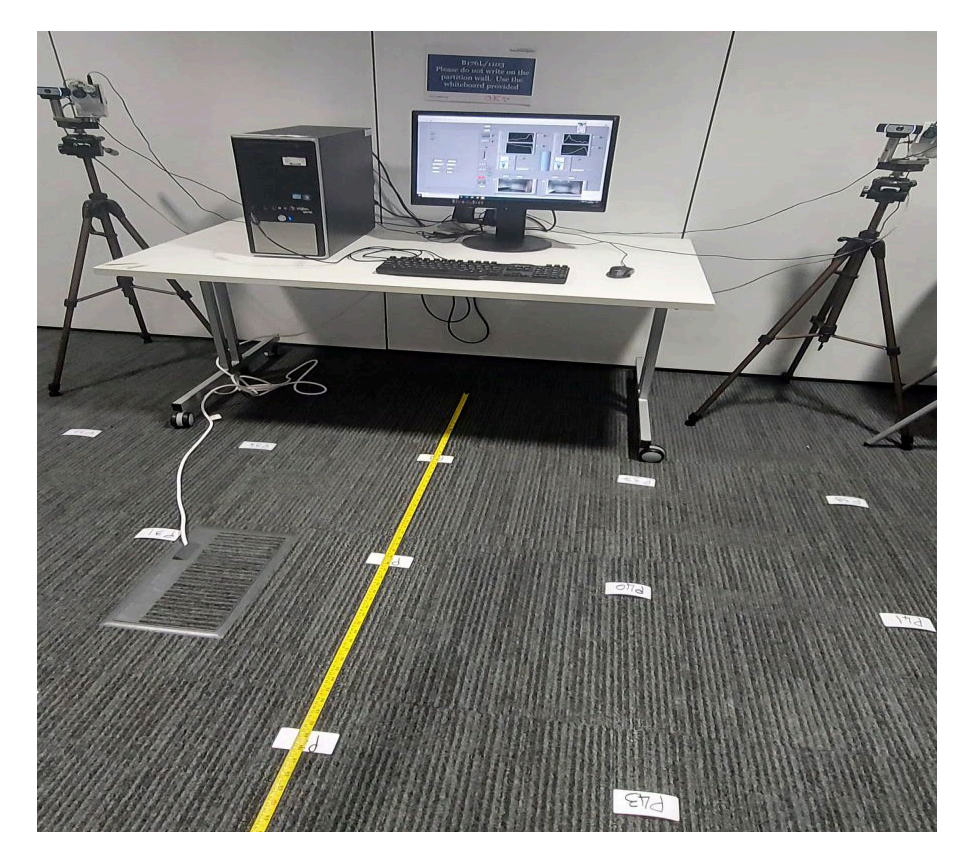


Figure 6.2 Two Leddar M16 – Two cameras showing the front view of the Engineering experimental setup.

The positions of the pedestrian at Position Px were defined by the X and Y coordinates, with X values ranging from -150 cm to 150 cm, and Y values ranging from 50 cm to 450 cm. The data collected from these experiments was processed using an initial Python code that was developed by Professor Otto Muskens.

For this experimental setup, there were modifications made to the Python code, and this is outlined in Appendix C. The goal was to adapt it to the changes made in the project due to human error. This includes slight change of Leddar angles, distance between Leddars, change of light, temperature etc. as data was collected over several days with different conditions. The same room was used during this experiment; however, it was not always available.

The graphs presented below in Figure 6.3 illustrate the various positions of the object (or pedestrian) using the input from two Leddar M16 sensors. This setup allowed examination of areas that might not be easily visible, often referred to as blind spots. Figure 6.4 shows the heat map for two LiDAR.

An analysis using heat map similar to the experimental work in chapter 5 was conducted of these blind spots. In this case, rather than calculating the intensity as previously done in chapter 5, the data was analysed using discrete variables: 0, 1, and 2. This indicates whether the object was seen by 1 Leddar, 2 Leddar or not seen at all. This analysis provided valuable insights and helped in the comparison with the previous experiment in order to draw conclusions.

As previously mentioned, the data was gathered using Python code, and Table 6.1 illustrates the coordinates of all the positions of the readings. The sequence starts from P1 (0, 450), the furthest point from the Leddar M16, and progresses towards P9 (0, 50), which is the closest point to the Leddar M16.

Figure 6.3 displays individual graphs, each depicting 16 points aligned along a blue line representing the Leddar M16 Sensor 1 and 16 points aligned along an orange line representing Leddar M16 Sensor 2. In this representation, 'X' denotes the pedestrian or object being studied. When these points form a line, whether blue or orange or both, it signifies that the object is detected by one or both of the sensors.

Points P1 to P8, located at the centre of the room, are visible to both LiDAR sensors. However, P9 is not detected by either sensor due to its close proximity, placing it within a blind spot area.

For example, in Figure 6.3, at position P3 (0,350), the object 'X' is visible to both LiDARs. In contrast, at position P57 (-150, 350), 'X' is only visible to the Leddar M16 Sensor 1, and at position P30 (150, 350), 'X' is solely visible to the Leddar M16 Sensor 2. Notably, P9 (0, 50) does not depict 'X,' indicating that it remains unseen by any sensor.

Upon observing the data displaying the camera views, and the overlay of the Leddar M16's 16 channels with the cameras, it is confirmed that at P9 (0, 50), 'X' is visible to at least one camera but is not detected by any of the sensors.

This situation occurs frequently, where the camera detects the object, but the sensors do not. This emphasizes the advantages of employing multiple sensors and highlights the concept of a sensor suite. This indicates that neither sensor is capable of detecting the object in these locations, suggesting the need for alternative sensors. Remarkably, P36 and P63 are the only positions consistently not visible to both cameras throughout the entirety of the experiment.

This situation occurs frequently, where the camera detects the object, but the sensors do not. This underscores the complementary advantages of employing additional sensors, highlighting the concept of a sensor suite. In table 6.1 below, dark orange presents object being seen by 2 Leddar M16, lighter orange seen by 1 Leddar M16 and grey shaded seen by none.

Table 6.1 Position coordinates reflecting heat map for illustration for Two LiDAR

| Y=450 | P55 | P46 | P37 | P1 | P10 | P19 | P28 |
|-------|--------|--------|-------|-----|------|-------|-------|
| Y=400 | P56 | P47 | P38 | P2 | P11 | P20 | P29 |
| Y=350 | P57 | P48 | P39 | P3 | P12 | P21 | P30 |
| Y=300 | P58 | P49 | P40 | P4 | P13 | P22 | P31 |
| Y=250 | P59 | P50 | P41 | P5 | P14 | P23 | P32 |
| Y=200 | P60 | P51 | P42 | P6 | P15 | P24 | P33 |
| Y=150 | P61 | P52 | P43 | P7 | P16 | P25 | P34 |
| Y=100 | P62 | P53 | P44 | P8 | P17 | P26 | P35 |
| Y=50 | P63 | P54 | P45 | P9 | P18 | P27 | P36 |
| | X=-150 | X=-100 | X=-50 | X=0 | X=50 | X=100 | X=150 |

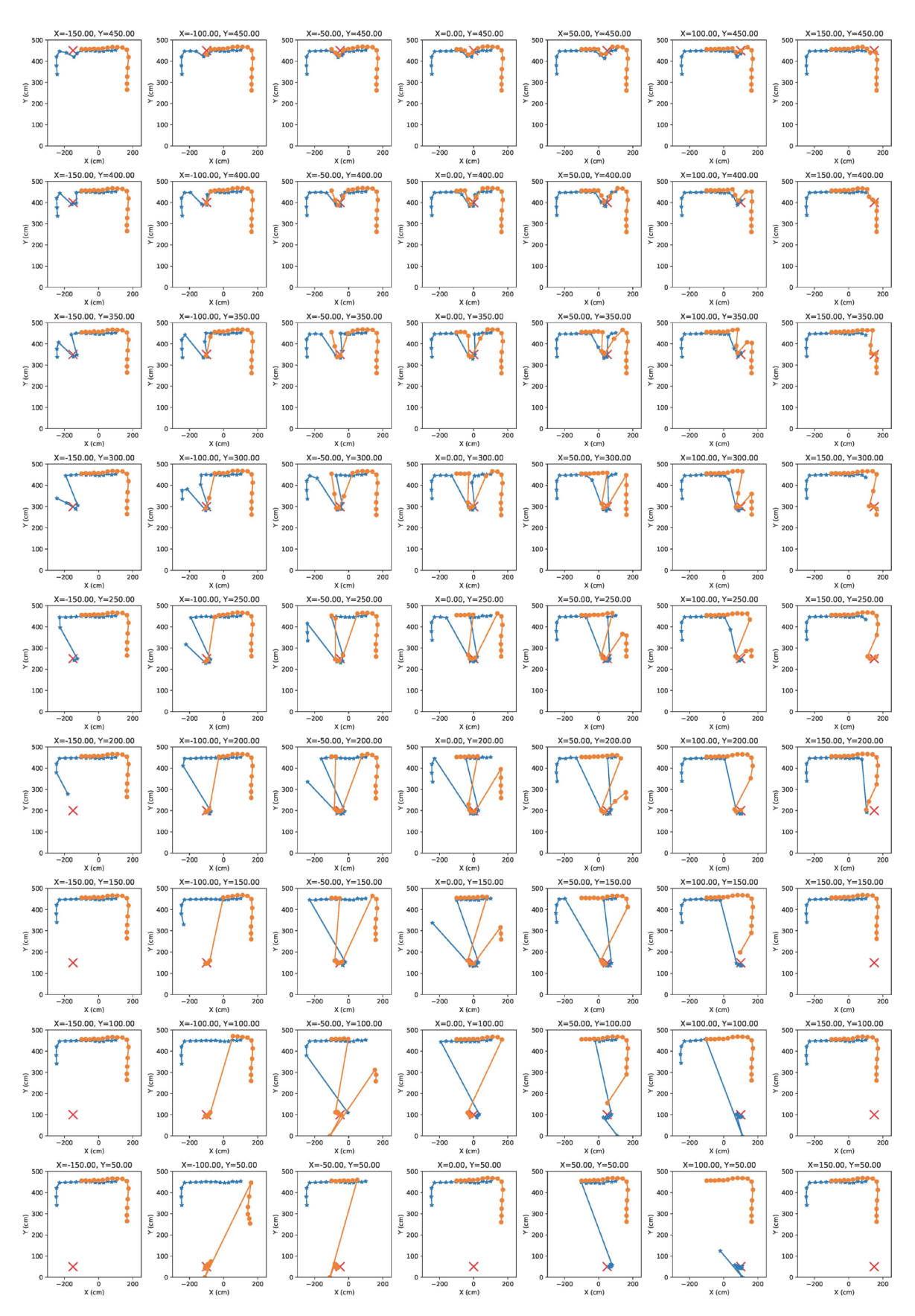


Figure 6.3 Full dataset object position using two Leddar M16 sensors.

Using the Python code, we were able to visually determine the positions where 'X' was detected by the Leddar M16 sensors. To simplify this analysis, we employed a discrete code system to categorize whether 'X' was identified by one Leddar M16, both Leddar M16s, or not seen at all. To further analyse and visualize this data, we utilized the SPSS program (version 27) to generate a heat map, depicted in Figure 6.10. In this heat map, numerical values were assigned, where '0' represents blind spots (white in colour), '1' indicates that the 'X' is detected by one sensor (light orange). In the case of 2 Lidar and '2' shows that the 'X' was identified by both Leddar M16 sensors (dark orange).

The darker orange shade (a '2') represents positions where 'X' was detected by both sensors. These include points such as P1 to P8, P10 to P16, P19 to P24, P37 to P43, and P46 to P51. The lighter orange shade illustrates positions where 'X' was detected by either one of the Lidars. These positions encompass P17, P18, P25 to P32, and P44, P45, P52 to P59. In contrast, the white dotted area signifies a blind spot ('0'), indicating that 'X' remained undetected by either sensor. These positions are P9, P33, P34, P35, P36, and P60 to P63. Remarkably, the heat map in Figure 6.10 displays complete symmetry in its arrangement, revealing interesting patterns in the detection capabilities of the Leddar M16 sensors.

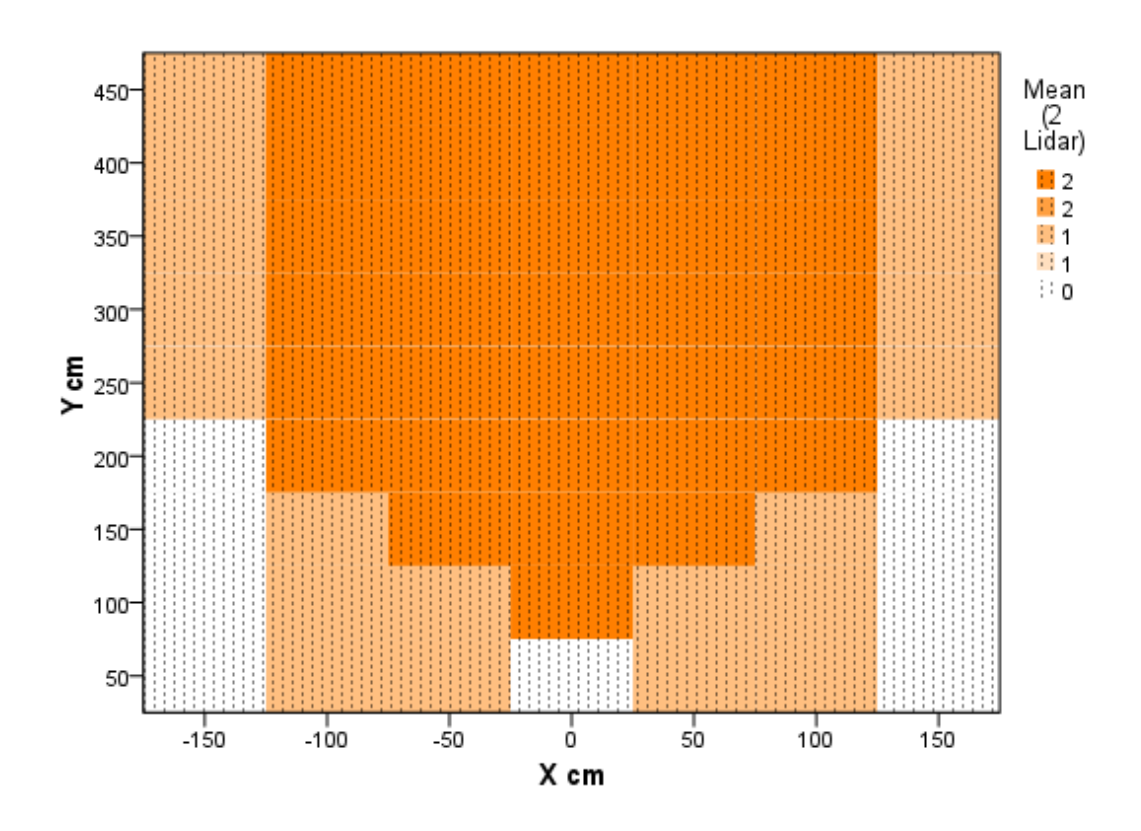


Figure 6.4 Heat Map for two Leddar M16 sensors.

6.2.2 One Leddar M16 and One Camera

The new experiment takes place in the same controlled environment as in (section 6.1). In this setup, the project uses a single Leddar M16 sensor and a camera, both positioned at the centre of the room, with the same height as in the previous experiment.

The details are as follows:

- 1. The experiment takes place in a room measuring 5×5 m² within Bolderwood Campus, University of Southampton.
- 2. A single Leddar M16 sensor and one camera are mounted on a tripod, both at a height of 122 cm.
- 3. A computer is used for Python integration and LabVIEW.
- 4. The distance between the Leddar M16 sensor and the camera is 15 cm.
- 5. The Leddar M16 sensor is aimed at the centre of the room, focusing on Point P5 (0, 250 cm).
- 6. The pedestrian or object being studied is represented as 'X'.

In this set of experiments, as shown in Figure 6.11, the pedestrian (the researcher) stood at 63 different positions within the room, where X values ranged from -150 cm to 150 cm and Y values ranged from 50 cm to 450 cm. The data was then analysed using the Python code developed by Professor Otto Muskens.

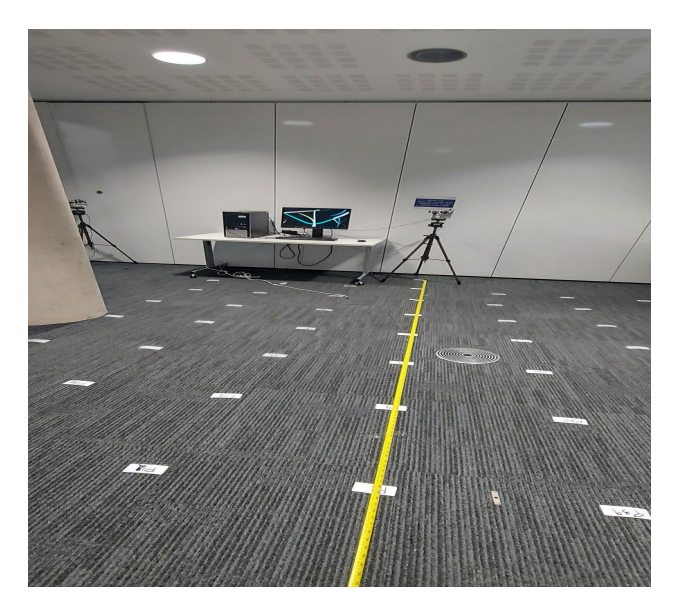


Figure 6.5 One Leddar M16, one camera setup

Figures 6.5 depicts the perspectives of a single Leddar M16 sensor and the camera, aimed at the object 'X'. The graphs illustrate the various positions of the object or pedestrian detected using the single Leddar M16 sensor.

The Python code was used to assess positions starting from P1 (0, 450), which is the furthest point from the Leddar M16, up to P9 (0, 50), which is closest to the sensor. This process

was repeated for all 63 points. Each image displays 16 points aligned along a blue line, representing the view of the single Leddar M16 sensor. This is illustrated in Figure 6.6 with cameras view results shown in Figure 6.7.

Points P1 to P24, situated at the centre of the room, are visible to the Leddar M16 sensor and present a cone-like view with no blind spots directly in front of the sensor. Similarly, P28 to P31, P37 to P51, and P55 to P58 were detected by the Leddar M16 sensor. On the other hand, positions such as P25, P26, P27, P32 to P36, P52, P53, P54, and P59 to P63 were not detected by the Leddar M16 sensor and therefore represent blind spots.

Two sample proportions tests assess whether the proportion in two populations (1 lidar and 2 lidar here), represented by two samples, are equivalent. The paired sample version of the test is more powerful and can be used here as the data points in the two samples can first be matched by the locations of the objects. This would therefore be the standard statistical test for this form of data.

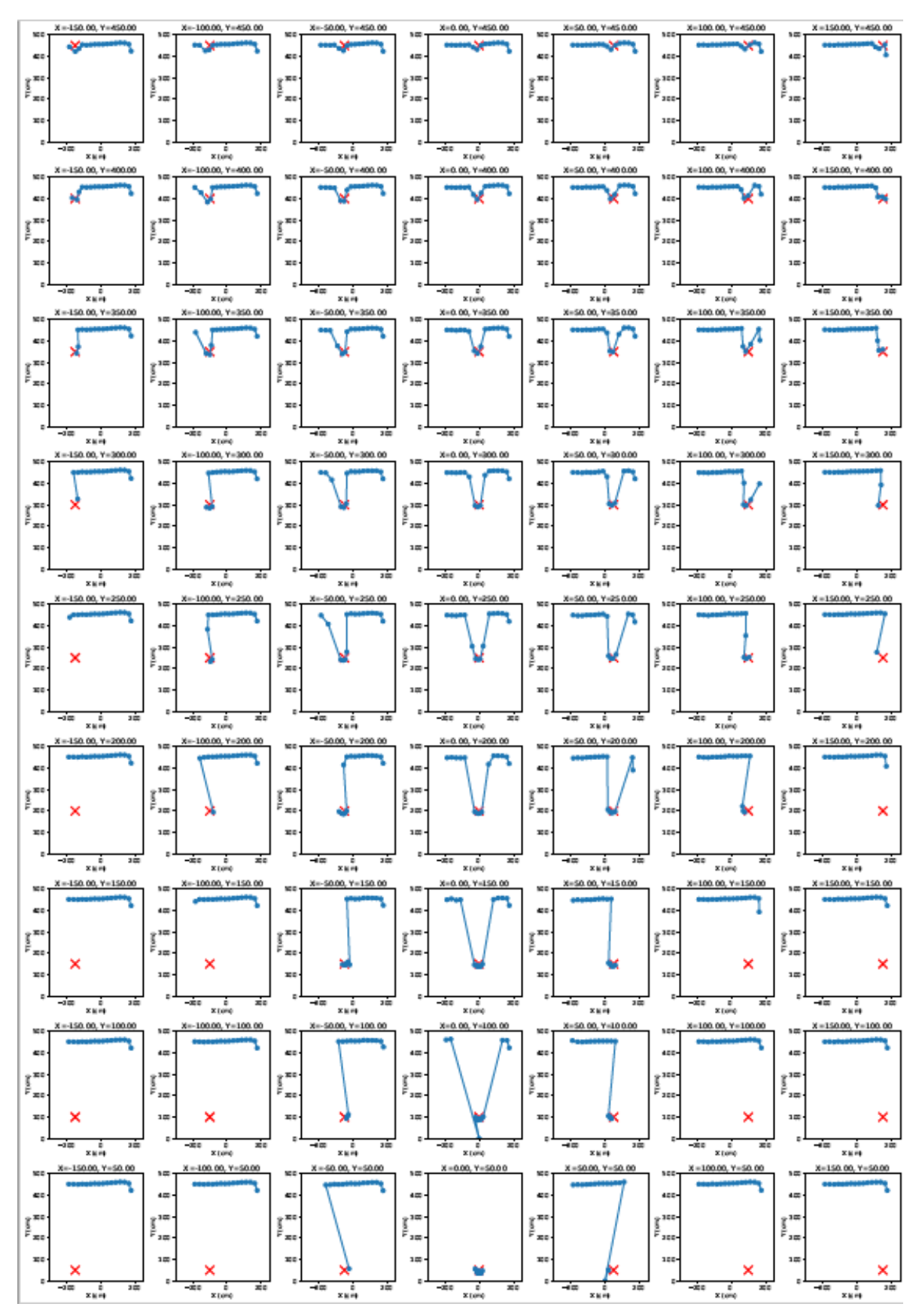


Figure 6.6 One Leddar M16 sensor looking at position X.



Figure 6.7 One camera looking at position X.

Figure 6.8 shows a heat map in which the dark orange area represents the positions detected by Leddar M16, and the white dotted area signifies blind spots. As with the previous experiment, the SPSS program was used to generate this heat map, using numbers 0 and 1, where '0' indicates a blind spot and '1' indicates detection of the pedestrian by the LiDAR sensor.

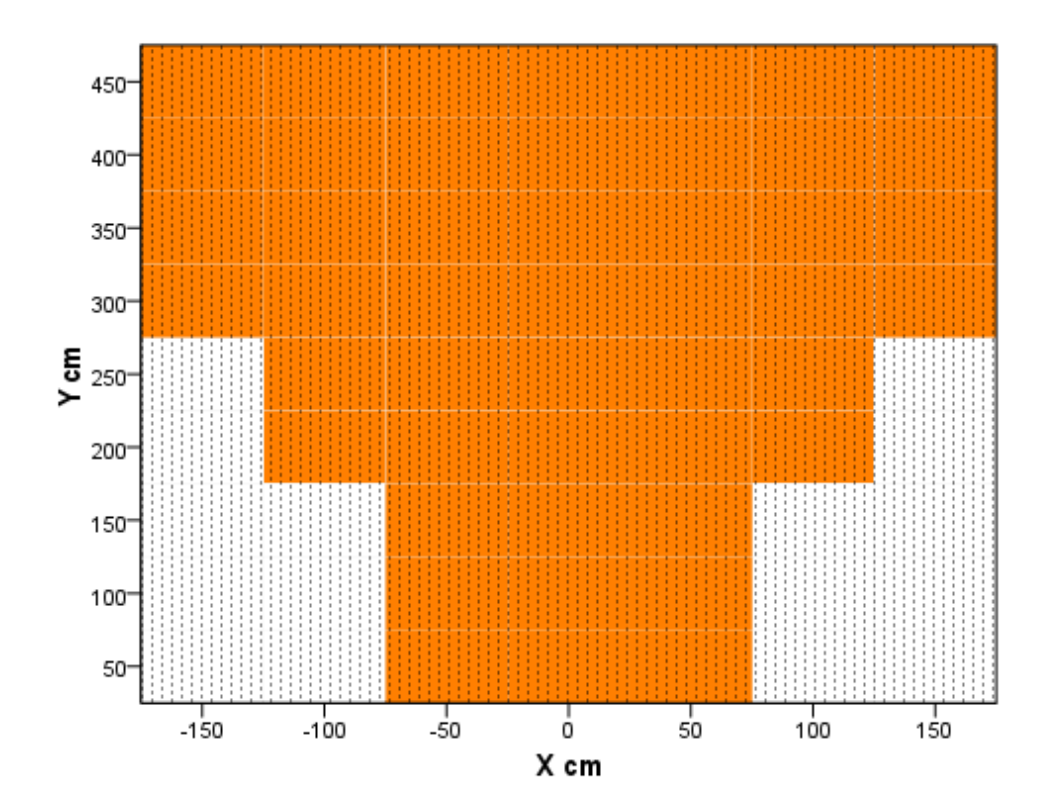


Figure 6.8 Heat map for one Leddar M16 sensor.

6.2.3 Data Description

Table 6.2 presents the frequency of detections using two Leddar M16 sensors. Out of 63 observations, there were nine instances where neither Leddar M16 detected the object (labelled as 'No'). There were 20 instances where one Leddar M16 detected the object ('Yes (1)'), and there were 34 instances where both sensors detected the object ('Yes (2)'). Results show 54% of the positions were detected by two sensors, yet 14.3% of the positions were identified as blind spots.

The frequency distribution was also conducted for the experiment using only one LiDAR sensor. Table 6.3 provides the details. Out of the 63 observations, there were 16 instances where the object was not detected by the Leddar M16 ('No'), and 47 instances where the Leddar M16 detected the object ('Yes').

Comparing the two Leddar M16 setups, 14.3% of the data points were blind spots when using two Leddar M16 sensors as opposed to 25.4% of the data points when using one sensor. Hence, the two LiDAR system is efficient in reducing blind spots.

In summary, the collected data was analysed using a discrete system (0 for no detection and 1 for detection). The results were tabulated to show the distribution of detections using either one or two Leddar M16 sensors, enabling us to make comparisons between the two setups.

Table 6.2 Frequency Distribution for Two LiDAR sensors

| Detection Type | Frequency | Percent |
|----------------|-----------|---------|
| No | 9 | 14.3% |
| Yes (1) | 20 | 31.7% |
| Yes (2) | 34 | 54.0% |

Table 6.3 Frequency Distribution for One Lidar

| Detection Type | Frequency | Percent |
|----------------|-----------|---------|
| No | 16 | 25.4% |
| Yes | 47 | 74.6% |

6.2.4 Data Comparison & Analysis

A comparison was conducted between the performance of a setup using one Leddar M16 and a similar setup using two Leddar M16 sensors. The data was analysed using discrete values 0 and 1, where 2 is considered equivalent to 1.

To determine if there is a significant difference between the two samples, we employed a statistical test known as the paired-sample proportions test. This test helps us decide whether the proportion of successes in the two samples is equal or not. If the calculated p-value (P) is greater than 0.05 this concludes there is not enough evidence to reject the idea that the proportions are not the same.

Equal or not. If the calculated p-value (P) is greater than 0.05 this concludes there is insufficient evidence to reject a hypothesis that the proportions are the equal (and if P is less than 0.05, there is sufficient evidence to reject the hypothesis that the proportions are equal). In our case.

If P is less than 0.05, there is a significant difference. In our case, the calculated Z-score is 2.33 and the one-sided p-value is 0.01, which is lower than 0.05. This means that we have enough evidence to reject the null hypothesis (the proportions are equal) at a 95% confidence interval. Consequently, we can conclude that there is a significant difference between the two samples.

The setup adopting 2 Leddar M16 sensors, had 54 successes out of 63 trials, resulting in a success proportion of 0.857, whereas the setup with one Leddar M16 sensor had 47 successes out of 63 trials, resulting in a success proportion of 0.746. The statistical analysis also provided

confidence intervals for the difference in proportions between the two systems. Depending on the method used, the confidence interval for this difference ranges from 0.011 to 0.204.

The test used is the McNemar tests ("McNemar's Test Using SPSS Statistics," n.d.). The McNamar test is used to assess whether the proportion of tested cases (63 locations for the one pedestrian experiment in 6.2.4 and 18 locations for the two pedestrian experiment in 6.3.4) indicate a significant increase in the proportion of cases successfully identified. The McNemar Test is used rather than a standard X2 or two sample proportion tests as it adjusts for the paired nature of the sample points in each experiment.

In conclusion, there is a significant difference between the proportion of object exposed by the two-sensor setup to the proportion of object detections by one sensor. Additionally, there is a 10% difference in success rate for the setup using two sensors compared to the setup with only one. This indicates that the two-sensor system has better overall performance.

Table 6.4 Paired-Samples Proportions Tests

| | | | | Significa | nce |
|-----------|---------------------------------|---------------------------------|-------|-----------------|-----------------|
| Test Type | Difference in Proportions | Asymptotic Standard Error | Z | One- Sided p | Two- Sided p |
| McNemar | .111 | .046 | 2.333 | .010 | .020 |

Table 6.5 Paired-Samples Proportions Statistics

| | | Successes | Trials | Proportion | Asymptotic Standard Error |
|--------|---------------|-----------|--------|------------|------------------------------|
| Pair 1 | 2 LiDAR = Yes | 54 | 63 | .857 | .048 |
| | 1 LiDAR = Yes | 47 | 63 | .746 | .063 |

6.3 Leddar M16 Experiments on Multiple Moving Objects

In the previous tests, we focused on a Leddar M16 system identifying a stationary pedestrian. However, this approach did not account for the blind spot situated behind the pedestrian. To address this limitation, it is necessary to study scenarios involving multiple pedestrians. In this section, we explore a scenario where two Leddar M16 sensors and two cameras are employed to monitor the movements of two pedestrians in different positions. This experimentation used the same setup described in section 6.2.3.

The table displayed below illustrates the positions of the first pedestrian X1 and the second pedestrian X2, as detected by the two Leddar sensors. This configuration allowed us to identify the blind spots. An analysis of these blind spots was carried out using discrete variables. This analysis provided valuable insights into the characteristics of these obscured regions. Table 6.6 provides the coordinates for the positions tested for both X1 and X2. The sequence commences with X1 located at position P7, accompanied by X2 positioned at P50, P5, P23, P48, P3, and P21.

The subsequent observation involves X1 at P5 with X2 at positions P50, P23, P48, P3, and P21. Following that, X1 is placed at P50, and X2 occupies positions P48, P3, P21, and P23. Subsequently, X1 is situated at P3, while X2 occupies positions P48 and P21. Finally, X1 is placed at P48, and X2 is positioned at P21.

These positions were selected since, to the naked eye, these positions would be visible in scenarios involving setups using two Leddar M16 sensors and one Leddar M16 sensor. However, in the case of two sensors, there is a possibility that P21 could be obscured by P5 or P7, as detected by Leddar M16 Sensor 1 – this requires further confirmation. Similarly, P48 could be obscured by P5 or P7 in situations involving two sensors. Furthermore, in scenarios involving one Leddar M16 sensor, P3 and P5 could be obscured by P7. These assumptions will be verified through experimentation described below based on X1 selected positions with different layouts 1 to 6 as illustrated in Tables 6.6 to 6.11. they are illustrated in Figure 6.9 to Figure 6.21.

Table 6.6 Position coordinates reflecting X1 and X2 Layout 1

| P55 | P46 | P37 | P1 | P10 | P19 | P28 | Y=450 |
|-----|-----|-----|----|-----|-----|-----|-------|
| P56 | P47 | P38 | P2 | P11 | P20 | P29 | Y=400 |
| P57 | P48 | P39 | P3 | P12 | P21 | P30 | Y=350 |
| P58 | P49 | P40 | P4 | P13 | P22 | P31 | Y=300 |
| P59 | P50 | P41 | P5 | P14 | P23 | P32 | Y=250 |

| P60 | P51 | P42 | P6 | P15 | P24 | P33 | Y=200 |
|--------|--------|-------|-----|------|-------|-------|-------|
| P61 | P52 | P43 | P7 | P16 | P25 | P34 | Y=150 |
| P62 | P53 | P44 | P8 | P17 | P26 | P35 | Y=100 |
| P63 | P54 | P45 | P9 | P18 | P27 | P36 | Y=50 |
| X=-150 | X=-100 | X=-50 | X=0 | X=50 | X=100 | X=150 | |

X1 X2

P7 (X0Y150) P50, P5, P23, P48, P3, P21

P5 (X0Y250) P50, P23, P48, P3, P21

P50 (X-100,Y250) P48, P3, P21, P23

P3 (X0Y350) P48, P21

P48 (X-100Y350) P21

6.3.1 Two M16 Leddar and Two Cameras

X1 at P7, X2 at P50, P5, P23, P48, P3, P21

For a setup of two Leddar M16 sensors, both X1 and X2 were identified at least once. Table 6.7 below shows X1 at P7 with X2 moving into six different positions relative to X1. The Python code was programmed to reflect on the positions of X2 relative to X1. It is shown below that at P48, P50, P21 and P23 X2 was identified by one sensor whereas at P3 and P5 X2 was observed by two. No blind spots were identified in this setup. The blue colour indicates the target object named X1 to separate from X2. Figure 6.9 shows the Full Dataset of X1 at P7 using two Leddar M16 sensors.

Table 6.7 Position coordinates reflecting X1 and X2 Layout 2

| X2 at P48 (1) | X2 at P3 (2) | X2 at P21 (1) |
|---------------|--------------|---------------|
| | | |
| X2 at P50 (1) | X2 at P5 (2) | X2 at P23 (1) |
| | | |
| | X1 at P7 | |

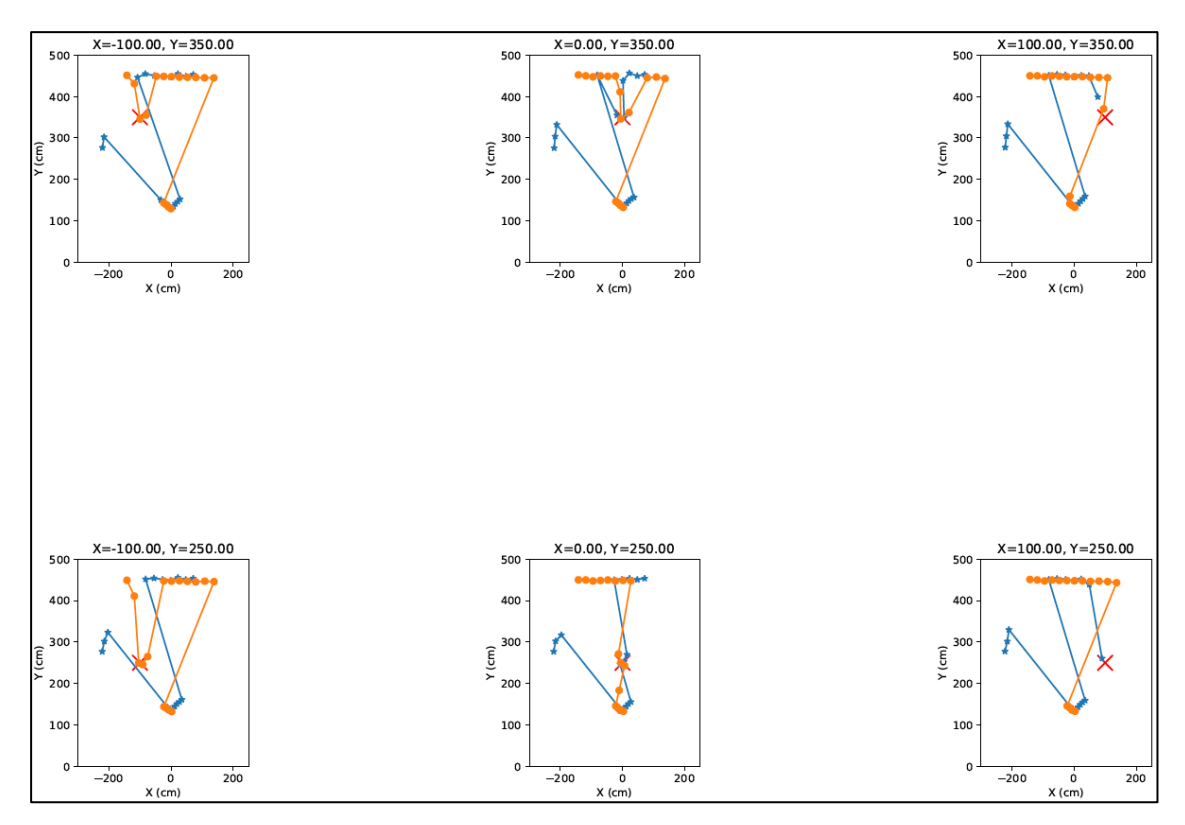


Figure 6.9 Full Dataset of X1 at P7 using two Leddar M16 sensors.

X1 at P5, X2 at P50, P23, P48, P3, P21

Table 6.8 below shows X1 at P5 with X2 moving into five different positions relative to X1. The Python code was programmed to reflect the positions of X2 relative to X1. At positions P48, and P21, X2 was located by one sensor whereas at P3, P23 and P50, X2 were observed by two. As before, no blind spots were identified in this setup.

Table 6.8 Position coordinates reflecting X1 and X2 Layout 3

| X2 at P48 (1) | X2 at P3 (2) | X2 at P21 (1) |
|---------------|--------------|---------------|
| | | |
| X2 at P50 (2) | X1 at P5 | X2 at P23 (2) |

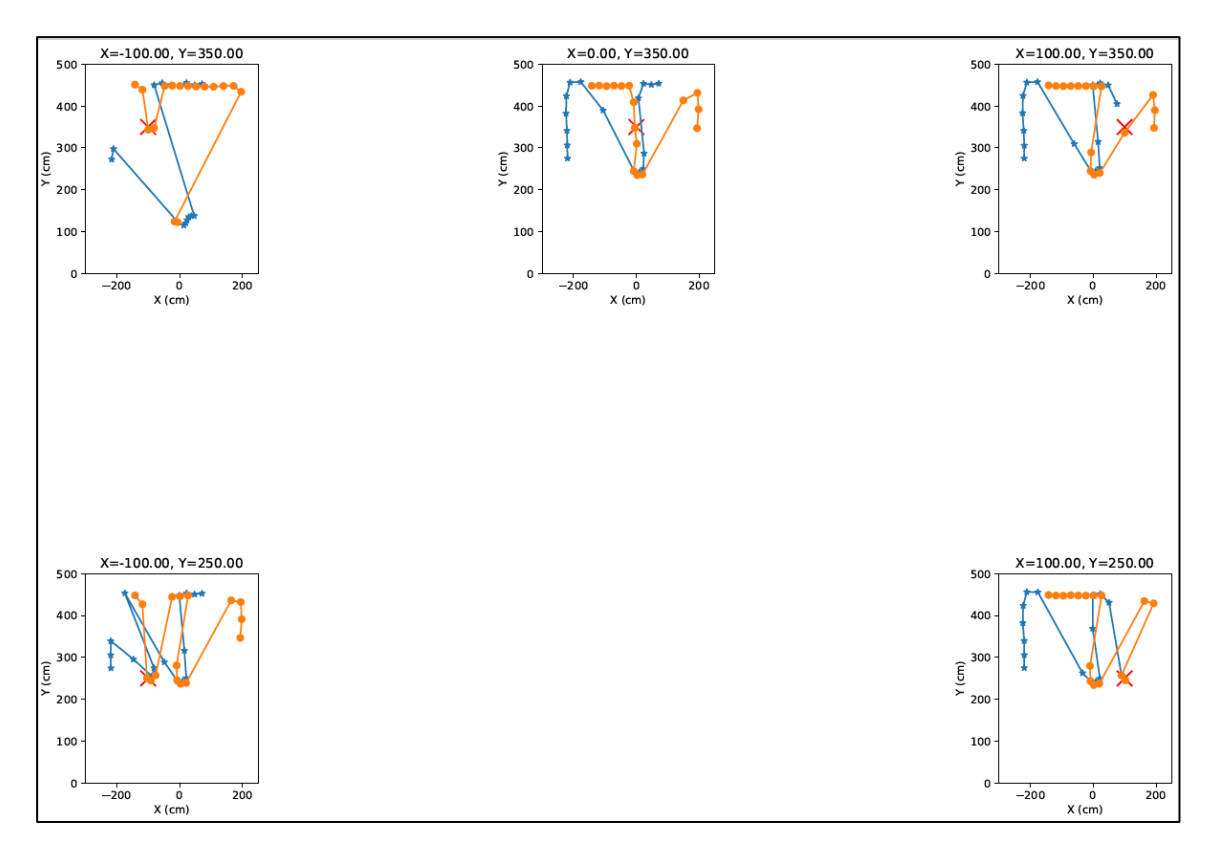


Figure 6.10 Full Dataset of X1 at P5 using two Leddar M16 sensors.

X1 at P50, X2 at P48, P3, P21, P23

Table 6.9 below shows X1 at P50 with X2 moving into four different positions relative to X1. The Python code was programmed locate the positions of X2 relative to X1 and it is seen below that at P48, P21, P3, and P23, X2 was identified by two sensors. Again, no blind spots were identified in this setup.

Table 6.9 Position coordinates reflecting X1 and X2 Layout 4

| X2 at P48 (2) | X2 at P3 (2) | X2 at P21 (2) |
|---------------|--------------|---------------|
| | | |
| X1 at P50 | | X2 at P23 (2) |

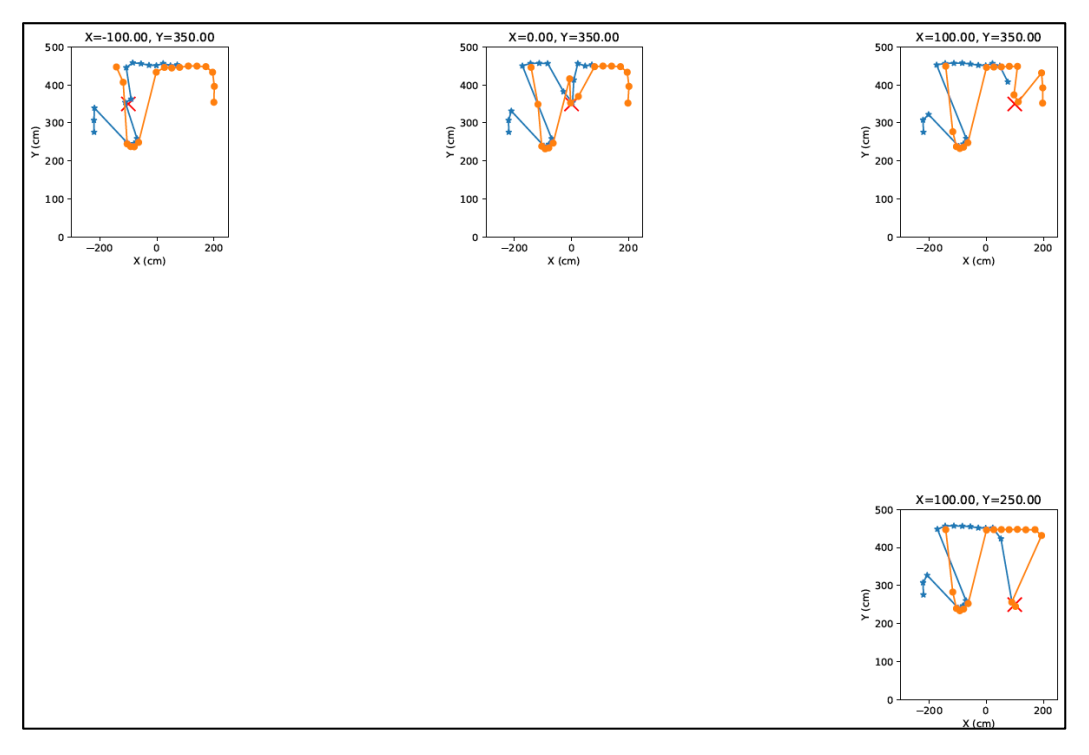


Figure 6.11 Full Dataset of X1 at P50 using two Leddar M16 sensors.

X1 at P3, X2 at P48, P21

Table 6.10 shows X1 at P3 with X2 moving into two different positions relative to X1. We see below that at P48 and P21, X2 was seen by two Leddar M16 sensors. No blind spots were identified in this setup.

Table 6.10 Position coordinates reflecting X1 and X2 Layout 5



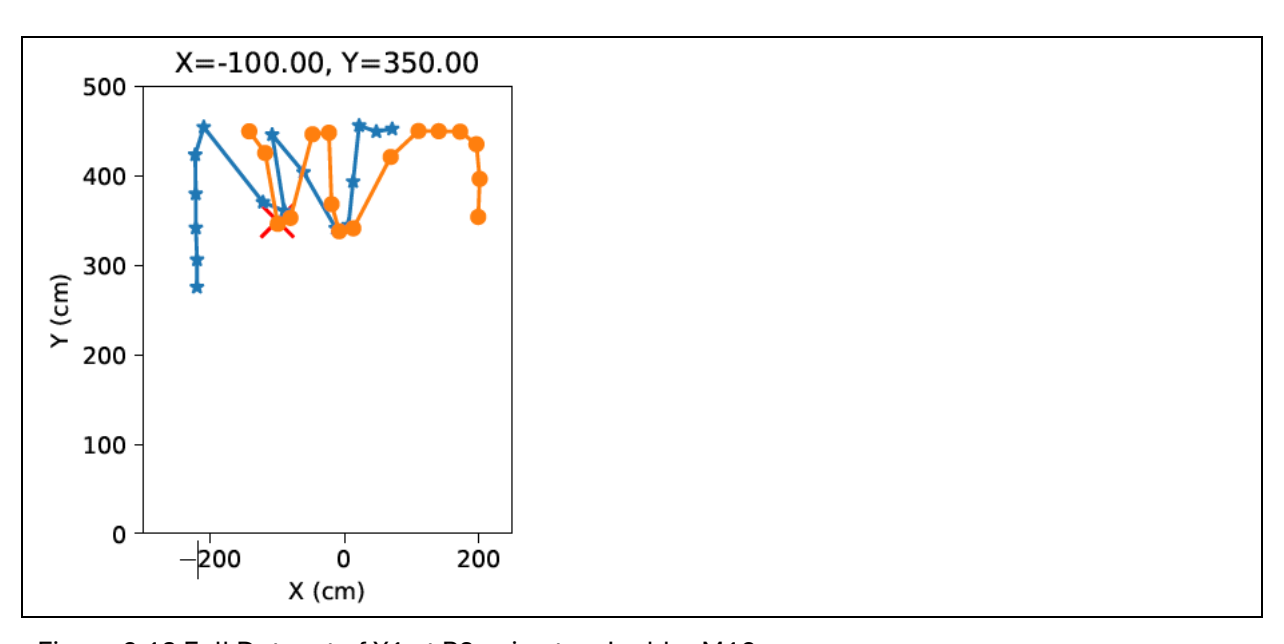


Figure 6.12 Full Dataset of X1 at P3 using two Leddar M16 sensors.

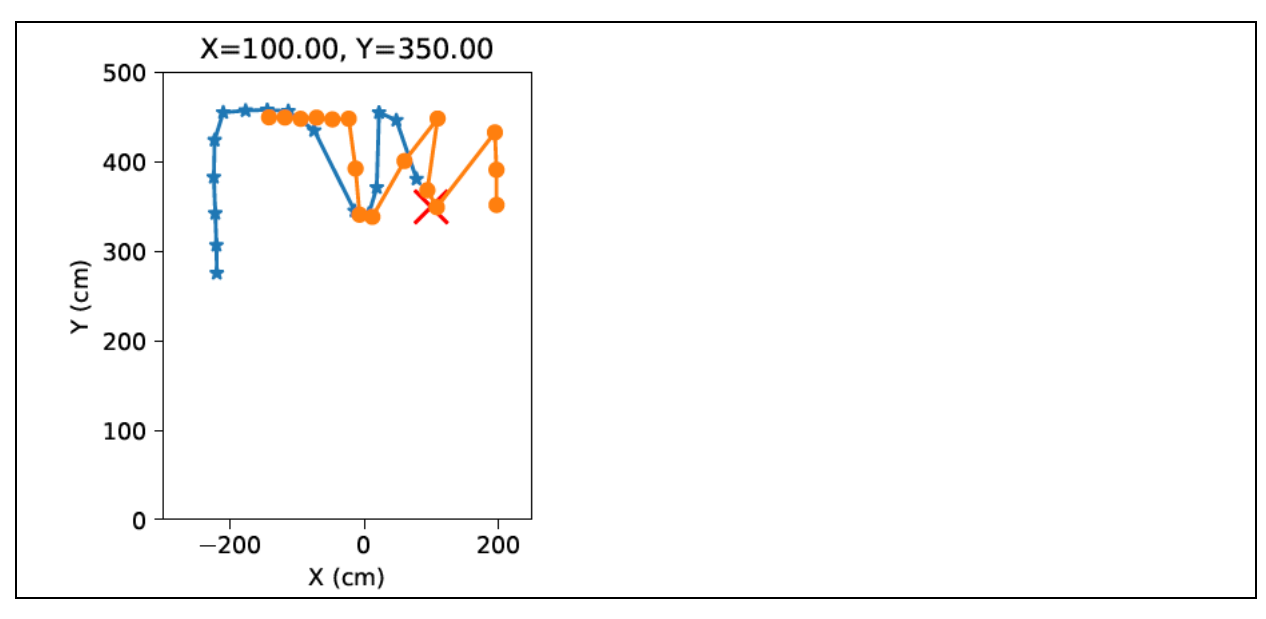


Figure 6.13 Full Dataset of X1 at P48 using two Leddar M16 sensors.

X1 at P48, X2 at P21

Table 6.10 below shows X1 at P3 with X2 moving into one position relative to X1. At P21, X2 was seen by two sensors. Again, no blind spots were identified in this setup.

Table 6.11 Position coordinates reflecting X1 and X2 Layout 6

| X1 at P48 | | X2 at P21 (2) |
|-----------|--|---------------|

6.3.2 One Leddar M16 and One Camera

Following the same steps as in section 6.3.1 and using the data in Table 6.6, the positions of X1 and X2 were taken to use in this section. This section looks at X1 and X2 using one Leddar M16 and one camera.

Table 6.12 below shows X1 at P7 with X2 moving into six different positions relative to X1. The Python code was programmed identify the positions of X2 relative to X1 and it is shown below that at P48, P50, P21 and P23, X2 was seen by one sensor whereas at P3 and P5, X2 was seen by two. Two blind spots were identified in this setup.

Table 6.12

Table 6.12 Position coordinates reflecting X1 and X2 for X1 at P7.



| X2 at P50 (1) | X2 at P5 (0) | X2 at P23 (1) |
|---------------|--------------|---------------|
| | | |
| | X1 at P7 | |

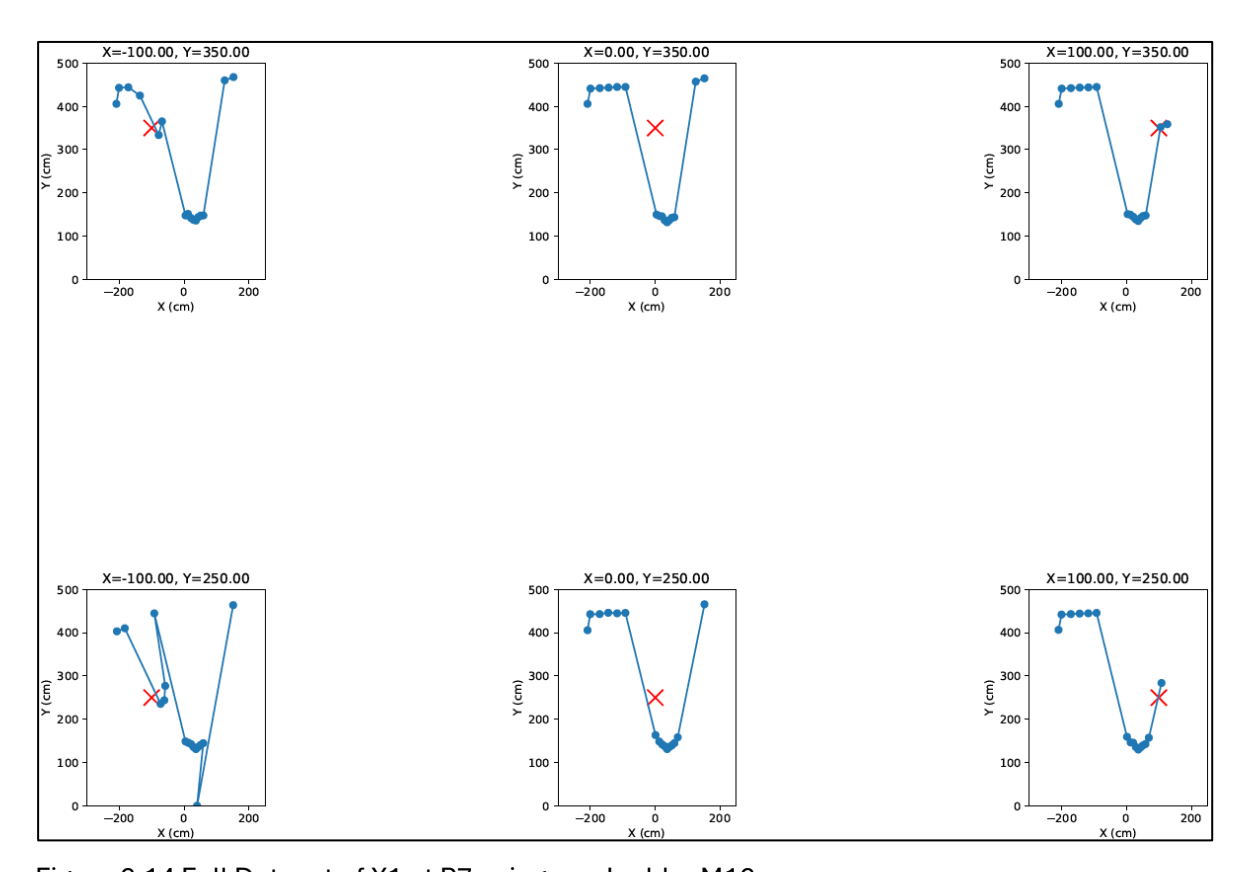


Figure 6.14 Full Dataset of X1 at P7 using one Leddar M16 sensor.

X1 at P5, X2 at P50, P23, P48, P3, P21

Table 6.12 shows X1 at P5 with X2 moving into five different positions relative to X1. At P48, P21, and P50, and partly P23, X2 was seen by the Leddar M16 whereas at P3, X2 was not seen. Comparing results with the camera view, X2 was seen by the camera at P23 in Figure 6.22 and was caught by Leddar M16 channels in Figure 6.23. Therefore, we can conclude that one blind spot was missed in this test.

Table 6.13 Position coordinates reflecting X1 and X2 for X1 at P5.

| X2 at P48 (1) | X2 at P3 (0) | X2 at P21 (1) |
|---------------|--------------|---------------|
| | | |
| X2 at P50 (1) | X1 at P5 | X2 at P23 (1) |

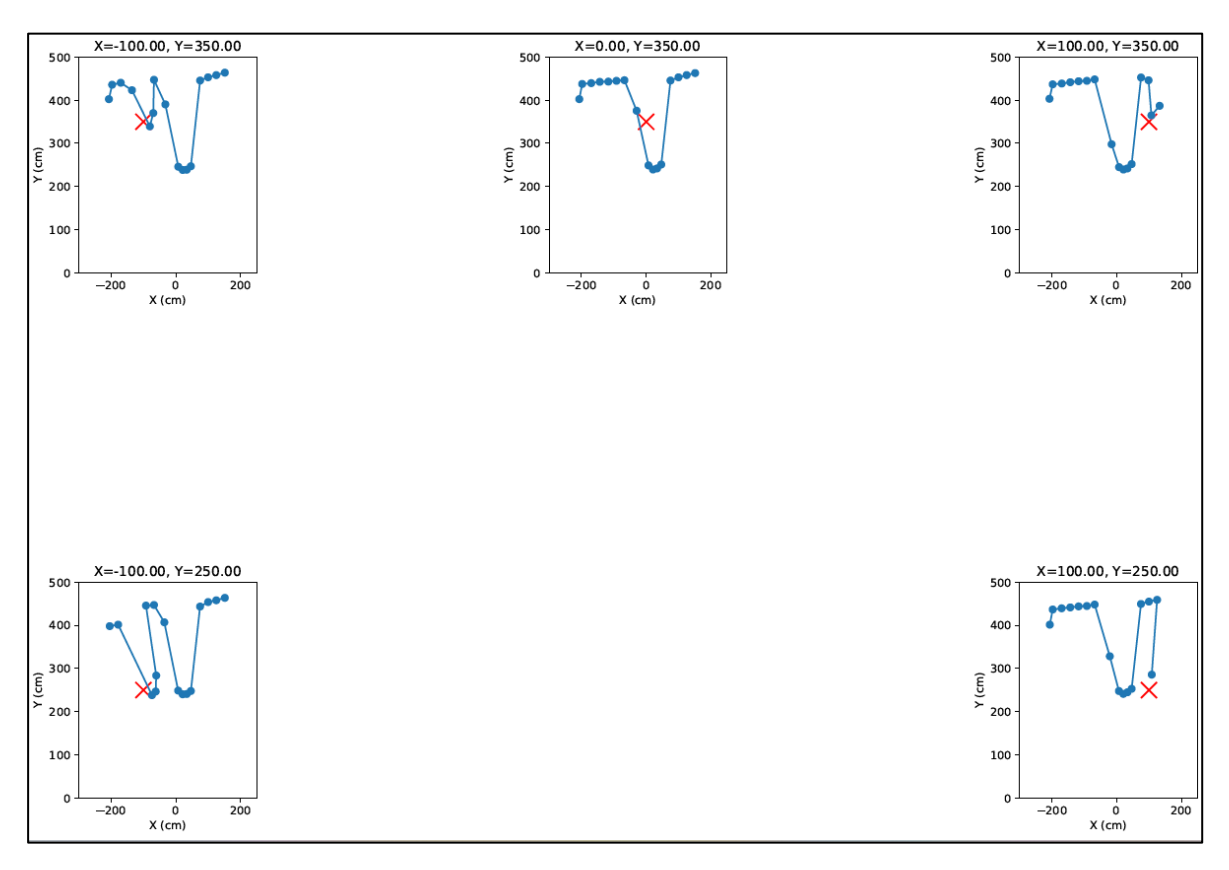


Figure 6.15 Full Dataset of X1 at P5 using one Leddar M16 sensor.

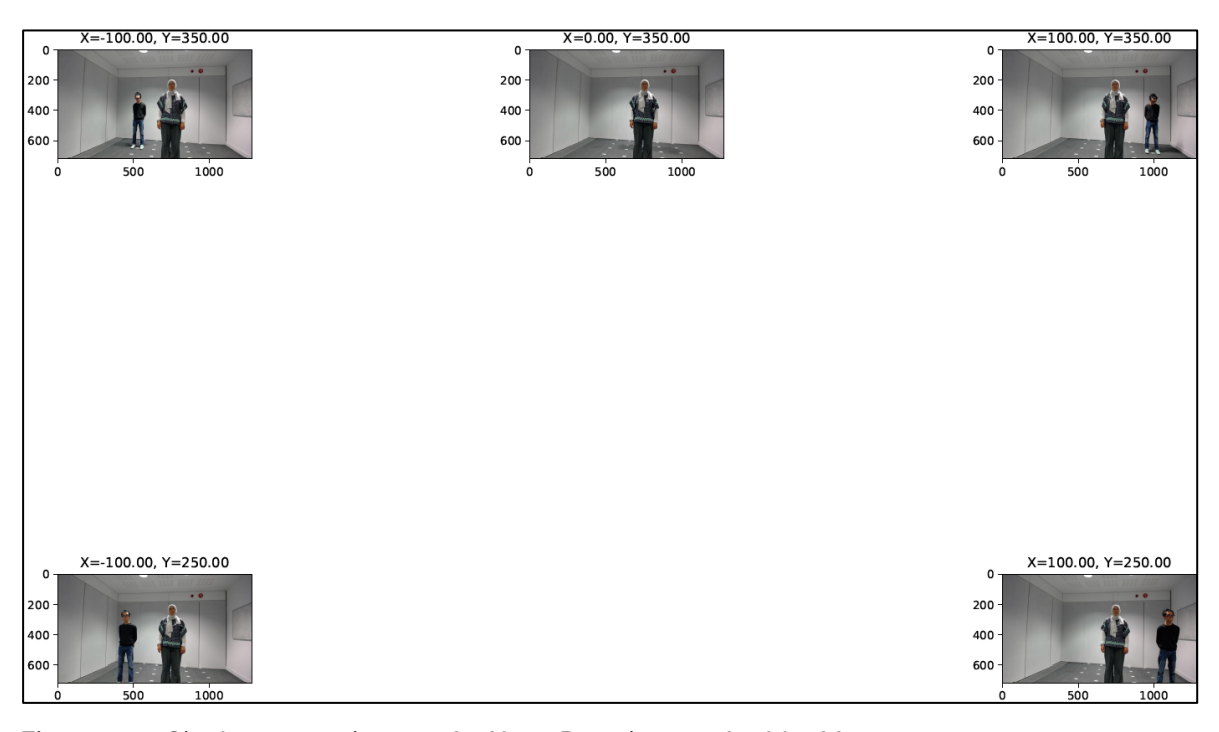


Figure 6.16 Single camera images for X1 at P5 using one Leddar M16 sensor.

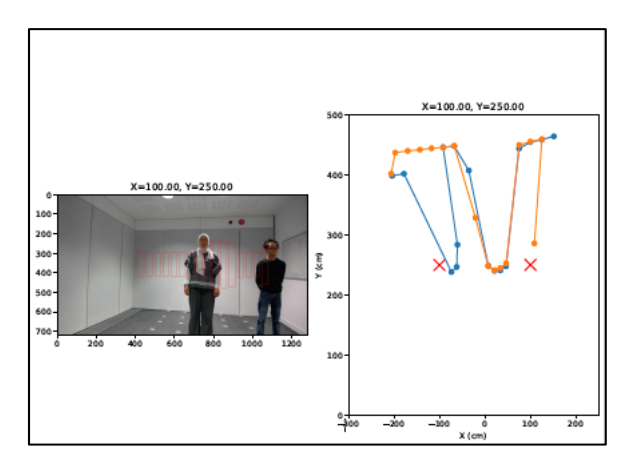


Figure 6.17 Overlay for Single camera and Leddar M16 sensor for X1 at P5 and X2 at P23

X1 at P50, X2 at P48, P3, P21, P23

Table 6.13 shows X1 at P50 with X2 moving into four different positions relative to X1. At P48, P21, P3, and P23, X2 was seen by the Leddar M16 sensor. No blind spots were identified in this setup.

Table 6.14 Position coordinates reflecting X1 and X2 for X1 at P50

| X2 at P48 (1) | X2 at P3 (1) | X2 at P21 (1) |
|---------------|--------------|---------------|
| | | |
| X1 at P50 | | X2 at P23 (1) |

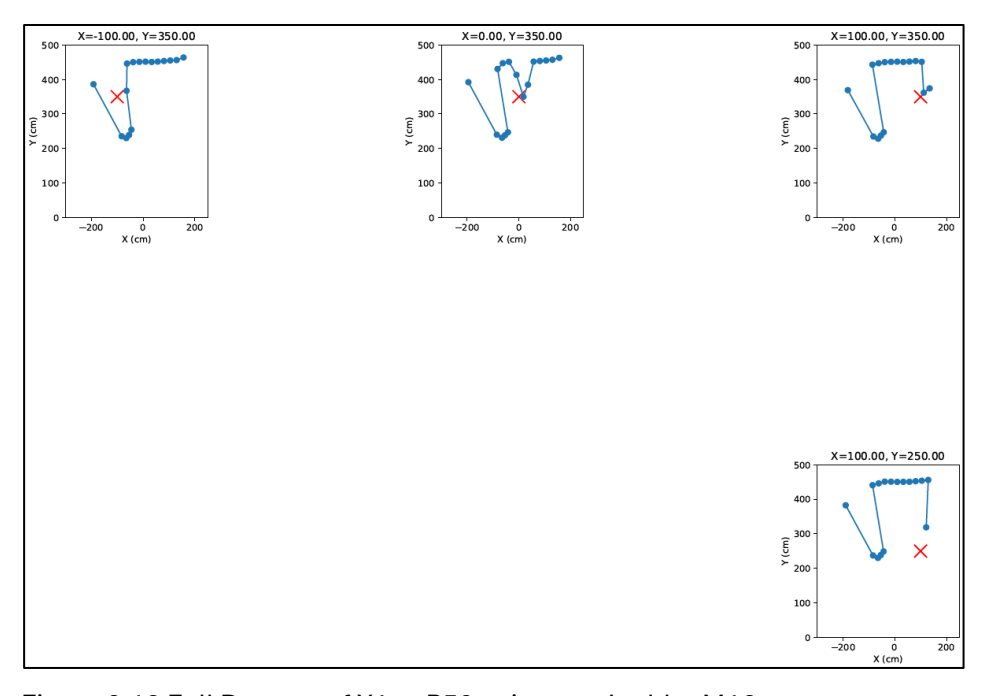


Figure 6.18 Full Dataset of X1 at P50 using one Leddar M16 sensor.

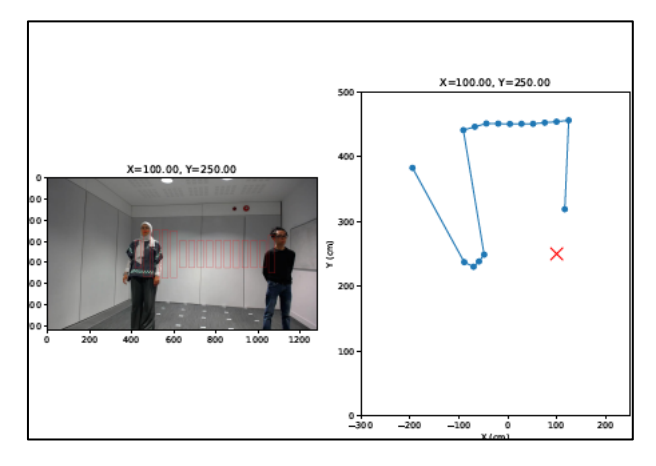


Figure 6.19 Overlay for Single camera and Leddar M16 sensor for X1 at P50 and X2 at P23

X1 at P3, X2 at P48, P21

X1 at P3 with X2 moving into two different positions relative to X1 was shown in Table 6.14. It shows that at P48 and P21, X2 was seen by the Leddar M16 sensor. No blind spots were identified in this setup.

Table 6.15 Position coordinates reflecting X1 and X2 for X2 at P48





Figure 6.20 Full Dataset of X1 at P3 using one Leddar M16 sensor.



Figure 6.21 Full Dataset of X1 at P48 using one Leddar M16 sensor.

X1 at P48, X2 at P21

Table 6.10 shows X1 at P3 with X2 moving into one position relative to X1. The Python code was programmed to reflect on the positions of X2 relative to X1 and we see below that at P21, X2 was seen by two of the sensors. As before, no blind spots were identified in this setup.

Table 6.16 Position coordinates reflecting X1 and X2 for X1 at P48



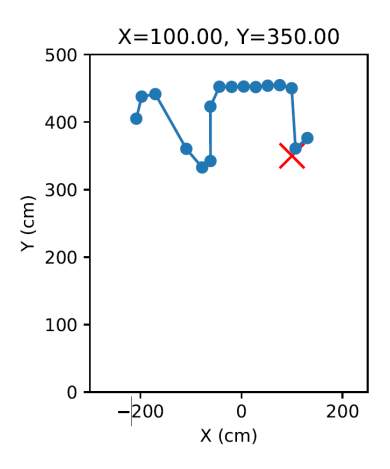


Figure 6.22 Full Dataset of X1 at P48 using one Leddar M16 sensor.

6.3.3 Data Description

In the data analysis, SPSS program was used to describe the data collected during the experiments using a discrete system. This system classified the observations as follows:

- 0 or blind spot: No detection
- 1 (detected by 1 Lidar): Detected
- 2 (detected by both Lidars): Detected

Table 6.17 presents the number of detections using two Leddar M16 sensors. Out of 18 observations, there were no instances where neither sensor detected the object (labelled as 'No'). There were four instances where one sensor detected the object ('Yes (1)'). Additionally, there were 14 instances where both Leddar M16 sensors identified the object ('Yes (2)'). This table helps us understand the distribution of detections based on the two sensors.

The data was also analysed using only one sensor, shown in Table 6.18 Of the 18 observations, there were three instances in which the object was not detected by the sensor ('No'), and 15 instances where the sensor detected the object ('Yes').

Comparing the two setups, the table shows that with two Leddars, detection occurred 100% of the time as opposed to the setup using one LiDAR that detected the object 83.8% of the time. This comparison shows that the two-sensor setup was more effective in terms of the area covered.

In summary, the collected data was analysed using a discrete system (0 for no detection and 1 for detection). The results were tabulated to show the distribution of detections using either 1 or 2 Leddar M16 sensors, enabling us to make comparisons between the two setups. Here's a summary of the distribution in percentages:

Table 6.17 Frequency Distribution for Two Lidars

| Detection Type | Frequency | Percent |
|----------------|-----------|---------|
| No | 0 | 0% |
| Yes (1) | 4 | 22.2% |
| Yes (2) | 14 | 77.8% |

Table 6.18 Frequency Distribution for One Lidar.

| Detection Type | Frequency | Percent |
|----------------|-----------|---------|
| No | 3 | 16.7% |
| Yes | 15 | 83.3% |

6.3.4 Data Comparison & Analysis

A comparison was undertaken to study the performance of a single Leddar M16 sensor system with that of two sensors. The data was processed using discrete values, where '0' indicated an object not seen and '1' represented a seen object. To analyse the results effectively, all the data from the experiment were combined into a single dataset. The variables were named 'Leddar 1' and 'Leddar 2' respectively.

To assess if there was a significant difference between the two sets of results, a paired-sample proportions test was employed. This test determines whether the proportions of successful outcomes in the two sets of data are equal or not. In our experiment, the McNemar test was used for this purpose. The calculated difference in proportions was found to be 0.167, with an asymptotic standard error of 0.088 and a Z-score of 1.732 as shown in Table 6.19. The calculated one-sided p-value was 0.042, while the two-sided p-value was 0.083, as detailed in Tables 6.19 and 6.20. Since the one-sided p-value was 0.04, which is less than the threshold of 0.05, the null hypothesis (that the proportions are equal) can be rejected with a 95% confidence level. The two-sided p-value is not relevant because we are looking specifically for an increase in successful detection with moving from 1 Leddar M16 to 2 Leddar M16. The appropriate p-value is therefore 0.042 which is significant at the 5% level. Mention of the two-sided pvalue has been removed from the thesis.

In conclusion, based on this analysis, we can confidently conclude that there is a significant difference between the proportions of objects detected by the two-sensor system and the "one-sensor system. The 17% difference is notable, with the setup with two Leddar M16s achieving a perfect success rate of 18 out of 18 trials compared to the one-sensor system's success rate of 15 out of 18 trials. This suggests that the system using two Leddar M16 sensors performs better at detecting objects.

Table 6.19 Paired-Samples Proportions Tests

| | | | Asymptotic | | Significance | |
|-------------------------|-----------|---------------|------------|-------|--------------|-------------|
| D.: 4.0 | | Difference in | Standard | | | |
| Pair 1: 2 Leddar - 1 | Test Type | Proportions | Error | z | One-Sided p | Two-Sided p |
| | McNemar | .167 | .088 | 1.732 | .042 | .083 |

Table 6.20 Paired-Samples Proportions Statistics.

| | Successe | Trials | Proportion |
|-------------------|----------|--------|------------|
| 2 Leddar = Yes | 18 | 18 | 1.000 |
| 1 Leddar = Yes | 15 | 18 | .833 |

Chapter 7 Conclusion & Future Work

7.1 Conclusion

Road traffic accidents are commonplace and improvements to road safety remains a challenge. The CAV claim to reduce traffic accidents by reducing human errors, the principal cause of collision. If all vehicles were to be equipped with the appropriate hardware and software, then human errors could be eliminated. The focus of this project was to explore how to improve road safety using LiDAR sensors by reducing blind spots. The proposed research question is whether multiple LiDAR can perform better than single LiDAR.

Previous work was conducted to explore single state LiDAR and how it can improve road safety. The work of this thesis took the previous work a step further and includes cameras and a triangulation method to locate an object, while reducing blind spots. The key areas in this research are LiDAR theory and practice, triangulation, pedestrian safety, autonomous vehicles, Advanced Driver Assistance Systems (ADAS), physics laboratory and engineering laboratory experiments. This study considered all these areas in order to improve pedestrian safety.

Based on the experiments conducted and data analysis achieved here, it can be concluded that Multiple/ Multistatic LiDAR sensors are better than Monostatic LiDAR in reducing blind spots. Hence, this could lead to improving road safety. The work began by understanding how a single LiDAR sensor works in a laboratory environment and then investigated Multiple LiDAR systems by investigating a single object using a triangulation method while focusing on optimal LiDAR sensors placement to reduce blind spots.

In the laboratory experiments, we used a Fianium laser and applied triangulation under different scenarios. We began with conventional LiDAR and investigated different scenarios of LiDAR combined with other sensors. The initial focus of this work was with optics improvements through experiments combined with data analysis and laboratory measurements.

Multistatic LiDAR was then used to examine and complete laboratory experiments for improved setup using triangulation pointing at a static single object. The second part of the experiment was performed in a real-life environment using SSL sensors combined with cameras pointing at single and multiple objects. The project compared the results of theoretical LiDAR sensors versus field experiment solid-state Leddar M16 sensors combined with cameras for testing and validation in real-life controlled. The field experiment included looking at single static and multiple moving objects or pedestrians.

There were many limitations in the field experiment, including the limited space and the unavailability of a dedicated space for this experiment. Therefore, the Leddar M16 sensor and camera setup needed to be dissembled and reassembled each time an experiment was taking place. This could have affected the results meaning some assumptions needed to be made. However, this did not affect the general conclusion that two LiDAR sensors are better than one for reducing blind spots. Thus, this research contributes to advancing the safety performance of a LiDAR setup when installed on CAV.

The results of the field experiment confirmed the conclusions of the laboratory experiment. In that experiment we worked on improving the optical setup. Both lab and field experiments used triangulation/trilateration,. The definition can differ between different scholars; however, the idea is to use two sensors pointing at an angle at one pedestrian and work out the setup to reduce blind spots. In the field experiment, there was a significant difference between the proportions of

objects detected by the two-sensor system and the one-sensor system. This suggests that the system with two Leddar M16 sensors performs better in detecting objects than a single Leddar M16 system. This answers the research question of this thesis.

7.2 Future Work

While this research has provided interesting insights into the comparison of single and multiple lidar configurations, it is noted that there remains a key area in which further investigation is recommended.

When looking at multiple objects and moving objects, the time trace will produce multiple peaks, each corresponding to a different object. It will be difficult to identify those peaks to each corresponding object since the peaks only inform of the presence of the objects in space and not specific objects. This means the analytical method of triangulation, relying on the known distance for a single object from multiple detectors, can no longer be used. In this case neural networks may be able to resolve this issue.

Neural networks are computing systems that use algorithms to recognise unknown patterns and correlate, classify and cluster raw data (Donahoe 1997). It is a method of data analysis that replicates how neural networks in human brains make decisions. The output will identify the peak belonging to the detected objects. Therefore, neural networks can help with multiple objects where analytical methods are not sufficient, it can also help with moving objects. In this situation, neural networks are recommended for further work in the laboratory using multiple Lidar sensors to detect multiple objects and moving objects.

Appendix A Object Location Using Mathematica

Code developed by O. Muskens modified by Z. Nazer Remove["@"] $d1[xo_,yo_]=Sqrt[xo^2+yo^2];$ $d2[xo_,yo_,x1_]=Sqrt[(xo-x1)^2+yo^2];$ $a[xo_{yo}, yo_{x1}] = (d1[xo_{yo}] + d2[xo_{yo}, x1])/2$ $1/2 \left(\sqrt{xo^2 + yo^2} + \sqrt{(-x1 + xo)^2 + yo^2} \right)$ $b[xo,yo,x1]=Sqrt[(a[xo,yo,x1])^2-(x1/2)^2]$ $\sqrt{-\frac{x1^2}{4} + \frac{1}{4} \left(\sqrt{x0^2 + y0^2} + \sqrt{(-x1 + x0)^2 + y0^2}\right)^2}$ ellipse1=(x-x1/2)^2/a[xo,yo,x1]^2+y^2/b[xo,yo,x1]^2==1 $(4 (x-x1/2)^2)/(\sqrt{xo^2 + yo^2} + \sqrt{(-x1 + xo)^2 + yo^2})^2 + y^2/(-(x1^2/4)+1/4)(\sqrt{xo^2 + yo^2} + yo^2)^2$ $\sqrt{(-x1 + x0)^2 + y0^2}_{1^2}$ ellipse2=(x-x2/2)^2/a[xo,yo,x2]^2+y^2/b[xo,yo,x2]^2==1 $(4 (x-x2/2)^2)/(\sqrt{xo^2+yo^2}_+\sqrt{(-x2+xo)^2+yo^2}_)^2+y^2/(-(x2^2/4)+1/4)(\sqrt{xo^2+yo^2}_+$ $\sqrt{(-x^2 + x^0)^2 + y^0^2}$ xobject=-0.3; vobject=0.6; xdet1=0.4; xdet2 = -0.4;solution=Solve[ellipse1,{x,y}]/.{x1->xdet1, xo->xobject, yo->yobject} $\{\{y->-\sqrt{0.556756+0.374773} x-0.936932 x^2\}, \{y->-\sqrt{0.556756+0.374773} x-\sqrt{0.936932} x^2\}$ $\sqrt{0.556756 + 0.374773 \times - 0.936932 \times^2}$ sol2y1[x]=solution[[2,1,2]] $\sqrt{0.556756 + 0.374773 \times - 0.936932 \times^2}$ graph1=Plot[sol2y1[x],{x,-1.0,1.0}];

solution2=Solve[ellipse2,{x,y}]/.{x2->xdet2, xo->xobject, yo->yobject}

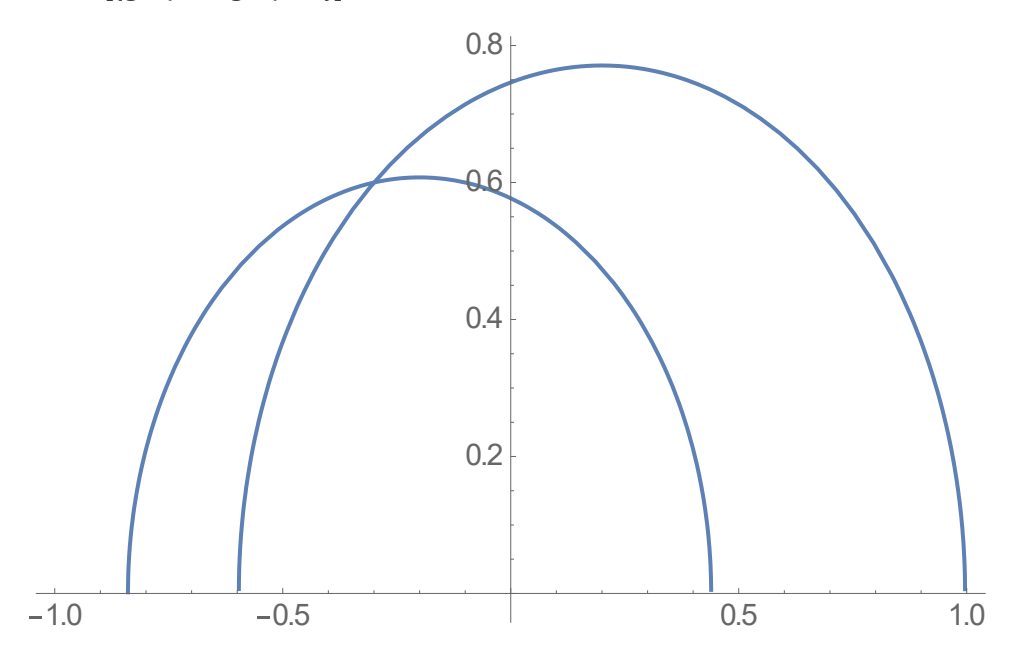
$$\begin{array}{l} \{\{y->_{-}\sqrt{0.332934}-0.360882\,x-0.902206\,x^2\,\}, \{y->_{-}\sqrt{0.332934}-0.360882\,x-0.902206\,x^2\,\}\} \end{array}$$

sol2y2[x]=solution2[[2,1,2]]

$$\sqrt{0.332934} - 0.360882 x - 0.902206 x^2$$

graph2=Plot[sol2y2[x],{x,-1.0,1.0}];

Show[{graph1,graph2}]



eq1=sol2y1[x]==sol2y2[x]

$$\sqrt{0.556756 - 0.374773 \times - 0.936932 \times^2} = \sqrt{0.332934 + 0.360882 \times - 0.902206 \times^2}$$

solutionx=Solve[eq1,x,Reals][[1,1,2]]

0.3

sol2y1[solutionx]

0.6

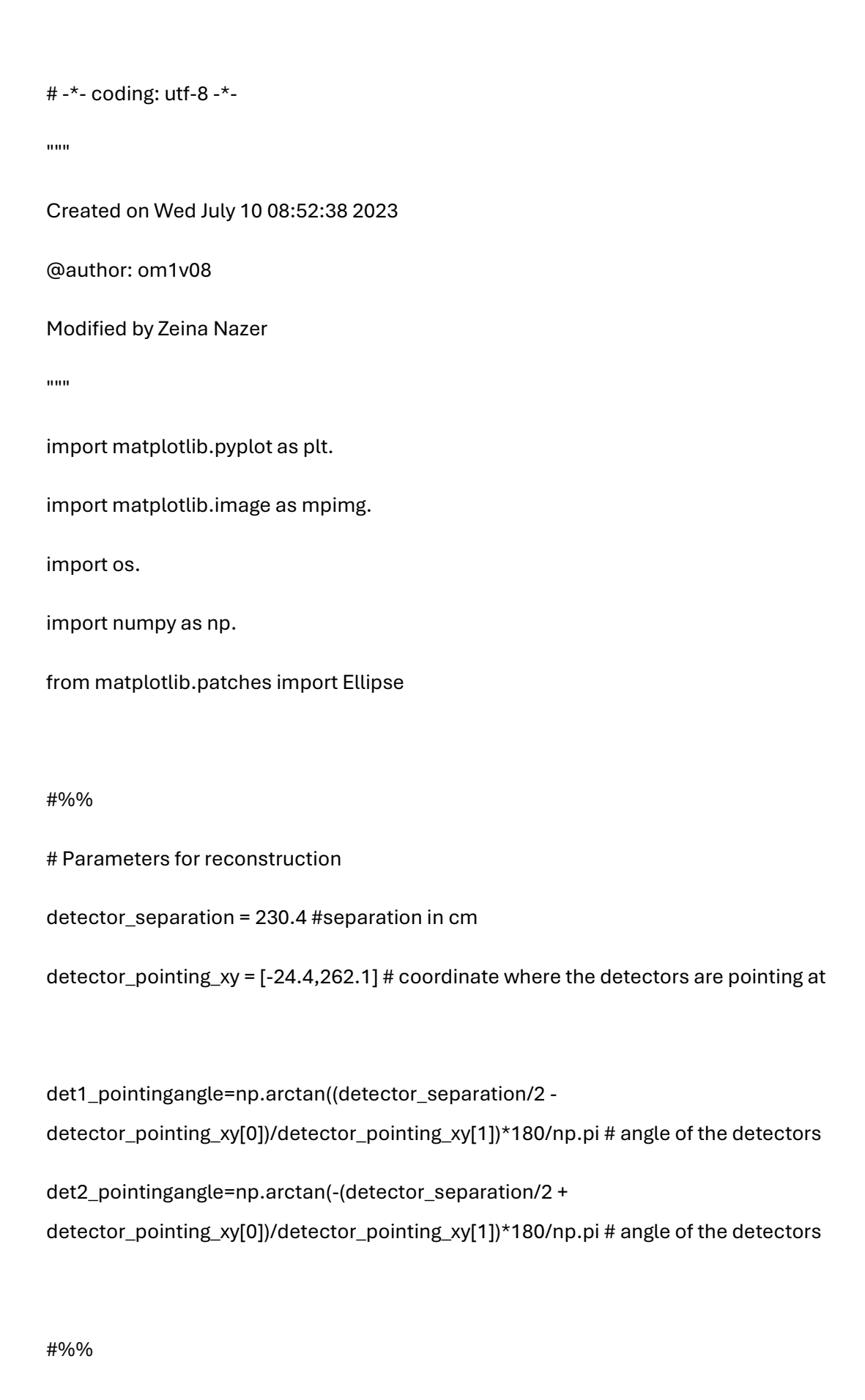
Appendix B Object Location Using Python Coding

```
#!/usr/bin/env python
# -*- coding: utf-8 -*-
illustration for optical triangulation
P.R. Wiecha, modified by Z Nazer on 20/07/2023.
import numpy as np.
import matplotlib.pyplot as plt.
#
# config geometry
## light source position
rs = np.array([0.0,0.5])
## detector positions
rd1 = np.array([0.0,0.0])
rd2 = np.array([0.3,0.0])
rd3 = np.array([0.6,0.0])
rd4 = np.array([0.9,0.0])
#rd_list = [rd1]
#rd_list = [rd2]
rd_list = [rd1, rd2]
rd_list = [rd1, rd2, rd3, rd4]
## object positions
ro1 = np.array([0.3, 0.4])
ro2 = np.array([0.5, 0.8])
```

```
ro_list = [ro1]
#ro_list = [ro1, ro2]
def get_ellipse(rs, rd, ro, N_points=100):
  .....
  ellipse parametrization, defined by foci (rs, rd) and some point (ro) on perimeter.
  ## ellipse parameters
  L = np.linalg.norm(rs - ro)+ np.linalg.norm(ro - rd)
  a = L/2.
  c = np.linalg.norm(rs - rd)/2.
  b = np.sqrt(a**2 - c**2)
    ## center position and rotation angle of ellipse
  r0 = (rs - rd)/2.
  angle = np.arctan2(r0[1], r0[0])
    ## calculate X/Y positions on positive half-ellipse
  Xellipse = np.linspace(-a, a, N_points)
  Yellipse = b/a * np.sqrt(a**2 - Xellipse**2)
  ## add roundtrip (second half of ellipse)
  Xellipse = np.concatenate([Xellipse, Xellipse[::-1]])
  Yellipse = np.concatenate([Yellipse, -1*Yellipse[::-1]])
    ## rotate and shift
  Xellipse_rot = Xellipse*np.cos(angle) - Yellipse*np.sin(angle)
  Yellipse_rot = Xellipse*np.sin(angle) + Yellipse*np.cos(angle)
  Xellipse = Xellipse_rot - r0[0]
  Yellipse = Yellipse_rot + r0[1]
    return Xellipse, Yellipse
#%%
# evaluate and plot
```

```
colors_det = ['C2', 'C1', 'C5', 'C6', 'C4']
colors_obj = ['c', 'm', 'b', 'k', 'g']
plt.figure(figsize=(7,7))
plt.subplot(aspect='equal')
## iterate detectors
for i_det, rd in enumerate(rd_list):
  ## plot detector and lightsource
  if i_det == len(rd_list)-1:
    label_src = 'src'; label_obj = 'obj'
  else:
    label_src = "; label_obj = "
  plt.scatter(rd[0], rd[1], color=colors_det[i_det], s=200, marker='s',
label='detector{}'.format(i_det), zorder=99)
  plt.scatter(rs[0], rs[1], color='r', s=150, marker='x', linewidth=3, label=label_src, zorder=99)
    ## iterate objects
  for i_obj, ro in enumerate(ro_list):
    ## plot exact position and detector/source ellipse
    plt.scatter(ro[0], ro[1], color=colors_obj[i_obj], s=70, marker='o', label=label_obj, zorder=99)
    Xellipse, Yellipse = get_ellipse(rs, rd, ro)
    plt.plot(Xellipse, Yellipse, color=colors_obj[i_obj], lw=1.25, zorder=10)
    plt.plot(Xellipse, Yellipse, dashes=[4,4], color=colors_det[i_det], lw=2, zorder=11)
  plt.xlabel("X (m)")
plt.ylabel("Y (m)")
plt.legend(loc=1, ncol=2)
#plt.savefig("plot_ToF_triangulation.png", dpi=150) # save figure as png
plt.show()
```

Appendix C Python Coding for Leddar M16



```
all_dist_det1 = [] # array of distances
all_dist_det2 = [] # array of distances
all_ampl_det1 = [] # array of amplitudes
all_ampl_det2 = [] # array of amplitudes
all_x = [] # array of coordinates
all_y = []
all_points = [] # array of point indices
all_image1 = [] # array of images
all_image2 = [] # array of images
all_overlay1 = [] # array of images
all_overlay2 = [] # array of images
P5-2Lidar"
SUFFIX = ".lvm"
PREFIX = "T"
filelist = sorted([f for f in os.listdir(data_folder) if (f.startswith(PREFIX) and
                 f.endswith(SUFFIX))])
for i_file, f in enumerate(filelist):
 if i_file%1==0:
   print("load {}".format(i_file))
   ## --- parse parameters
```

```
if f.find('_leddar1')!=-1:
  #point = float(f.split('T')[1].split('X')[0])
 x = float(f.split('X')[1].split('Y')[0])
 y = float(f.split('Y')[1].split('multi')[0])
  #load data
  dataset=np.loadtxt(os.path.join(data_folder, f))
  #all_points.append(point)
  all_x.append(x)
  all_y.append(y)
  all_dist_det1.append(dataset[0:16,0])
  all_ampl_det1.append(dataset[0:16,1])
if f.find('_leddar2')!=-1:
  #point = float(f.split('P')[1].split('X')[0])
  #x = float(f.split('X')[1].split('Y')[0])
  #y = float(f.split('Y')[1].split('X')[0])
  #load data
  dataset=np.loadtxt(os.path.join(data_folder, f))
  #all_points.append(point)
  #all_x.append(x)
  #all_y.append(y)
  all_dist_det2.append(dataset[0:16,0])
  all_ampl_det2.append(dataset[0:16,1])
```

#%%

```
SUFFIXJPG = ".jpg"
PREFIX = "T"
filelistjpg = sorted([f for f in os.listdir(data_folder) if (f.startswith(PREFIX) and
                    f.endswith(SUFFIXJPG))])
for i_file, f in enumerate(filelistjpg):
  if i_file%1==0:
   print("load {}".format(i_file))
    ## --- parse parameters
  if f.find('_camera1')!=-1:
    #load data
   jpgset= mpimg.imread(os.path.join(data_folder, f))
    all_image1.append(jpgset)
  if f.find('_camera2')!=-1:
    #load data
   jpgset= mpimg.imread(os.path.join(data_folder, f))
    all_image2.append(jpgset)
  if f.find('_overlay1')!=-1:
    #load data
   jpgoverlayset= mpimg.imread(os.path.join(data_folder, f))
```

```
all_overlay1.append(jpgoverlayset)
  if f.find('_overlay2')!=-1:
    #load data
   jpgoverlayset= mpimg.imread(os.path.join(data_folder, f))
   all_overlay2.append(jpgoverlayset)
#%%
#fileidx=1 # select one dataset from the total
anglearr=np.arange(0,16)*3.0-22.5 # angles covered by the leddar channels in degrees
det1_anglearr=(anglearr-det1_pointingangle)*np.pi/180 # in radians
det2_anglearr=(anglearr-det2_pointingangle)*np.pi/180
#%%
# for fileidx in np.arange(0, len(all_x)):
# dist_det1=all_dist_det1[fileidx]
# dist_det2=all_dist_det2[fileidx]
# x=all_x[fileidx]
# y=all_y[fileidx]
```

```
#define the object
  object1 = Ellipse((x,y), width=50, height=50, facecolor='r')
   det1_tox=dist_det1*np.cos(det1_anglearr)
   det1_toy=dist_det1*np.sin(det1_anglearr)+detector_separation/2
   det2_tox=dist_det2*np.cos(det2_anglearr)
  det2_toy=dist_det2*np.sin(det2_anglearr)-detector_separation/2
   fig,ax = plt.subplots(figsize=(6.5,6))
   ax.plot(det1_toy,det1_tox,'-*')
   ax.plot(det2_toy,det2_tox,'-o')
   plt.xlim([-300,250])
   plt.ylim([0,500])
   ax.add_patch(object1)
   plt.title('reconstruction X={:.2f}, Y={:.2f}'.format(x,y))
   plt.xlabel('X (cm)')
   plt.ylabel('Y (cm)')
   plt.show()
#%%
# all graphs in one large display
fig=plt.figure(figsize=(20,29))
```

```
for fileidx in np.arange(0, len(all_x)):
  dist_det1=all_dist_det1[fileidx]
  dist_det2=all_dist_det2[fileidx]
  x=all_x[fileidx]
  y=all_y[fileidx]
  det1_toy=dist_det1*np.cos(det1_anglearr)
  det1_tox=dist_det1*np.sin(det1_anglearr)+detector_separation/2
  det2_toy=dist_det2*np.cos(det2_anglearr)
  det2_tox=dist_det2*np.sin(det2_anglearr)-detector_separation/2
  subplotidx=int((x+150)/50+((450-y)/50)*7)
  plt.subplot(9, 7, subplotidx+1)
  plt.scatter(x,y, marker='x', color='r', s=200)
  plt.plot(det1_tox,det1_toy,'-*')
  plt.plot(det2_tox,det2_toy,'-o')
  plt.xlim([-300,250])
  plt.ylim([0,500])
  plt.title('X={:.2f}, Y={:.2f}'.format(x,y))
  plt.xlabel('X (cm)')
  plt.ylabel('Y (cm)')
plt.tight_layout()
  #plt.show()
plt.savefig('Fulldataset.pdf',
```

format='pdf', bbox_inches='tight', transparent=True, dpi=600) # bbox_inches='tight'

```
#%%
# all images in one large display
fig=plt.figure(figsize=(10,29))
for fileidx in np.arange(0, len(all_x)):
  image_det1=all_image1[fileidx]
  image_det2=all_image2[fileidx]
  x=all_x[fileidx]
  y=all_y[fileidx]
  subplotidx=int((450-y)/50*2)
  dist_det1=all_dist_det1[fileidx]
  dist_det2=all_dist_det2[fileidx]
  det1_toy=dist_det1*np.cos(det1_anglearr)
  det1_tox=dist_det1*np.sin(det1_anglearr)+detector_separation/2
  det2_toy=dist_det2*np.cos(det2_anglearr)
  det2_tox=dist_det2*np.sin(det2_anglearr)-detector_separation/2
  plt.subplot(5, 2, subplotidx+2)
  plt.scatter(x,y, marker='x', color='r', s=200)
  plt.plot(det1_tox,det1_toy,'-*')
  plt.plot(det2_tox,det2_toy,'-o')
  plt.xlim([-300,250])
  plt.ylim([0,500])
```

```
plt.title('X={:..2f}, Y={:..2f}'.format(x,y))
  plt.xlabel('X (cm)')
  plt.ylabel('Y (cm)')
  overlay_det1=all_overlay1[fileidx]
  overlay_det2=all_overlay2[fileidx]
  x=all_x[fileidx]
 y=all_y[fileidx]
  plt.subplot(5, 2, subplotidx+1)
  combined_image = np.concatenate((overlay_det1, overlay_det2), axis=0)
  plt.imshow(combined_image)
  plt.title('X={:.2f}, Y={:.2f}'.format(x,y))
plt.tight_layout()
  #plt.show()
plt.savefig('Overlays.pdf',
     format='pdf', bbox_inches='tight', transparent=True, dpi=600) # bbox_inches='tight'
```

Definitions and Abbreviations

- AASHTO. 2018. A Policy on Geometric Design of Highways and Streets 2018 7th Edition.
- Adam Frost. 2018. "LeddarTech Launches Two New Solid-State Lidar Sensors for ITS Applications at World Congress." *Traffic Technology Today*, September.
- Angelov, Aleksandar, Andrew Robertson, Roderick Murray-Smith, and Francesco Fioranelli. 2018. "Practical Classification of Different Moving Targets Using Automotive Radar and Deep Neural Networks." *IET Radar, Sonar & Navigation* 12 (10): 1082–89. https://doi.org/10.1049/iet-rsn.2018.0103.
- Armenta, Antonio. 2021. "Safety Considerations for LiDAR Sensors."

 Https://Control.Com/Technical-Articles/Safety-Considerations-for-Lidar-Sensors/. 2021.
- Arrow.com. 2018. "How Does an Ultrasonic Sensor Work."

 Https://Www.Arrow.Com/En/Research-and-Events/Articles/Ultrasonic-Sensors-How-They-Work-and-How-to-Use-Them-with-Arduino#:~:Text=Ultrasonic%20sensors%20work%20by%20emitting,Based%20on%20the %20time%20required. 2018.
- Bo Liu Yu Yang Jiang Shuo. 2019. "Review of Advances in LiDAR Detection and 3D Imaging." Guangdian Gongcheng/Opto-Electronic Engineering.
- Bole, Alan, Alan Wall, and Andy Norris. 2014. "The Radar System Technical Principles." *Radar and ARPA Manual*, January, 29–137. https://doi.org/10.1016/B978-0-08-097752-2.00002-7.
- Bosch, Thierry. 2001. "Laser Ranging: A Critical Review of Usual Techniques for Distance Measurement." *Optical Engineering* 40 (1): 10. https://doi.org/10.1117/1.1330700.
- Bucsuházy, Kateřina, Eva Matuchová, Robert Zůvala, Pavlína Moravcová, Martina Kostíková, and Roman Mikulec. 2020. "Human Factors Contributing to the Road Traffic Accident Occurrence." *Transportation Research Procedia* 45:555–61. https://doi.org/10.1016/j.trpro.2020.03.057.
- Burke, Katie. 2019. "How Does A Self-Driving Car See?"

 Https://Blogs.Nvidia.Com/Blog/2019/04/15/How-Does-a-Self-Driving-Car-See/#:~:Text=Autonomous%20vehicles%20rely%20on%20cameras,To%20provide%20long%2Drange%20visuals. 2019.

- Caramazza, Piergiorgio, Alessandro Boccolini, Daniel Buschek, Matthias Hullin, Catherine F Higham, Robert Henderson, Roderick Murray-Smith, and Daniele Faccio. 2018. "Neural Network Identification of People Hidden from View with a Single-Pixel, Single-Photon Detector OPEN." Scientific REPORts | 8:11945. https://doi.org/10.1038/s41598-018-30390-0.
- Cprime. n.d. "CAV vs AV." Accessed March 19, 2024.

 https://www.cprime.com/resources/blog/connected-and-autonomous-vehicles-main-differences-promising-benefits-and-concerns/#:~:text=The%20main%20difference%20between%20connected,synonym%20for%20self%2Ddriving%20cars.
- Critchley, Liam. 2019. "LiDAR vs. Radar."

 Https://Www.Azooptics.Com/Article.Aspx?ArticleID=1527. 2019.
- Crouch, Stephen. 2019. "Frequency-Modulated Continuous-Wave Lidar Has All-Weather Capabilities." *Laser Focus World*, no. June. https://www.laserfocusworld.com/lasers-sources/article/14035383/frequency-modulated-continuous-wave-lidar-has-all-weather-capabilities.
- Crowe, Robert. 2024. "SwRI DEVELOPS OFF-ROAD AUTONOMOUS DRIVING TOOLS FOCUSED ON CAMERA VISION." San Antonio.
- Dahlia Sam E. Evangelin Cyril RAJ Velanganny. 2015. "Improving Road Safety for Pedestrians in Black Spots Using a Hybrid Vanet of Vehicular Sensors and Pedestrian Body Unit ." ARPN Journal of Engineering and Applied Sciences, January.
- Dai, Zhuoqun, Alexander Wolf, Peer-Phillip Ley, Tobias Glück, Max Caspar Sundermeier, and Roland Lachmayer. 2022. "Requirements for Automotive LiDAR Systems." *Sensors* 22 (19): 7532. https://doi.org/10.3390/s22197532.
- Donahoe, John W. 1997. "Chapter 1 The Necessity of Neural Networks." *Advances in Psychology* 121 (C): 1–19. https://doi.org/10.1016/S0166-4115(97)80087-8.
- Doughty, S.R., K. Woodbridge, and C.J. Baker. 2007. "Improving Resolution Using Multistatic Radar." In *IET International Conference on Radar Systems 2007*, 23–23. IEE. https://doi.org/10.1049/cp:20070498.
- Emery, William, and Adriano Camps. 2017. "Remote Sensing Using Global Navigation Satellite System Signals of Opportunity." *Introduction to Satellite Remote Sensing*, January, 455–564. https://doi.org/10.1016/B978-0-12-809254-5.00006-3.

- Fölster, Florian, Hermann Rohling, and Senior Member. 2005. "Data Association and Tracking for Automotive Radar Networks." *IEEE TRANSACTIONS ON INTELLIGENT TRANSPORTATION SYSTEMS* 6 (4). https://doi.org/10.1109/TITS.2005.858784.
- Ge, Yi, Peter J. Jin, Tianya T. Zhang, and Anjiang Chen. 2023. "Roadside LiDAR Sensor Configuration Assessment and Optimization Methods for Vehicle Detection and Tracking in Connected and Automated Vehicle Applications." *Transportation Research Record:* Journal of the Transportation Research Board, June. https://doi.org/10.1177/03611981231172949.
- Gentile, R. 2019. "Algorithms to Antenna: Modeling Multistatic Radar Systems."

 Https://Www.Mwrf.Com/Technologies/Embedded/Systems/Article/21849980/MathworksAlgorithms-to-Antenna-Modeling-Multistatic-Radar-Systems. 2019.
- German Sharabock. 2020. "Why Tesla Won't Use LIDAR." Towards Data Science, September.
- GIS. 2023. "Differences between Triangulation and Trilateration." 2023.
- Gottinger, Michael, Marcel Hoffmann, Mark Christmann, Martin Schütz, Fabian Kirsch, Peter Gulden, and Martin Vossiek. n.d. "Coherent Automotive Radar Networks: The Next Generation of Radar-Based Imaging and Mapping."

 https://doi.org/10.1109/JMW.2020.3034475.
- Gouda, Maged, Alexander Epp, Rowan Tilroe, and Karim El-Basyouny. 2022. "Traffic Sign Extraction Using Deep Hierarchical Feature Learning and Mobile Light Detection and Ranging (LiDAR) Data on Rural Highways." https://doi.org/10.1080/15472450.2022.2074792.
- Hadji, Bahman. 2021. "Demystifying LiDAR: An In-Depth Guide to the Great Wavelength Debate." Https://Www.Eetimes.Com/Demystifying-Lidar-an-in-Depth-Guide-to-the-Great-Wavelength-Debate/. 2021.
- Hearst Autos Research. 2020. "How Many Miles Does a Car Last?"

 Https://Www.Caranddriver.Com/Research/A32758625/How-Many-Miles-Does-a-Car-Last/.
- Hecht, Jeff. 2013. "PHOTONIC FRONTIERS: OPTICAL ANTENNAS: Optical Antennas Concentrate Light and Direct Beams," 2013.
- "IEC60825-1 Safety of Laser Products." n.d. http://www.iec.ch.

- Ignatious, Henry Alexander, Hesham El-Sayed, and Manzoor Ahmed Khan. 2023. "Sensor Technology for Autonomous Vehicles." *Encyclopedia of Sensors and Biosensors: Volume*1-4, First Edition 1–4 (January):35–51. https://doi.org/10.1016/B978-0-12-822548-6.00122-9.
- Jim Hyen Park. 2008. "Multiple Scattering Measurements Using Multistatic LiDAR." https://slate.com/technology/2023/07/cruise-autonomous-vehicles-safety-waymo-self-driving-cars-ad-new-york-times.html.
- Jin Hyen Park. 2008. "MULTIPLE SCATTERING MEASUREMENTS USING MULTISTATIC LIDAR." University of Pennsylvania.
- John Dinan. 2021. "Using Solid-State Flash LiDAR Technology to Access Better and Lower-Cost Vehicle Profiling Data in E-Tolling Applications." *Leddar Tech White Paper*, October.
- Johnson, Steven, Miles J. Padgett, Catherine Higham, and Roderick Murray-Smith. 2021. "LIDAR Using a Deep-Learning Approach." In *AI and Optical Data Sciences II*, edited by Ken-ichi Kitayama and Bahram Jalali, 20. SPIE. https://doi.org/10.1117/12.2576884.
- Kim, Tae-Hyeong, and Tae-Hyoung Park. 2020. "Placement Optimization of Multiple Lidar Sensors for Autonomous Vehicles." *IEEE Transactions on Intelligent Transportation Systems* 21 (5): 2139–45. https://doi.org/10.1109/TITS.2019.2915087.
- LeddarTech. 2019. 54A0040-3EN M16 Laser User Guide, issued 2019.
- Leddartech. 2022. "An Explanation of LiDAR Components and Their Functions in a LiDAR Sensor for ADAS and Autonomous Vehicles ."
- Lemmetti, Juha, Niklas Sorri, Ilkka Kallioniemi, Petri Melanen, and Petteri Uusimaa. 2021. "Long-Range All-Solid-State Flash LiDAR Sensor for Autonomous Driving." In *High-Power Diode Laser Technology XIX*, edited by Mark S. Zediker, 22. SPIE. https://doi.org/10.1117/12.2578769.
- Li, You, and Javier Ibanez-Guzman. 2020. "Lidar for Autonomous Driving: The Principles, Challenges, and Trends for Automotive Lidar and Perception Systems." *IEEE Signal Processing Magazine* 37 (4): 50–61. https://doi.org/10.1109/MSP.2020.2973615.
- Lopac, Nikola, Irena Jurdana, Adrian Brnelić, and Tomislav Krljan. 2022. "Application of Laser Systems for Detection and Ranging in the Modern Road Transportation and Maritime Sector." Sensors 22 (16): 5946. https://doi.org/10.3390/s22165946.

- McManamon, Paul F. 2019. "Design Considerations for an Auto LiDAR." In *ODS 2019: Industrial Optical Devices and Systems*, edited by Ryuichi Katayama and Yuzuru Takashima, 16. SPIE. https://doi.org/10.1117/12.2531442.
- McManamon, P.F. 2015. Field Guide to Lidar. SPIE.
- "McNemar's Test Using SPSS Statistics." n.d. Https://Statistics.Laerd.Com/Spss-Tutorials/Mcnemars-Test-Using-Spss-Statistics.Php.
- "MEMS Sensors." n.d. Https://Www.Caplinq.Com/Passive-Components/Sensors/Mems-Sensors/.
- Mishchenko, Michael I., Mikhail D. Alexandrov, Brian Cairns, and Larry D. Travis. 2016. "Multistatic Aerosol–Cloud Lidar in Space: A Theoretical Perspective." *Journal of Quantitative Spectroscopy and Radiative Transfer* 184 (November):180–92. https://doi.org/10.1016/j.jqsrt.2016.07.015.
- Motaz Khader. 2020. "An Introduction to Automotive LIDAR." Texas Instruments.
- "Multistatic Radars." 2004. In *Bistatic Radar*, 191–95. Institution of Engineering and Technology. https://doi.org/10.1049/SBRA003E_ch11.
- Nikzad, N., Hoenk M.E. 2020. High Performance Silicon Imaging.
- Novitsky, E. J., and C. R. Philbrick. 2005. "Multistatic Lidar Profiling of Urban Atmospheric Aerosols." *Journal of Geophysical Research Atmospheres* 110 (7): 1–10. https://doi.org/10.1029/2004JD004723.
- O'Hagan, Daniel W., Shaun R. Doughty, and Michael R. Inggs. 2017. "Multistatic Radar Systems." *Academic Press Library in Signal Processing, Volume 7: Array, Radar and Communications Engineering*, December, 253–75. https://doi.org/10.1016/B978-0-12-811887-0.00005-5.
- Paleja, Ameya. 2024. "US Ditches LIDAR, Develops New Stealth Camera Tech to Tackle Laser Detection," March 2024.
- Paschotta, Rüdiger. 2020. "Collimated Beams." Https://Www.Rp-Photonics.Com/Collimated_beams.Html. 2020.
- Petrović, Đorđe, Radomir Mijailović, and Dalibor Pešić. 2020. "Traffic Accidents with Autonomous Vehicles: Type of Collisions, Manoeuvres and Errors of Conventional Vehicles' Drivers." *Transportation Research Procedia* 45:161–68. https://doi.org/10.1016/j.trpro.2020.03.003.

- Piatek. 2017. "LiDAR and Other Techniques Slawomir Piatek Technical Consultant, Hamamatsu Corp. Measuring Distance with Light for Automotive Industry."
- Piggott, Alexander Y. 2022. "Understanding the Physics of Coherent LiDAR."
- Royo, Santiago, and Maria Ballesta-Garcia. 2019. "An Overview of Lidar Imaging Systems for Autonomous Vehicles." https://doi.org/10.3390/app9194093.
- RUMAR, KÂRE. 1990. "The Basic Driver Error: Late Detection." *Ergonomics* 33 (10–11): 1281–90. https://doi.org/10.1080/00140139008925332.
- S Holmström, Sven T, Utku Baran, Hakan Urey, and Senior Member. 2014. "MEMS Laser Scanners: A Review." *JOURNAL OF MICROELECTROMECHANICAL SYSTEMS* 23 (2). https://doi.org/10.1109/JMEMS.2013.2295470.
- Sonbul, Omar and KALASHNIKOV, Alexander. 2014. "Determining the Operating Distance of Air Ultrasound Range Finders: Calculations and Experiments."

 Https://Shura.Shu.Ac.Uk/12087/.
- Teschler, Lee. 2021. "Automotive LiDAR Slides down the Cost Curve."

 Https://Www.Microcontrollertips.Com/Automotive-Lidar-Slides-down-the-Cost-Curve/.

 2021.
- Thakur, Rajeev. 2016. "Scanning LIDAR in Advanced Driver Assistance Systems and Beyond:
 Building a Road Map for next-Generation LIDAR Technology; Scanning LIDAR in Advanced
 Driver Assistance Systems and Beyond: Building a Road Map for next-Generation LIDAR
 Technology." *IEEE Consumer Electronics Magazine* 5.
 https://doi.org/10.1109/MCE.2016.2556878.
- United Nations. 2018. "The World Cities in 2018."
- US-NHTSA. 2022. "Nearly 70% of Car Crashes Linked to 'self-Driving' in US Were Tesla: Report." Business Standard, June.
- Vince, Pasquale. 2022. "A Study on the Use of Multi-Static Radar for Automotive Applications."

 Milan: Politecnico University.
- Warren, Mial E. 2019. "Automotive LIDAR Technology." In 2019 Symposium on VLSI Circuits, C254–55. IEEE. https://doi.org/10.23919/VLSIC.2019.8777993.
- William Poor. 2023. "Lidar Remains the Secret Sauce for Truly Autonomous Cars (despite What Musk Says)." The Verge. June 28, 2023.

Wu, Yunhan, Shuai Shao, Yixuan Li, Xiangzheng Chen, Dongbo Che, Jiayu Chen, Kunyang Du, Ruitao Jiang, Xunqing Huang, and Dongping Kan. 2022. "Multi-Beam Optical Phase Array for Long-Range LiDAR and Free-Space Data Communication." *Optics & Laser Technology* 151 (July):108027. https://doi.org/10.1016/J.OPTLASTEC.2022.108027.

Yole Developpement. 2018. "The Automotive LiDAR Market," April.

Zhang, Yuxiao, Alexander Carballo, Hanting Yang, and Kazuya Takeda. 2023. "Perception and Sensing for Autonomous Vehicles under Adverse Weather Conditions: A Survey." *ISPRS Journal of Photogrammetry and Remote Sensing* 196 (February):146–77. https://doi.org/10.1016/j.isprsjprs.2022.12.021.

Zhao, Junxuan, Hao Xu, Zhihui Chen, and Hongchao Liu. 2023. "Accurate Detection of Vehicle, Pedestrian, Cyclist and Wheelchair from Roadside Light Detection and Ranging Sensors."

Journal of Intelligent Transportation Systems, August, 1–17.

https://doi.org/10.1080/15472450.2023.2243816.